Ultrasound and motion capture analysis for pre-operative planning in lower limb joint replacement surgeries

By Frederick Greatrex

Supervisor: Prof. Claudia Mazzà
Co-Supervisor: Prof. Josef Kozak (Aesculap, Germany)
DDP Supervisor: Prof. Damien Lacroix/Dr. Alberto Marzo

A thesis submitted in partial fulfilment of the requirements for the degree of
Doctor of Philosophy

The University of Sheffield
Faculty of Engineering
Department of Mechanical Engineering

July 2019

Acknowledgements

Abstract

Pre-operative planning in total knee and hip arthroplasty is important for surgical outcome and patient satisfaction. Current clinical gold standards for pre-operative planning include imaging methods which are invasive to the patient and limited to one position of analysis. Lower limb and pelvic alignment are assessed in planning for total knee and hip arthroplasty respectively and have shown to vary in their measurements between standing and supine. B-mode ultrasound has shown to be a promising method for gaining superficial structures like muscles and bones. B-mode ultrasound can be performed rapidly and is relatively cheap and measurements can be conducted with the patient in various positions. The aim of this thesis is to establish non-invasive protocols for pre-operative planning in knee and hip surgeries.

Several approaches were developed to non-invasively measure lower limb and pelvic alignment. These consisted of using integrated motion capture and ultrasound system (OrthoPilot, Aesculap). A *smart system* (Aesculap) which consisted of a smart phone, smart tablet and ultrasound device was used to measure pelvic tilt from the anterior pelvic plane. A motion capture system on its own was used to measure the pelvic tilt in alternative manners. And finally, a synchronised ultrasound and motion capture setup was used for three-dimensional reconstructions of bone geometries. Supine and standing measurements were conducted which showed the flexibility of the measurements unlike common alternatives (X-Ray, MRI, CT).

Several operators performed precise measurements of key lower limb parameters. For example, varus-valgus was shown to be measured within 1 degree across operators. Femur and tibia segment lengths were also consistent (<5mm maximum variation between operators). Femur and tibia torsion measurements were less reliable (up to 10-15 degrees of variation between operators). Pelvic tilt measurements were also found to be unreliable regardless of the measurement technique. Initial promise and feasibility of three-dimensional reconstructions of all lower limb joint axis for implementation into musculoskeletal models was also shown. Joint contact forces differences between the implementation of MRI and ultrasound parameters into the models were less than 1 body weight.

Overall, ultrasound has shown to be useful in the assessment of lower limb parameters and bone geometries. This work has built upon previous findings to continue its development in the field of pre-operative planning and musculoskeletal modelling. Further work will include a large validation of subject-specific musculoskeletal modelling from ultrasound reconstructions. Improvements to the lower limb assessment with OrthoPilot will also be investigated.

Table of Contents

Nomenclature

LLA - Lower limb alignment

PT - Pelvic tilt

MRI - Magnetic resonance imaging

CT - Computed tomography

US - Ultrasound

GRF - Ground reaction forces

TKA - Total knee arthroplasty

THA - Total hip arthroplasty

AJC - Ankle joint centre

KJC - Knee joint centre

HJC - Hip joint centre

APP - Anterior pelvic plane

SD - Standard deviation

ICC - Intra-class correlation coefficient

MSK - Musculoskeletal

OA - Osteoarthritis

Chapter I

Introduction

1.1 Background

Pre-operative planning for total knee and hip arthroplasty has always been an essential part of the surgical period. The analysis performed has considerable impact on the decision-making during surgery and therefore the post-operative outcome and most importantly, satisfaction of the patient. The demand for both procedures in the USA and UK has been predicted to rise exponentially in the next few decades (Kurtz, 2007; Culliford *et al.*, 2015). Without substantial surgical and prosthesis improvements, these authors also suggest that revision rates will remain stable, meaning potentially larger burdens on healthcare systems. Kurtz *et al.* (2005) showed in the USA, from 1990-2002, significant increases in total hip arthroplasty (THA) and total knee arthroplasty (TKA) surgeries and subsequently, revision procedures. The percentage of THA and TKA cases which required revision surgery were 16.3% and 7.8% respectively in 2005 (Kurtz, 2005). THA will require more attention with respect to decreasing the amount of revision and current causes of extra surgery which have resulted in this high figure. These percentages are not predicted to decrease significantly (14.5% and 7.2% for THA and TKA revisions) up to 2030 (Kurtz, 2007). Therefore, as primary surgeries increase, large increases in revision procedures will also occur. In terms of the economic impact this translates to, a theoretical reduction of 1% in THA and TKA revision surgeries in 2002 would save between $96 million and $211.0 million for the USA health services.

In the UK, estimates based on exponential extrapolation of the past hip and knee arthroplasty data forecast large increases in surgery by 2035. Estimates range from approximately 98,000 to 1,100,000 estimated surgeries for THA in 2035 and 110,000 to 1,200,000 for TKA surgeries (Culliford *et al.*, 2015). It is likely the conservative estimation will highly underestimate the amount of procedures in 2035, therefore putting the real figure perhaps closer to the larger estimate. These figures for

the UK will put a high burden on the healthcare and pre-operative planning will be a crucial service.

The impact pre-operative analysis has on patient outcome is slightly harder to break down. Identifying the reasons for failure is often not reported (Kurtz, 2005). A report on the Swedish population however, describes the main contributions for revision (Robertsson *et al.*, 2001). The most common cause for revision in Sweden was implant loosening, which accounted for 44% of all cases (1411/3918). Interpreting this information, however, has its challenges as specific pre and post-operative information, such as knee alignment was not described.

For total knee arthroplasty, the Swedish Knee Arthroplasty Register showed that osteoarthritis accounted for 85% of all TKA surgeries between 1988 and 1997, meaning it's by far the leading cause for undertaking the procedure (Robertsson *et al.*, 2001). The issue of knee mal-alignment, commonly described by the hip-knee-ankle angle, or lower limb alignment, is of continuous interest and its importance is debated. For example, there are many studies which show mal-alignment as a factor that accelerates the rate of osteoarthritis progression, whether the patient has a varus or valgus knee (Sharma *et al.*, 2010). However, it is suggested that those who do not have osteoarthritis and have valgus aligned knees, are less likely to progress to osteoarthritic knees compared to those who have varus aligned knees (Sharma *et al.*, 2010). This is therefore an important step to consider, and how much this natural alignment developed by the individual effects the post-operative walking habits. Normally, the patient will be realigned to $0°\pm3°$, distributing the tibiofemoral loading evenly over the implant. This is currently the gold standard method, described as mechanical alignment restoration. However, its effectiveness has been questioned due to unnatural post-operative function (Bellemans *et al.*, 2012). Other surgical methods, such as kinematic alignment have recently been proposed as a more robust re-alignment of the knee, which considers the pre-arthritic alignment of tibiofemoral parameters. Importantly, kinematic alignment is a dynamic and 3D alignment and can only be partially represented by a plain X-ray (Schiraldi *et al.*, 2016).

For total hip arthroplasty, the Swedish Total Hip Arthroplasty Register showed that osteoarthritis accounted for 75% of all THA surgeries between 1992 and 2000 (Malchau *et al.*, 2002). Like the knee, this restricts movement and causes continuous

discomfort for the individual. To optimise the implant orientation, and similarly to TKA, standing radiographs are the clinical gold standard for analysing the anatomy of the patient. A key issue is the amount of functional change in the acetabulum position, in the sagittal plane, between several key positions such as sitting, standing and supine (Pierrepont *et al.,* 2017; Uemura *et al.,* 2017; Philippot *et al.,* 2009;). Optimum cup anteversion and inclination are sort after to avoid implant impingement or dislocation. By considering several positions, the surgeon can optimise the cup orientation during the surgery and not solely rely on a single position obtained from a standing radiograph. In many cases, the amount of acetabular cup orientation change between sitting and the surgical position (supine) is often a significant amount.

Pre-operative planning for both surgeries have been based on radiographs since their inception. The importance of the information obtained from radiographs was recognised and was the primary source of pre-operative planning through the majority of the 20th century (Wiles, 1958; Shiers, 1960). Joint surgeries of the lower limb present a continuous challenge to the global community. Non-invasive pre-operative planning is still a novel concept, as the diagnostic capabilities of X-rays which commonly lead to a positive outcome, greatly outweigh the potential harm they cause. However, the potential for non-invasive alternatives which can accurately measure lower limb and pelvic parameters could remove the need for invasive imaging techniques.

1.2 Aims and Objectives

The aim of this thesis is to establish non-invasive protocols for pre-operative planning in knee and hip surgeries with the use of ultrasound and motion capture technologies. Measurements included detecting several lower limb internal and palpable external anatomical landmarks to quantify knee varus-valgus and pelvic tilt for knee and hip surgeries respectively.

To this purpose, the following objectives were defined:

- Testing the capability of a prototype system based on motion capture and ultrasound to provide accurate and reliable data for pre-operative planning in knee replacement.

- Testing the capability of a prototype system based on motion capture and ultrasound to provide accurate and reliable data for pre-operative planning in hip replacement.

- Use the knowledge gained by the previous two investigations to develop a new combined protocol for the estimate of both knee and hip pre-operative planning, which could also be used in the framework of patient-specific musculo-skeletal modelling.

According to this context, the thesis is structured as follows:

Chapter II: First, this chapter presents a brief overview of the common measurements used for joint alignment quantification throughout the thesis. Secondly, an explanation of the equipment and techniques for the measurements. Thirdly, a literature review summarising the gold standards of joint alignment measurements of the knee and pelvis and the current alternatives. And fourthly, further literature on the quantification between different subject measurement positions; supine and standing for example.

Chapter III: This chapter investigates the use of an integrated motion capture and ultrasound device to measure several lower limb parameters which are essential in pre-operative planning for total knee arthroplasty surgeries. This includes the measurement of lower limb alignment, femur and tibia torsion, and femur and tibia lengths. The experiments include an intra- and inter-operative reliability assessment on a phantom and small subject cohort to quantify operator dependency of the measurement process.

Chapter IV: This chapter proposes three approaches to quantify pelvic tilt, which is essential in pre-operative planning for total hip arthroplasty surgeries, using external, palpable landmarks on the pelvis. A combination of ultrasound and motion capture systems were used for the experiments. The first approach involved the use of an integrated ultrasound and motion capture setup for the measurement of pelvic tilt from the anterior pelvic plane (APP). The second approach performed the same measurement of the APP with the use of motion capture only. And the third approach quantified pelvic tilt from alternative palpable landmarks on the pelvis with motion capture only.

Chapter V: This chapter examines the use of ultrasound and motion capture as a tool for image based musculoskeletal modelling, potentially replacing current techniques based on MR-imaging. Through 2D freehand ultrasound measurements of the hip and knee joints, tracked with a motion capture system, 3D reconstructions of the femur head, posterior femur condyles and talar dome were conducted on one subject to determine the joint rotation axis of the hip and knee. A sensitivity analysis on a subject specific musculoskeletal model was performed to assess the difference in output of gait simulations for the same subject in comparison to MR-imaging inputs.

Chapter VI: The final chapter summarises each chapter, suggests how has influenced the individual fields of research and the limitations of the findings. Improvements to the current protocols and plans for future work are suggested.

Chapter II

Definitions and literature summary

This chapter introduces the basic concepts of the thesis and discusses the relevant literature in the areas of pre-operative planning for total knee and hip replacements.

2.1 Definitions

Each chapter will focus on different anatomical measurements of the lower limb and consist of several approaches for their measurements. Table 2.1 shows a summary of each study and what approaches are taken. Following this are the basic definitions of the key parameters measured within each chapter.

Lower limb alignment (LLA) is one of the most common parameters assessed in pre-operative planning for knee surgeries (Sharma *et al.*, 2003). It is commonly defined as the angle formed between the mechanical axis of the femur and mechanical axis of the tibia in the frontal plane. The mechanical axis of the femur is measured as a line connecting the hip joint centre (HJC) and knee joint centre (KJC). The mechanical axis of the tibia is measured as the line connecting the KJC and ankle joint centre (AJC). Typically, the HJC is annotated as the centre of a circle fitted on the X-ray to the femur head, the KJC as the trochlea notch of the femur and the AJC as the mid-point of the talus. This is how the joint centres are defined for the LLA in this thesis, though it varies slightly within the literature. This is visualised in Figure 2.1. The LLA angle is shown pre- and post-operatively for a high tibial osteotomy surgery.

Table 2.1. Summary of the three main studies

Chapter	Hypothesis	Instruments	Protocol	Subjects/ Operators	Parameters
III	Reliable measurements of lower limb parameters with ultrasound in supine and standing positions	• OrthoPilot (Aesculap) consisting of an ultrasound and two-camera infrared system • Phantom (Aesculap); a precision machined, two segment plastic device of non-realistic human lower limb geometries (all dimensions known)	• Nine ultrasound images of the lower limb were gained to measure 6 lower limb parameters • This was performed on the phantom first and then on a small healthy subject cohort	• Phantom measurements: 4 operators • Subject measurements: 3 operators, 3 subjects • Subject measurements: 1 operator, 9 subjects	• Varus-valgus, flexion-extension, femur and tibia torsion and segment lengths
IV	Reliable measurements of pelvic tilt (PT) through several different approaches	• Portable smart system (Aesculap; iPhone, surface tablet, ultrasound device) • Motion capture system (10 camera Vicon) • Palpating wand for anatomical landmark detection	• Measurements of PT with respect to the anterior pelvic plane (APP) with the smart system • Measurements of PT with motion capture of the same parameter as the smart system (APP) and quantification of PT in separate approaches from the measurement of other palpable pelvic landmarks	• Phantom measurements: 1 operator • Subject measurements: Up to 4 subjects, 1 operator	• PT measurements with respect to the anterior pelvic plane • PT measurements with respect to the iliac crest height difference
V	Measurements of joint axis from ultrasound measurements can potentially replace measurements currently performed from MRI	• Synchronised motion capture (10-camera Vicon) and ultrasound system • A femur phantom (plastic) of realistic geometries but void of mimicking soft tissue	• Freehand sweeps of the ultrasound probe were performed on a phantom and on one healthy subject	• Phantom measurements: 1 operator • Subject measurements: 1 operator, 1 subject	• Hip, knee and ankle joint axis

Femur torsion and tibia torsion are defined in the transverse plane and are commonly assessed in hip and knee surgeries, and typically measured by MRI scans (Kulig *et al.*, 2010). Femur torsion is defined from the difference between a vector formed by the femur neck axis and posterior condylar axis in the transverse plane. Tibia torsion is defined as the difference between a vector formed by the tibia plateau and the anterior distal tibial in the transverse plane. Both these parameters are show in Figure 2.2.

Naturally, from the measurements of LLA, femur and tibia lengths are defined as the distances from the HJC to the KJC and KJC to AJC respectively.
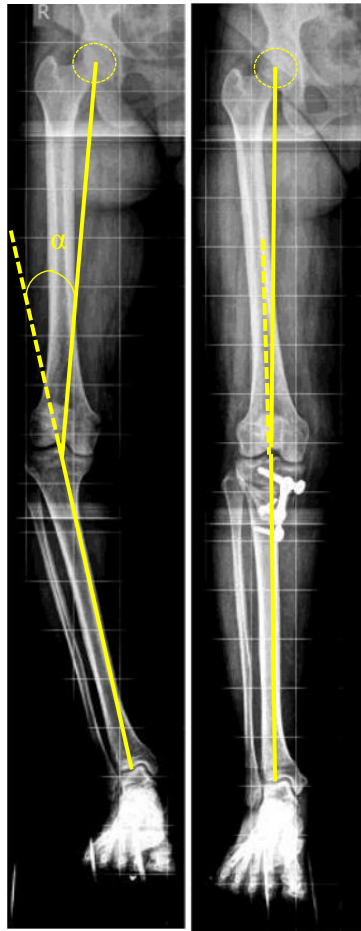
Figure 2.1. Lower limb alignment difference between pre-operative (left) and post-operative (right) high tibial osteotomy surgery (Durandet *et al.*, 2013). A large proportion of the tibiofemoral load is on the medial section of the knee joint, this is known as a varus knee. A more equal load distribution is shown on the right post-operatively.
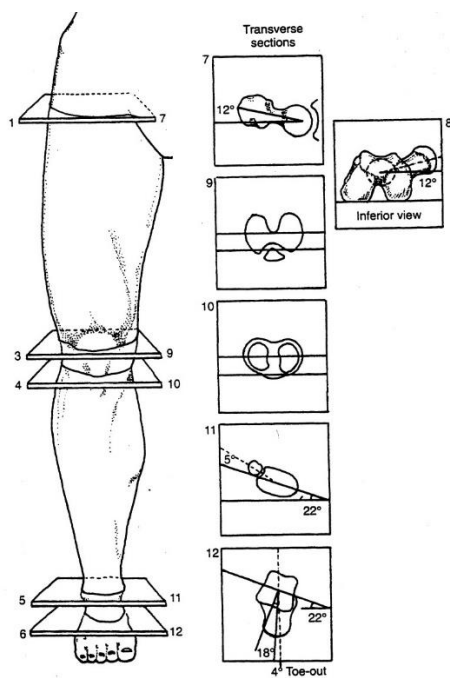
Figure 2.2. Femur (sections 7 and 9) and tibia (sections 10 and 11) torsion shown with respective transverse views of the axis needed to calculate the parameters (Michaud, 2011).

Measurement of pelvic tilt (PT) is a key process in the pre and intra-operative parts of total hip arthroplasty (Lewinnek *et al.*, 1978; Gajdosik *et al.*, 1985; Anda *et al.*, 1990). This parameter (Figure 2.3), amongst others such as the sacral slope (SS) and pelvic incidence (PI), is used to estimate the angle of the acetabular cup during THA. The three parameters are related in the following way:

$$PI = SS + PT \qquad (2.1)$$

The gold standard measurement is performed on radiographs and is defined as the angle between a tangent drawn from the centre of the femoral head to the S1 mid-point, and the coronal plane. This is shown in Figure 2.3.
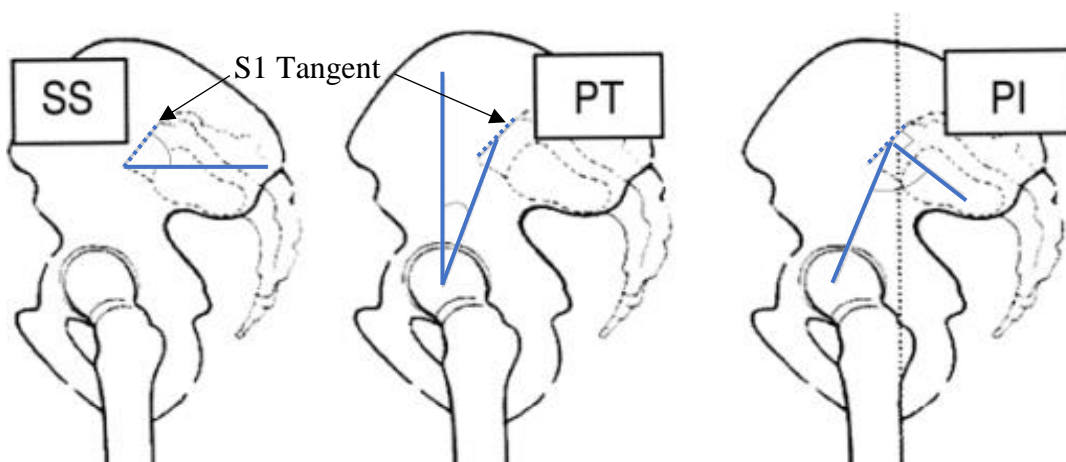
Figure 2.3. Schematics of three sagittal pelvic parameters which help surgical decision making. The sacral slope (SS) is defined as the angle between the sacral endplate, S1 tangent, and the transverse plane. Pelvic tilt (PT) is defined as the angle between a tangent drawn from the centre of the femoral head to the S1 mid-point, and the coronal plane. Pelvic incidence (PI) is the sum of the previous two angles but is defined anatomically by the angle formed by a line perpendicular to the sacral endplate tangent and a line from the centre of the femoral head to the sacral endplate midpoint. Figure adapted from (Oh, Chung and Lee, 2009).

Measurement techniques which cannot obtain internal landmarks such as the S1 mid-point, rely on different PT definitions. Three other definitions will be defined here. Firstly, PT can be defined with respect to three palpable points on the pelvis which form the anterior pelvic plane (APP). The three points are the left and right anterior superior iliac spines (LASIS, RASIS) and the pubic symphysis (PS). The PT is then defined as the angle between the APP and the coronal plane. This is shown in Figure 2.4.
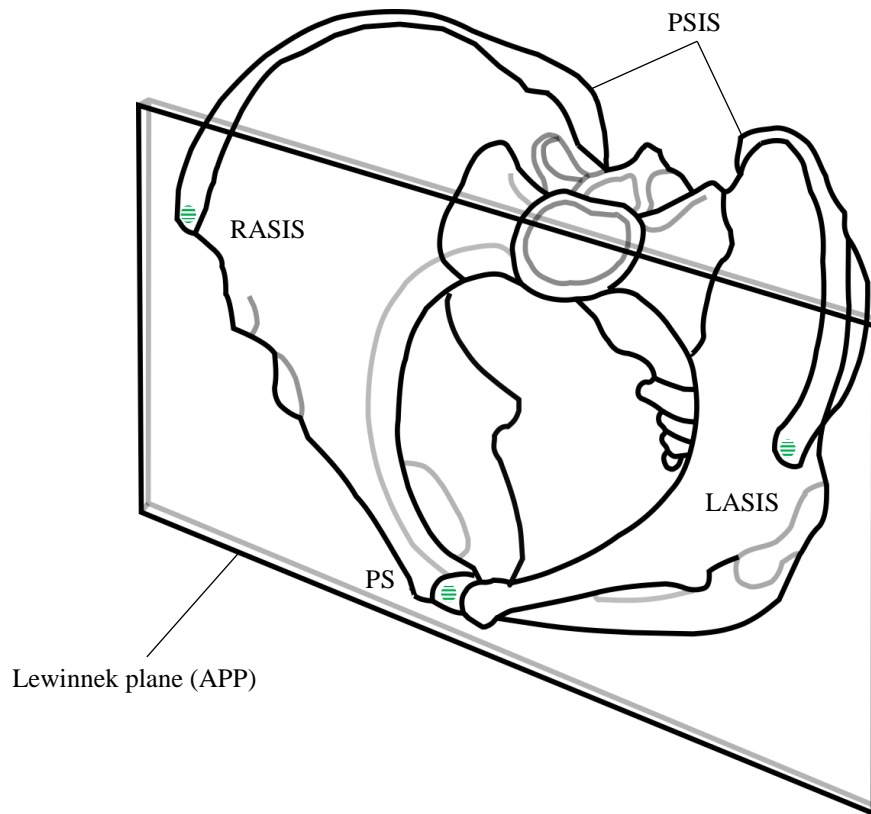
Figure 2.4. Pelvis schematic showing the three key landmarks which define the Lewinnek plane (shaded in green) or also known as the anterior pelvic plane (APP). These are the left and right anterior superior iliac spines (LASIS and RASIS) and the pubic symphysis (PS). In this schematic, the pelvis coincides with the coronal plane, i.e. showing no pelvic tilt either anteriorly or posteriorly. The posterior iliac spines (PSIS) are also shown in this diagram as they can also be used to estimate the tilt of the pelvis.

Secondly, PT can be defined from the pelvic plane, formed from the LASIS, RASIS, and the left and right posterior iliac spines (LPSIS, RPSIS). PT is then defined in the sagittal plane as the angle between the plane formed from the four pelvic landmarks and the transverse plane. This is shown in Figure 2.5.
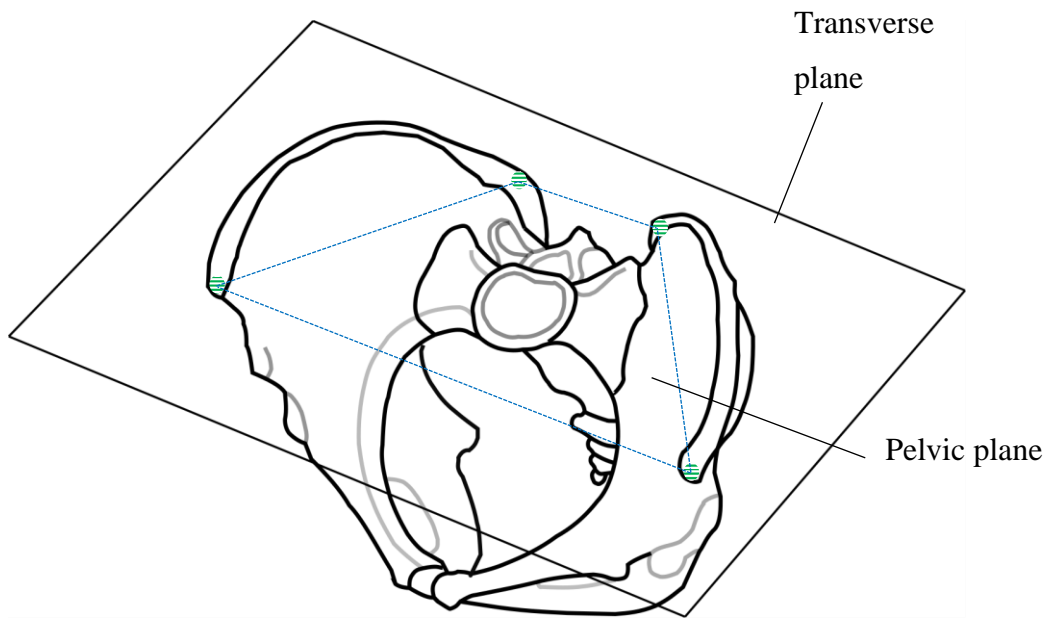
Figure 2.5. Transverse plane and pelvic plane (formed by the right and left anterior and posterior iliac spines). The angle between the two planes in the sagittal plane is the pelvic tilt. The angle between the two planes in the frontal plane is the pelvic obliquity.

Thirdly, measurements are performed with respect to iliac crest height difference, the calculations were performed in a similar fashion to Gajdosik *et al.* (1985) and visually shown in Figure 2.6. In brief, it follows a trigonometric calculation as:

$$sin\theta = \frac{side\ opposite}{hypotenuse} \qquad (2.2)$$

where *side opposite* is the height difference between the PSIS and the floor and the ASIS and the floor, and the *hypotenuse* was the distance between the PSIS and ASIS (Gajdosik *et al.*, 1985). The left and right anterior and posterior iliac spines are investigated individually as shown in Figure 2.6.
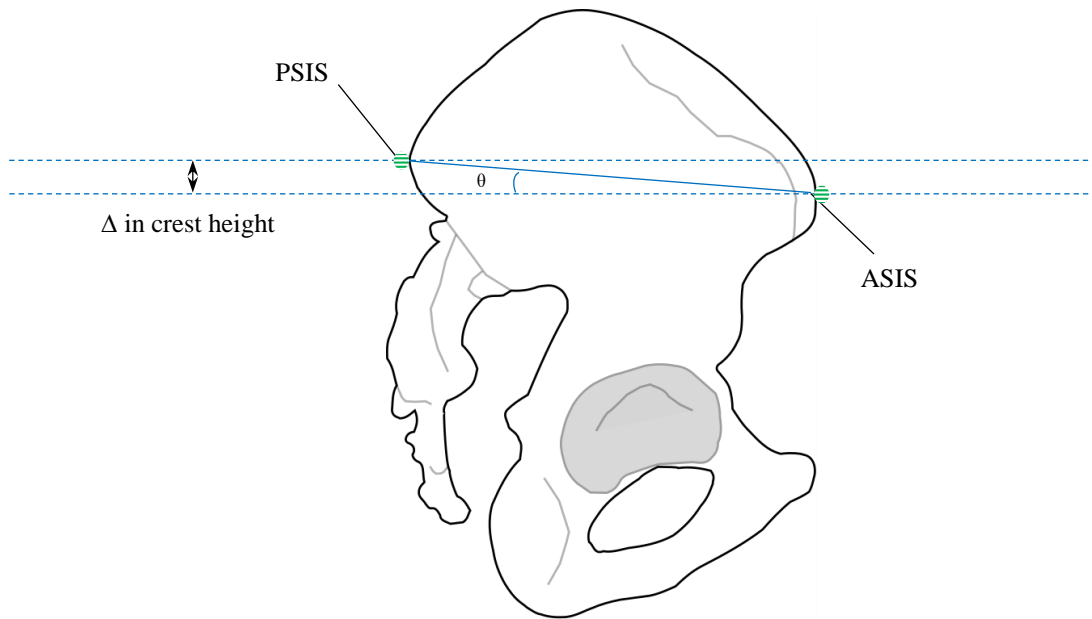
Figure 2.6. Sagittal plane view of the pelvis. The difference in the height of most posterior point (PSIS) and most anterior point (ASIS) of the pelvis is shown. Theta represents the PT measured from this method and in this example, the pelvis is anteriorly tilted.

2.2 Measurement Techniques

2.2.1 Ultrasound imaging

A recurring theme throughout this thesis is the use of B-mode ultrasound for anatomical measurements. B-mode ultrasound is ideal for medical imaging as superficial anatomical features such as muscles, tendons and bones can be measured with relative ease. Each chapter uses the same ultrasound technology. A key limitation is that ultrasound is dependent on the expertise of the operator. Another limitation is that deep structures are difficult to image. However, its portability, non-invasiveness and relative cost to other imaging methods are highly advantageous. A single ultrasound image of the femur head is shown in Figure 2.7.
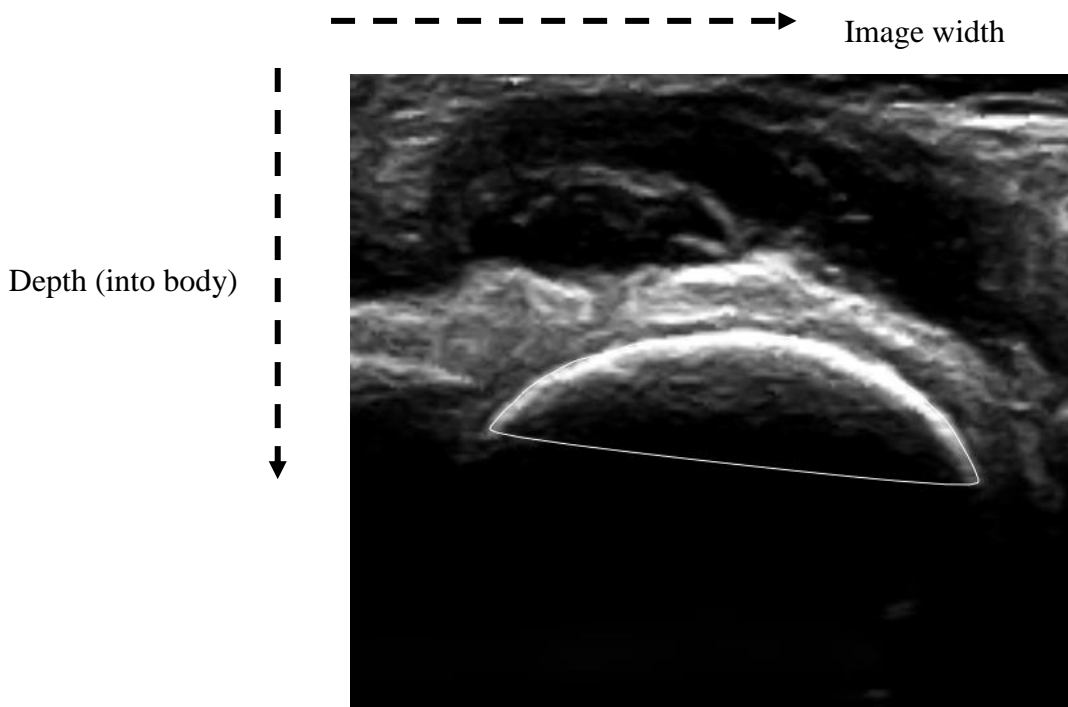
Figure 2.7. Ultrasound image of the femur head with the probe positioned transversely.

2.2.2 Motion capture

Equally common throughout the thesis is the use of motion capture technologies. This is broken down into three separate technologies, with three different systems (or a combination of the three) used in Chapters 3, 4 and 5 respectively. Each system identifies retro-reflective markers to track the positions of the ultrasound probe and subject to gain their positions in three-dimensional space. In Chapter 3, a two-camera, Polaris (NDI Polaris Spectra optical tracking system) camera

system is used with sub-mm accuracy and is pre-dominantly used in intra-operative navigation surgeries. Its main advantage is its accuracy and relative portability which can be used in surgical theatres. Its main disadvantage is its field of view which is limited to 2-3 metres. In Chapter 4, two motion capture systems were used. Firstly, a *smart system*, which consisted of an iPhone for the detection of the reflective markers. A key limitation is that it only has one camera for the detection of markers in 3D. This relies on a robust calibration procedure which is partly investigated in this thesis. Its portability and cost, however, is a key advantage. And secondly, a comprehensive, 10 camera Vicon motion capture system. In Chapter 5, the same Vicon motion capture system was utilised for the measurements. The main disadvantage of this system is its cost. However, it is the gold standard in motion capture technologies.

2.2.3 Musculoskeletal models

A subject-specific musculoskeletal model was built in Chapter 5 using OpenSim for the simulation of gait to calculate internal joint contact forces (JCF) of the hip, knee and ankle (Delp *et al.*, 2007).

2.3 Literature Review

2.3.1 Measurement alternatives for lower limb alignment

The drive for pursuing other planning methods is high, and alternative, non-invasive methods are emerging more prominently in a clinical setting. Several other techniques exist which have also been used for pre-operative analysis. Imaging methods such as CT-scans and MR-imaging have been thoroughly validated against radiographs which are still considered the clinical gold standard for lower limb alignment measurements (Liodakis *et al.*, 2011; Winter *et al.*, 2014). MR-imaging is a relatively common procedure, which is performed in clinical settings, however a main disadvantage is the expense per scan. CT-scans subject the patient to radiation, meaning it is not ideal for pre-operative evaluation and repeat measurements.

Easily obtaining information between weight bearing and non-weight bearing positions currently relies on multiple imaging techniques and have not been extensively researched (Brouwer *et al.*, 2003; Specogna *et al.*, 2006; Sabharwal *et al.*, 2007). The lack of flexibility in the measurement of subjects potentially inhibits a full

understanding of LLA in terms of everyday functionality. However, EOS, a relatively new X-ray imaging device which has a significantly lower radiation dosage compared to standard radiographs, can analyse subjects in various positions. This is a significant advantage, but does not operate in the supine position (Lazennec *et al.*, 2011; Escott *et al.*, 2013). The device uses the invention of Professor Georges Charpak who developed a gaseous particle detector with a multi wire proportional chamber which limits the dosage of X-rays subjects are exposed too. The technology provides both anteroposterior and lateral, full body scans which can then be reconstructed into 3D with their SterEOS software. However, the reconstruction is not automatic and requires training Its current availability for clinical measurements however, is limited due to its market access (Meijer *et al.*, 2016).

Three dimensional motion capture has become an increasingly popular choice for LLA during motion and has been integrated with experiments when gait analysis is performed pre- and post-operatively for patients (Hunt *et al.*, 2008; Mündermann *et al.,* 2008; Vanwanseele *et al.,* 2009; Duffell *et al.*, 2014). By measuring the varus-valgus over a gait cycle, a dynamic interpretation can be made and potentially give the surgeon a greater understanding of dynamic changes in LLA. However, methods quantifying parameters such as LLA from skin marker measurements have been questioned over their accuracy. Soft tissue artefact presents a consistent challenge in motion capture research within biomechanics, and certain compensation techniques have been investigated (Rouhandeh *et al.*, 2014). Certain landmarks, such as the HJC, rely on accurate measurements of external landmarks, or functional calibration techniques. The propagation error for quantifying lower limb parameters is extreme if the measurements are not performed correctly (Stagni *et al.*, 2000; Chiari *et al.*, 2005; Fiorentino *et al.*, 2016). Therefore, limitations currently exist in the interpretation of measurements performed from skin marker measurements. Removing the error produced from soft tissue artefact with ultrasound is a relatively novel approach and has been investigated by several researchers (Rouhandeh *et al.*, 2014; Jia *et al.*, 2016; Niu *et al.*, 2018). Whilst these areas are progressing the use of ultrasound in dynamic tasks, the use of ultrasound for static lower limb alignment measurements has only recently progressed (Greatrex *et al.*, 2017; Kochman *et al.*, 2017).

Hinman *et al.* (2006) presented five clinical measures of the LLA to find a valid method of the measurement compared to radiographs. Calliper, plumb-line,

inclinometer, goniometer and Magee's method were all performed with the subjects standing and compared against standing radiographs (Hinman *et al.,* 2006). These methods provided cheap and easy to use methods for LLA assessment compared to lower limb and knee radiographs. Forty patients with OA were assessed and out of the 5 clinical measures used, the inclinometer demonstrated the strongest correlation with the mechanical axis measured from the radiographs (r = 0.8, p < 0.001). This method involved measuring the orientation of the tibia with respect to the vertical, however, it does not consider the orientation of the femur. The results of the inclinometer and standing radiographs were 176°±3° and 174.2°±4.9° respectively (varus as < 180°). Their sample size and consequent population average for the LLA compares well with another study who performed a large prospective study on 236 patients and measured a mean LLA alignment of 5.4°±3.5° (varus as positive) (Cahue, *et al.*, 2003). This also compares to a study who investigated self-reported knee confidence and its association with varus-valgus, amongst other knee OA indicators, and found a mean LLA alignment of 176.8°±3.5° (varus as < 180°) in 100 patients measured on standing radiographs (Skou *et al.*, 2014).

Inclinometers and goniometers have also been used in other studies of LLA (Vanwanseele *et al.,* 2009; Deep *et al.*, 2016). One study performed a simple clinical measurement which involved measuring the LLA with a goniometer (Deep *et al.*, 2016). This was compared with two reference measurements; standing radiographs and an intra-operative navigation system. The differences between the clinical measurement and the two reference measurements were 0.8° (range: -12° to 12°) and 0.3° (range: -10.5° to 9°), where positive indicates an over estimation with respect to the reference. However, the authors maintain that the clinical method is an estimate of the true deformity with a very wide error margin (Deep *et al.*, 2016). Another study measured the mechanical axis during gait analysis and compared their results to standing radiographs, and inclinometer measurements (Vanwanseele *et al.*, 2009). The mean mechanical axis measurements for the three techniques respectively were 4.6°±6.5°, 0.7°±7.2° and 0.06°±3.6°. Similarly, however, only 11 patients were enrolled in this study, meaning comparing results with other studies may be limited.

Previous studies have successfully measured leg length discrepancy and femur torsion values with ultrasound in the past (Terjesen *et al.*, 1991; Hudson *et al.*, 2006; Kulig *et al.*, 2010b). Studies which integrate motion capture have investigated lower

extremity parameters such as hip joint centre calculations and torsion measurements, but not extensive analysis of lower limb alignments (Hicks & Richards, 2005; Upadhyaya *et al.,* 2015; Passmore *et al.*, 2016). Despite being very encouraging for further exploitation of the techniques, none of these studies provided a thorough analysis of all the variables that might be needed for fully determining lower limb alignments for pre-operative planning.

2.3.2 Sensitivity of lower limb alignment to subject positioning

During pre-operative analysis to obtain the LLA and other parameters, it is debated whether this should be conducted in supine, as the subject will be during surgery or as is most common, in standing. The literature on the amount of change between different positions is extensive. Typically, research has focussed on supine and standing positions, but gait analysis has also been conducted to quantify dynamic changes. A summary of the findings in this section is shown in Table 2.1.

Table 2.2. Literature findings for measurements of lower limb alignment and differences between various postures.

Group	Author	Methods	Subjects/ Operators	Results	Conclusions
Large differences between positions of analysis	Brouwer, 2003	Radiographs in supine and standing	20 patients, 2 assessors	• 2° more varus deviation in the standing than in the supine • Intraobserver and interobserver variability were low, ICC = 0.98; 95% CI = 0.94–0.99 and ICC = 0.97; 95% CI = 0.94–0.99, respectively.	• A WLR in supine is recommended for patients with abnormal laxity of the lateral collateral ligament • Supine radiographs are recommended
	Sabharwal, 2008	Intra-operative fluoroscopy, standing radiographs	80 patients (102 limbs). 46 pre, 34 post. 1 assessor	• Mean difference of 13.4 mm for the mechanical axis deviation between standing radiograph and the fluoroscopic images	• Surgeons can be confident of the estimation of the lower limb alignment with use of this method
	Mündermann, 2008	Motion capture, standing radiographs	62 patients, 1 assessor	• Motion capture: $3.8 \pm 4.7°$; radiograph: $2.6 \pm 4.4°$ • For 90% of the knees, results for the same knee were within 5.3°	• Quantifying mechanical axis alignment using motion capture correlates well with the gold standard
	Vanwanseele, 2009	3D gait, inclinometer, standing radiographs	11 patients (20 limbs), 1 assessor	• Mean mechanical axis radiographs: $0.7° \pm 7.2°$ • Mean HKA angle with the static 3D analysis technique was $4.6° \pm 6.5°$	• The inclinometer and static trials are reproducible methods to estimate the mechanical alignment of the knee
	Duffell, 2014	3D motion capture, MRI, CT	15 patients (CT + MOCAP) + 9 healthy patients (MRI + MOCAP)	• 2–4° increase in knee adduction angle during gait when compared to static conditions	• Static imaging alone appears insufficient to document the degree of functional knee adduction
	Winter, 2014	MRI & Standing radiographs	45 patients, 3 assessors	• Lower limb alignment was identical in 10/45 • Under-estimated in 31/45 • Over-estimated in 4/45 (9%)	• Supine MRI underestimates the degree of deformity at the knee join
	Deep, 2015	Non-invasive navigation measurements (OrthoPilot)	132 healthy subjects (264 knees), 1 assessor	• $2.2° \pm 3.6°$ more varus in the standing position compared with supine	• Implications for the assessment of alignment in TKA • Non-weight-bearing conditions may not represent weight-bearing scenarios
Small differences between positions of analysis	Hunt, 2008	3D motion capture, standing radiographs	80 patients, 1 assessor	• Radiograph-based LLA: $-4.8° \pm 5.8°$. Gait analysis based: $-4.8° \pm 6.0°$	• Variance (29%) in proposed measure of dynamic lower limb alignment
	Kornaropoulos, 2010	CT, functional assessment, regression method	13 patients (15 limbs), 1 assessor	• CT and Functional-mFTA predicted the mFTA angle to within 1° • The difference between the CT and Regression-mFTA was significant	• The results suggest that the novel techniques are relevant for both clinical and scientific use
Differences not quantified	Hinman, 2006	Calliper, plumb-line, inclinometer, goniometer, Magee's method, radiographs	40 patients, 1 assessor	• Inclinometer method demonstrated the strongest correlation with the mechanical axis	• Inclinometer and calliper methods (varus only) methods shown to be valid alternatives to radiographs
	Boonen, 2016	Standing radiographs, CT Scan	24 patients, 6 assessors (radiographs), 1 CT assessor	• Means of $1.3° \pm 1.5°$ and $1.8° \pm 2.1°$ between the deviations of the femoral and tibia components of the prosthesis	• LLR are an adequate tool for analysing alignment of TKA components
	Deep, 2016	Clinical measurement, standing radiographs, intra-operative navigation	54 patients, 2 assessors (radiographs)	• Mean difference of the clinical measurement and radiographs was 0.8° (-12° to 12°) • Mean difference of the clinical measurements and navigation was 0.3° (-10.5° to 9°).	• Potential that weight bearing measurements impacts alignment • Clinical measurement is a rough estimate of the true amount of deformity

Contrasting studies exist which investigate the changes in LLA. One study showed for radiographs in standing and supine, that there is a mean difference of 2°±0.45° (range: 1°-3°) more varus deviation for the standing position (Brouwer *et al.*, 2003). Similar results were obtained in another study, but with MR-imaging for the supine analysis (Winter *et al.*, 2014). They concluded that MR-imaging underestimates the deformity of the knee by an average of 2°±3° (range: 0°-8°). A greater spread of data is shown in this study which potentially limits the interpretation of the comparison. In contrast, another study compared up-right MRI scans to standing radiographs and showed comparable results (Liodakis *et al.*, 2011). LLA angles of 4.5°±4.4° and 4.1°±3.3° were found respectively for the two measurement techniques. This suggests that the under estimation found by Winter *et al.* (2014) was due to the non-weight bearing position of the subjects.

Dynamic variation of the varus-valgus angle was assessed and their results were compared to static trials and CT scans in a patient population (Duffell *et al.*, 2014). The same protocol was applied to a healthy subject group, but their motion capture results were compared to MRI measurements. For all subjects, there was an approximate 2°-4° increase in knee adduction angle (KAA) during gait when compared to static conditions. Interestingly, KAA when measured in supine where significantly higher than those measured in the static standing posture measured with the motion capture system. The drawback of this study is the cohort size, 15 patients and 9 healthy subjects, meaning the results should be interpreted with caution (Duffell *et al.*, 2014). A similar study was conducted with a larger cohort (62 patients) and compared the mechanical axis during gait analysis with standing radiographs (Mündermann, *et al.,* 2008*)*. For both methods, the mean mechanical axis was 3.8°±4.7° for the gait analysis and 2.6°±4.4° for the radiographs. A key finding was that varus malalignment measured with the motion capture increased as OA severity increased (measured with Kellgren-Lawrence grades).

Lower limb alignment of 132 healthy subjects was measured with an intra-operative device OrthoPilot® (Aesculap, Tuttlingen), like the one shown in Chapter 3 (Deep, *et al.,* 2015). Supine and standing measurements were conducted. Whilst normally used to aid TKA, this device was used non-invasively to quantify the LLA. Certain functional tasks were performed with clusters attached to the subject so that the device could track the subject's movements. With this, a pointer, handled by the

assessor was also tracked, and aided the palpations of bony landmarks. With this information, the LLA was measured and there was a mean of 2.2°±3.6° more varus in standing than supine (Deep, *et al.,* 2015). This agrees with the previously described literature which shows supine measurements underestimate LLA.

To optimise the knee implant, the correct alignment needs to be measured intra-operatively. Quantifying this is not rudimentary, but some novel techniques have been attempted. One such technique, using intra-operative fluoroscopy, was attempted (Sabharwal and Zhao, 2008). They retrospectively analysed 80 patients requiring various surgeries and baseline imaging was either pre- or post-operative and therefore split into two groups. They quantified the amount of LLA by assessing the mechanical axis deviation (MAD) which measured the perpendicular distance from the mechanical axis (line joining the HJC and AJC) to the mid-point of the tibial splines (defined as the centre of the knee in this case). The mean MAD for the standing radiographs was 7.1mm medial (range; 86mm lateral to 126mm medial) and for the fluoroscopy was 7.7mm medial (range; 74mm lateral to 136mm medal). This study analysed a relatively young population (80 patients, 88% are ≤ 18 yr.), and their main limitation was the implication of the fluoroscopy technique on obese individuals, which would likely be a large proportion of persons undergoing TKA in a typical population of patients (Sabharwal and Zhao, 2008).

2.3.3 Measurement alternatives for pelvic tilt

The Palpation Meter (PALM, Performance Attainment Associates, St. Paul, MN, USA) has been a popular measurement method for performing anatomical measurements on the pelvis since 1998 (Hagins *et al.*, 1998). This has included the assessment of leg length discrepancy by measuring the iliac crest height difference on both sides of the pelvis (pelvic torsion) and the measurement of the sagittal plane PT using the anterior and posterior iliac spines (Petrone *et al.*, 2003; Herrington, 2011). Whilst these landmarks are regarded as simple to palpate over soft tissue, there is contrasting literature on the reliability of performing palpations on the pelvis (Cooperstein and Hickey, 2016). Specifically, low inter and intra-operator agreement on the palpation of the PSIS and ASIS landmarks has been shown (Kmita and Lucas, 2008). Their rigorous experimental procedure, which focussed on the standardisation of the palpation techniques, was the highest scoring paper for overall quality (Cooperstein and Hickey, 2016). Four examiners participated, and a Cohen's kappa score was calculated from their categorical results. Scores range from -1 to 1 with scores close to 0 showing no agreement and it considers the possibility of agreement occurring by chance. In this study, only one instance of a kappa score between two operators was found for the ASIS palpation, and none for the PSIS landmarks. Agreement was found to be irrespective of operator experience (Kmita and Lucas, 2008). Their main limitation was the low sample sized used (n=9) which meant population-based assumptions could not be made. Their palpations were performed in the prone and supine positions only, whereas several studies have also assessed the palpation reliability in standing and sitting positions (van Kessel-Cobelens *et al.*, 2008). It was found that palpation of the PSIS landmarks in the sitting position within a cohort of pregnant woman to assess pelvic asymmetry was unreliable. Kappa scores were consistently below 0.5 after a similar categorical measurement procedure was used (Kmita and Lucas, 2008; van Kessel-Cobelens *et al.*, 2008).

A similar method assessed the reliability of measuring the PT with a digital pelvic inclinometer (DPI, Sub-4 Limited, UK) (Beardsley *et al.,* 2016). This involved simultaneously palpating the anterior and posterior iliac spines and reading off the angle in the sagittal plane as the pelvic tilt. This method is appealing as it is fast and efficient. Like this, but measured slightly differently, is research conducted by measuring the PT by palpating the posterior and anterior superior iliac spines and

simultaneously measuring the distance from each landmark, to the floor (Gajdosik *et al.*, 1985). This method allowed the calculation of a height difference between the most posterior and anterior points on the pelvis and consequently, a pelvic angle (Gajdosik *et al.*, 1985). Intra-operator reliability was good with Pearson coefficients of 0.88 for the standing pelvic tilt tests. Imposed anterior and posterior pelvic tilt measurements had r values of 0.92 and 0.88 respectively. Inter-operator reliability was not assessed and considered one of the main limitations of the study.

EOS imaging has shown great appeal since its introduction into clinical and research settings (Melhem *et al.*, 2016). A key advantage of the EOS is the measurement of pelvic parameters in sitting, squatting and standing positions (Lazennec *et al.*, 2015). Its accuracy for lower limb measurements has been compared to CT scans and has shown robust results. For femur torsion measurements one study found values of 13.4°±9.1° and 13.7°±9.4° for EOS and CT respectively. For tibia torsion measurements, they found values of 30.8°±8.8° and 30.3°±9.6° for EOS and CT respectively (Folinais *et al.*, 2013). It is a promising replacement but is currently expensive (€500,000 implementation plus yearly maintenance) and not cost-effective compared to X-rays which may be a reason it is not in many clinical settings (Lazennec *et al.*, 2011; Faria *et al.*, 2013; Melhem *et al.*, 2016; Thelen *et al.*, 2016).

Another technique involved the use of a digitising arm, which could digitise the bony landmarks needed to measure the APP (Mayr *et al.*, 2005). The difficulty in this technique, however, is the palpation of the PS landmark through the soft tissue without causing discomfort for the subject. In subjects with a large amount of soft tissue, this technique becomes problematic.

Motion capture in the context of clinical biomechanics is used in gait analysis experiments to measure lower extremity joint kinematics and kinetics. In most cases, passive reflective markers are placed in clusters and on bony landmarks of the subject and detected by a series of non-invasive stereophotogrammetric infrared cameras. Estimates of the PT angle have been measured with respect to four markers attached to the anterior and posterior iliac spines (Vicon®, 2002; Perrott *et al.*, 2017). However, the main problem with this approach for measuring PT is the STA associated with movement of the skin with respect to the underlying bony landmark. This in turn is linked to the palpation of the PSIS landmarks which has shown to be a cause of error

(Cooperstein and Hickey, 2016). Almost all the studies reviewed showed inter-operator reliability was not attainable and this was irrespective of operator experience. All studies which calculated kappa agreements were noted to be less than substantial (< 0.60). Therefore, locating landmarks through conventional methods, such as radiographs is currently a favourable and more reliable method.

Recently, an ultrasound system has been developed to measure the APP to offer an alternative to current methods (Martin 2016; Kochman *et al.,* 2017; Marques *et al.*, 2018). However, current results are highly variable, and, as emphasised, before introducing APP ultrasound measurements on a patient cohort, improvements in the ultrasound setup will be necessary for further studies to be pursued. Large variation is potentially explained by the operator dependence of ultrasound measurements or the identification of the pubic symphysis landmark. Therefore, expertise in ultrasound imaging is highly advised and there are several operator dependent processes (measurements, and then ultrasound image annotation) which potentially increase the variability in measurements (Kochman *et al.*, 2017). As well as this, current attempts of APP measurements in positions apart from supine resulted in even greater variability. The main advantage of ultrasound is that it can penetrate through soft tissue and potentially overcome errors associated with STA. It is therefore an appealing technique which could be a useful tool in a clinical setting, if it can perform reliably and accurately. The device tested in this group of studies is also used in this chapter to partly try and determine the cause of the excessive intra-operator variability of subject measurements currently observed (Kochman *et al.,* 2017; Marques, *et al.*, 2018).

Having reviewed several non-invasive techniques for PT measurement in this chapter, a combination of techniques was used to measure the PT. Shown in Chapter 4, this included measurements of the anterior and posterior iliac spine height difference, palpation of the anterior pelvic plane, and ultrasound measurements of the anterior pelvic plane (Gajdosik *et al.*, 1985; Mayr *et al.*, 2005; Martin, 2016).

2.3.4 Sensitivity of pelvic alignment to subject positioning

During pre-operative analysis to obtain the APP and other parameters, a continuous discussion is present as to whether this should be conducted in supine, as the subject will be during surgery, or in other positions which might provide insight

into the amount of PT change between typically assumed positions. The literature on the amount of change between different positions is extensive. Typically, research has focussed on supine, standing and sitting PT positions, but squatting and gait analysis have also been conducted to quantify dynamic changes. The sitting position is commonly analysed due to the importance of the acetabular cup positioning and the severity of the hip flexion angle when an individual is in a sitting position. If this position is not analysed, then vital information may be missing in the pre-operative analysis, as the amount of change between supine and sitting PT has been shown to be significant. A summary of the discoveries in this section is shown in Table 2.2.

Table 2.3. Summary of literature findings for measurement of pelvic tilt.

Group	Author	Methods	Subjects/ Operators	Results	Conclusions
Large differences between positions of analysis	DiGioia, 2006	Radiographs (standing, sitting)	84 patients, 1 assessor	• Mean APP in standing and sitting of 1.2° (-22 to 27°) and -36.2° (-64° to 4°) • No significant differences from pre to post-operative measurements	• There were unpredictable variations in pelvic orientation when comparing standing and sitting results
	Philippot, 2009	Radiographs (supine, sitting, standing)	67 patients, 1 assessor	• Means of the standing and lying PT are similar • Difference between the sitting position and the others is approximately 21°	• Determine the position of the Lewinnek plane preoperatively when standing, lying, and during surgery
	Lazennec, 2011	EOS, conventional radiographs (sitting, standing)	50 patients, 2 assessors	• Very similar results for the two techniques • Mean of the standing at sitting PT were 2.4°±7.3° and 16.9°±9.1° respectively	• The image accuracy achieved using the EOS 2D imaging system is like conventional X-rays
	Taki, 2012	Radiographs (supine, standing)	86 patients, pre, post at 1st, 2nd, 3rd (55) and 4th (32) year	• Mean PT in standing and supine pre-operatively was 22.6°±10.4°& 18.5°±8.0° • Mean PT significantly changed at each time point apart from 4th year	• Older patients showed larger change in PT after THA • Suggest obtaining standing and supine pelvic radiographs to check PT
	Kanawade, 2014	Radiographs (standing and sitting)	85 patients, pre and post	• Mean difference between standing and sitting PT, pre and post-operatively was 28.7°±8.6° & 25.6°±10.6°	• Cup positioning at surgery is not the same when the patient stands or sits • Acetabular component should be implanted with respect to ante-inclination during sitting
	Lazennec, 2015	EOS (standing, sitting, squatting)	224 patients	• Mean PT in standing and sitting was 18.3°±11.2° & 36.0°±15.2° • Pelvic tilt increased posteriorly during squatting	• A global analysis was performed in the true standing, sitting and even squatting positions • The comparison of standing and sitting positions shows importance of outlier detection for APP measurements
	Ranawat, 2016	Radiographs (standing, sitting)	68 patients, 2 assessors	• Mean change between standing and siting was -21.4°±12.5° • High inter & intra- observer reliability	• Significant change in PT from standing to sitting, especially in patients with a flexible spine
	Kochman, 2017	Ultrasound smart system (standing, sitting, supine)	20 patients (14 sitting)	• Mean in standing, supine and sitting was 19°±24.9°, -6.9°±16.2° & -63.3°±13.6°	• Large spread of data compared to literature, but averages in line with previous results • Sitting analysis was considerably out of range with other studies
Small differences between positions of analysis	Mayr, 2005	Digitising arm (supine and standing)	120 subjects (several groups)	• Mean supine and standing inclination were 5.6° (4.4-6.1) and 6.7° (5.2-8.7) respectively • 3.0°±5° difference on average in elderly group	• The PT in the standing position increases when people become older • Changes in PT from standing to supine position were low in all but the elderly group
	Tamura, 2014	CT, radiographs	163 patients, 1assessor	• Mean change from supine to standing was -6.9°±5.7°	• Aging and spinal degeneration are related to PT
	Tamura, 2015	Radiographs (supine and standing), CT, motion capture	44 patients, 2 groups (group 1, greater than 10° of PT, group 2, less than)	• Mean APP in standing and supine was -8.9°±18.0° & 1.3°±11.6° • Large differences for all motion capture results of PT • Sitting produced by far the largest change in PT	• This study provides guidance for the pelvis and hip kinematics in the early postoperative period
	Tamura, 2017	CT, radiographs	70 patients, 10 years post THA	• Mean change of -2.9°±5.6° in supine after 10 years • Standing PT showed a -11.4°±13.2° reduction on average	• PT in the standing position showed continuous reclining, thought to be caused by spinal degeneration and aging
	Uemura, 2017	CT, radiographs	422 patients, 1 assessor	• Mean change between standing and supine was -7.2° (-10.7° to 3.3°) • In 20% of the cases, there was over 10° of change	• The odds ratio of a ≥10° change of PSI from supine to standing increased 3.5% as patient age increased by 1 year

As previously stated, the clinical gold standard for PT measurements is standing radiographs, and supine analysis is performed by CT scans. Comparisons of pelvic parameters between various positions became increasingly of interest in the early 2000s. It was hypothesised that pelvic parameters would significantly change during dynamic tasks, particularly from sitting to standing or lying to standing (Ala Eddine *et al.*, 2001). Therefore, quantifying the differences and compensating for them by optimising the cup position during surgery became a popular approach by clinicians.

One study measured the PT change between standing and supine with the use of radiographs at five time points (pre-operatively, post-operatively, 1, 2, 3 and 4 years post-operatively) (Taki *et al.,* 2012). This comprehensive study looked at the effect time had on pelvic parameters and determined small differences between standing and supine at all time points. Mean PT differed by about 4° on average in standing and supine pre-operatively. Mean PT significantly changed posteriorly at each time point apart from 4th year, with a reduction of 7° when moving from standing to supine respectively). Twenty five percent of the patients showed a PT change of over 10° between two time points (Year 1 and 3) in the standing position. Increases in PT causes an increase in cup anteversion which could potentially lead to dislocation or impingement. Therefore, measuring the PT over time post-operatively has given important information on implant position and potential longevity (Taki *et al.,* 2012). Similarly, other research has shown a continuous posterior recline in PT over a 10 year period, thought to be caused by spinal degeneration associated with aging (Tamura *et al.*, 2017). Large differences between supine and standing were found in other studies (Tamura *et al.,* 2014; Uemura *et al.*, 2017) which is different to the results in other studies (Philippot *et al.*, 2009; Taki *et al.*, 2012). Differences between supine and standing across the literature, however, were found rarely to exceed 10°.

For differences between standing and sitting, much greater changes are observed (DiGioia *et al.*, 2006; Philippot *et al.*, 2009; Kanawade *et al.,* 2014; Ranawat *et al.*, 2016). The most recent study used two assessors to perform inter and intra-assessor reliability on the radiographic measurements and found high agreement (Ranawat *et al.*, 2016). Similar results were reported who also performed supine radiographs and found mean differences of approximately 22° between both supine and sitting and standing and found a small difference of 1° between supine and

standing (Philippot *et al.*, 2009). Large differences between standing and sitting has also been found in other research but concentrated on the difference between pre- and post-operative PT where the mean difference for both time points was approximately 26° and 29° respectively (Kanawade, Dorr and Wan, 2014). Another study also concentrated on the pre-and post-operative change but measured the APP and found large ranges of approximately 38° between standing and sitting at both time points (DiGioia *et al.*, 2006).

The use of low-dose radiographs with EOS imaging has been used for the past decade and published several studies which include standing, sitting and squat measurements of the APP and PT in a bid to reduce the use of conventional radiographs (Lazennec *et al.*, 2011, 2016; J. Lazennec *et al.*, 2015; J. Y. Lazennec *et al.*, 2015). Similar results were found for standing measurements in their first validation study with EOS but lower sitting values were measured (DiGioia *et al.*, 2006). For their EOS measurements, the mean of the standing and sitting were approximately 3° and 18°. The mean of the standing and sitting APP were approximately 2° and 17° respectively for their conventional X-ray measurements (Lazennec *et al.*, 2011). The results showed that EOS could be a promising alternative to conventional X-rays. Their research continued further and an article showing their first 8 years using the technology summarised all their initial findings including the measurement of over 300 THA patients in standing, sitting and squatting positions (J. Lazennec *et al.*, 2015). A key finding from one of the studies questioned the usefulness of the Lewinnek safe zone which assumed a vertical APP for all positions. Such information has shown to be difficult to ignore and the 'safe zone' in contradicting studies has shown dislocation to be just as likely when positioned to the 'safe' specification previously described. Another author also pursued the use of EOS and focussed on the 3D orientation of the acetabulum in healthy subjects in the standing position only (Thelen *et al.*, 2016). This included the measurement of the PT defined with respect to the sacral segment S1 with a mean value over the whole population (102 subjects) of 11.5°±6.4°. This is comparable to a study which also used EOS to measure pelvic, femoral and acetabular parameters on healthy subjects in the standing position who found a mean PT of approximately 15 with a sample size of 30 (Bendaya *et al.*, 2015). Their measurements were also performed on an OA population and found

almost identical pelvic tilt values which is much lower than results previously discussed in this section.

Another study went one step further in their research by analysing and comparing APP measurements during gait with supine and standing radiographs, and three other dynamic movements (1. picking up an object whilst seated on a chair, 2. stretching the Achilles tendon and 3. bending backwards holding both hands up) to mimic hip flexion and extension tasks, all measured with a motion capture system (Tamura *et al.*, 2015). Two groups were analysed in this study, one for patients who, on the standing and sitting radiographs, exhibited a change in APP greater the 10° and one group of a change of less than 10°. On average for all patients, the change in APP over the gait cycle was 5.3°±2.1°. There was no significant difference for this parameter (Arc of APP sagittal tilt during walking) between the two groups. The four motions analysed gave an estimated maximum degree of change in sagittal pelvic kinematics which is why they were chosen. Such movements will not be analysed in this thesis but are certainly clinically relevant for determining the most effective cup orientation for THA based on tasks which may be performed by individuals post-operatively.

Herrington measured the PT of 120 healthy subjects with the Palpation Meter (PALM). Average anterior and posterior PT for males and females were very similar with no significant differences between the two groups. Differences were apparent between the left and right side of the pelvis however, for males but not for females (Herrington, 2011).

One study conducted their PT measurements with a digital inclinometer on 18 healthy subjects in the standing position. Their technique of measuring the PT with the DPI on key palpable landmarks, allows measurements on both sides of the pelvis. For the right and left side of the subjects, the PT measured was 10.6°±5.0° and 10.5°±5.8° anteriorly respectively (Beardsley *et al.,* 2016). Whilst it is difficult to link these results to more typical techniques (X-rays), these measurements are comparable to previously discussed results (Bendaya *et al.*, 2015; Thelen *et al.*, 2016). However, the results contrast slightly another study who found much lower values, especially in the female group (2.71° and 2.51° on average for the left and right side respectively,

SD not quoted) (Herrington, 2011). Though, comparing these two results should be interpreted with caution, as Herrington (2011) used a much larger sample of subjects.

Another study measured a large cohort of 120 subjects split into 4 groups (young healthy, old healthy, hip arthroplasty and coxarthrosis) to measure the APP with a digitising robotic arm in both supine and standing positions (Mayr *et al.*, 2005). Similar results were found in all groups, however, interestingly, the largest difference was between the young and old healthy groups in standing. Low measurements of the APP have also been found by previously discussed results (Lazennec *et al.*, 2011). The fact that such small changes were found between supine and standing positions questions the clinical relevance of measuring the APP in the two positions. This contradicts previously described studies which show large differences between the two positions.

One study measured 20 THA patients in standing, supine and sitting positions and their results were considerably more dispersed compared to other studies which measured the APP (Kochman *et al.*, 2017). This currently underlines the need for investigating the excessive spread of the measurements performed with the device to improve its clinical viability.

Overall, whilst non-invasive pelvic tilt and varus-valgus measurements have been investigated, there is still the need for a simple measurement process which can be easily translated into clinical settings. It is also apparent that these measurements need to be conducted in at least supine and standing positions for varus-valgus measurements and additionally, sitting should be measured for pelvic tilt quantification. The degree to which both measurements change between different positions has been conveyed by various authors and this thesis will take this impact into consideration through attempting to observe these differences through non-invasive measurements. Chapter 3 conveys the reliability of an ultrasound and motion capture device for lower limb characterisation in supine and standing positions. Chapter 4 introduces several approaches for measurements of pelvic tilt through ultrasound and motion capture techniques in supine, standing and sitting. And chapter 5 focusses on a preliminary pipeline for lower limb joint axes calculations but currently in supine only.

Chapter III

Reliability of an integrated ultrasound and stereophotogrammetric system

This chapter investigates the reliability of an integrated ultrasound and motion capture system. Considering what was discussed in the introduction, this chapter aims to show that ultrasound can be an efficient method for measuring several key lower limb parameters, all essential for pre-operative planning of total knee and hip replacements.

A considerable part of the material presented in this section is based on:

Greatrex, F., Montefiori, E., Grupp, T., Kozak, J., & Mazzà, C. (2017). "Reliability of an Integrated Ultrasound and Stereophotogrammetric System for Lower Limb Anatomical Characterisation**". *Applied bionics and biomechanics*.** doi: https://doi.org/10.1155/2017/4370649

3.1 Introduction

TKA is a common procedure for individuals suffering from severe knee pain, most commonly caused by osteoarthritis (Kurtz, 2007). Such a procedure requires meticulous planning in order to achieve a long surviving implant and long term patient satisfaction (Pietsch *et al.*, 2013). Preoperative planning partly consists of anteroposterior lower limb standing radiographs which image bone geometry and orientation that can be digitally annotated, aiding crucial surgical decision making such as the relative position of the femur with respect to the tibia (DiGioia *et al.*, 2006; Hunt *et al.*, 2008; Babazadeh *et al.*, 2013). Whilst this is considered the clinical gold standard, it is an invasive procedure which subjects the patient to significant radiation dosages (Hart and Wall, 2004). This method is also subject to rotation and magnification errors which significantly impact the measured lower limb angles

(Radtke *et al.*, 2010; Archibeck *et al.*, 2016; Maderbacher *et al.*, 2017). Key information gained during the pre-operative planning stage is LLA, described by the hip-knee-ankle angle, which for the purpose of this chapter, it is defined as the angle formed between the mechanical axis of the femur and mechanical axis of the tibia.

As well as LLA, several other parameters are important in pre-operative planning for TKA, such as leg length and femoral torsion. Maintaining leg length equality is important due to the potential post-operative impact it may have on an individual's gait and comfort (Lang *et al.*, 2012; Goldstein *et al.*, 2016; Chinnappa *et al.*, 2017). Therefore, measuring and compensating for the cuts made during the surgery is essential and accurate leg length measurements are important. This is also measured on standing radiographs, as leg length can be easily annotated. It is typically measured as a straight line from the centre of the femoral head to the mid-point of the medial and lateral malleoli.

Rotational alignment of the knee is also an important factor in TKA due to the positioning of the femoral component of the implant. This can be associated with several different definitions with respect to the knee orientation. For example, femoral cuts are often conducted parallel to the epicondylar axis and in turn, is out of line with the posterior condylar axis, which is often used to measure the torsion of the femur (Whiteside and Arima, 1995).

Pre-operative analysis is typically conducted in one position. For example, standing, with feet shoulder width, at a comfortable, but not extreme foot rotation position for full lower limb radiographs (Hunt *et al.*, 2006). Foot rotation, either externally or internally above 15° has shown to have an impact on alignment measurements conducted with standing radiographs (Hunt *et al.*, 2006). As this is considered the gold standard setup, other methods of analysis are typically not conducted, for example, MR images or CT scans. Research into the importance of whether other positions should be analysed, typically the supine position as it is non-weight bearing on the lower limb, is extensive. Studies have shown differences between measuring the LLA in weight bearing and non-weight bearing positions (Sabharwal and Zhao, 2008; Winter *et al.*, 2014). Therefore, as well as being non-invasive, new methods should have the flexibility to conduct measurements in at least standing or supine and if possible, other positions such as sitting.

Currently, the pre-operative planning is based on the weight-bearing approximation of the LLA, not the supine value, which potentially offsets the true value of the knee alignment when the surgery is being performed. However, it is the combination of the two positions of interest which would be most informative for the surgical planning and currently, whilst studies have addressed and quantified the differences, its implementation into a clinical setting is not known. Therefore, two questions arise which form the main themes of this chapter:

1. What alternatives currently exist to overcome the invasiveness?

2. Is it clinically relevant to consider the positional (lying/standing) change during the pre-operative planning stage?

The advantages and disadvantages of various techniques to quantify LLA that have been highlighted in Chapter 2 with emphasis on the need for a non-invasive alternative which can be used for supine and standing measurements. The aim of this chapter was to assess the reliability of OrthoPilot® in its integration with an ultrasound system for pre- and post-operative non-invasive lower limb anatomical analysis, by initially performing measurements on a phantom and then by assessing the lower limb alignments in standing and supine positions in healthy subjects.

3.2 Methods

The OrthoPilot® (Aesculap, Tuttlingen) system, shown in Figure 3.1, is a medical navigation system most commonly known for its use in computer assisted surgery in knee, hip and spine procedures. During surgery, it relies upon registration processes which aid the surgeon in identifying landmarks necessary for optimising the surgical outcome (Hauschild *et al.*, 2009). OrthoPilot consists of two infrared cameras (NDI Polaris Spectra optical tracking system) which are used to detect two, pre-calibrated rigid bodies. One is attached to the proximal tibia and the other is securely fastened to an ultrasound probe. The ultrasound device (7MHz transducer with 128 piezoelectric elements and a width of 90mm, penetration depth of 60mm, an axial resolution of 0.3mm and a lateral resolution of 0.5mm) is synchronised with the system and software is used to measure six variables of interest (varus-valgus, flexion-extension, femur and tibia lengths, and femur and tibia torsions) from the acquisition of a series of ultrasound images and their immediate annotation.

Two infrared cameras (Polaris Spectra)

Computer for ultrasound acquisition and analysis

Ultrasound device (7MHz transducer)
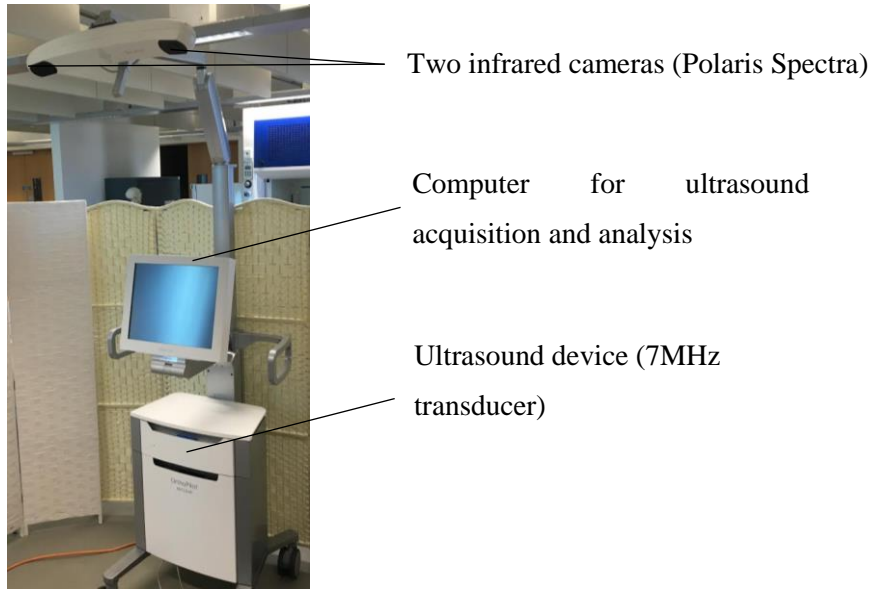
Figure 3.1 The Orthopilot device and its main components.

This section consists of two main sub-sections involving the validation of the integrated system on a phantom and then the assessment of its reliability on healthy subjects. Firstly, a summary of each variable of interest and how it is calculated is explained.

3.2.1 Investigated variables

Nine images are needed for measuring all the variables in this chapter. Figure 3.2 shows a schematic with the orientation of the probe at each landmark for each image taken. The following paragraphs will describe the image acquisitions in more detail.

(1, 2) Longitudinal and transverse femur head image

(3) Femur neck orientation

(5) Transverse posterior condyles

(4) Transverse trochlea notch

(6) Transverse posterior tibia plateau

(7) Transverse distal tibia

(8) Transverse talus

(9) Longitudinal tibia-talus interface
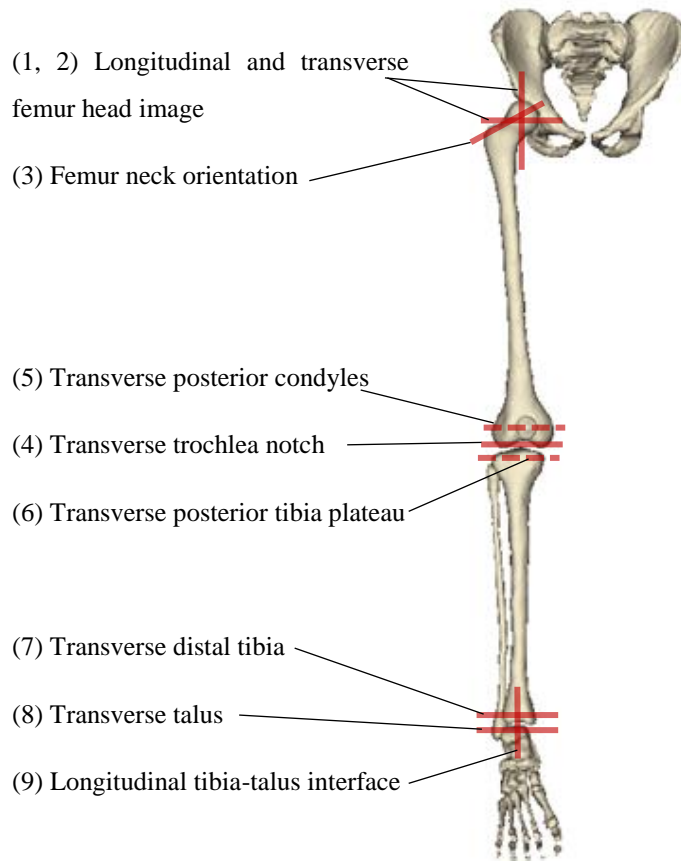
Figure 3.2. The orientation of the probe for the 9 images (imaging order in brackets) needed for full quantification of the lower limb. The dashed lines indicate images taken posteriorly on the limb.

A transverse and longitudinal image of the femoral head (Figure 3.3) determine the HJC. In the post-processing step, circles are manually fitted (automatic fittings not yet possible) to the femoral head curvature and cross-correlated to determine the HJC.
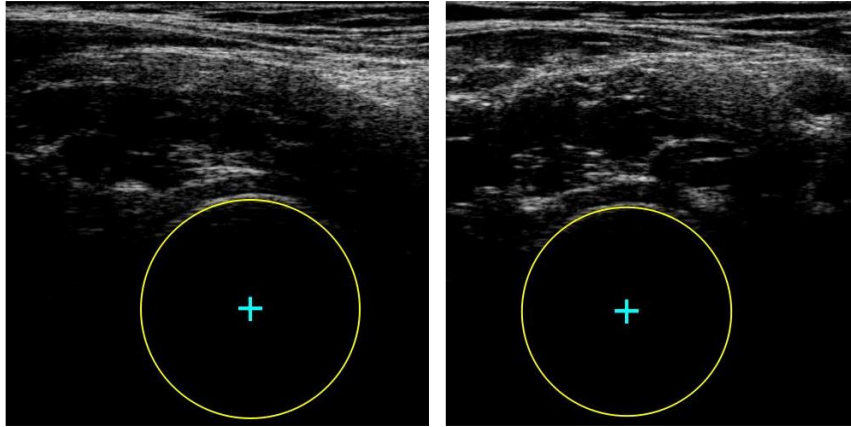
Figure 3.3. Femoral head in transverse and longitudinal probe positions with circle fittings shown.

A transverse image along the axis of the femoral neck and a transverse image of the posterior femoral condyles are needed to calculate the femur torsion (Figure 3.4). The relative difference in the angle formed by the two lines in the transverse plane, manually fitted during the post-processing, calculates the torsion.
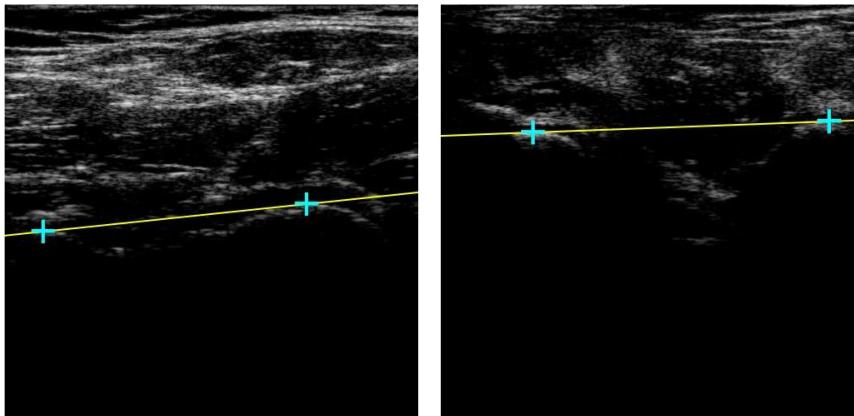
Figure 3.4. Left; femoral neck. Right; posterior femoral condyles.

One transverse, posterior image of the proximal tibia plateau, a transverse image of the anterior distal tibia and a transverse image of the talus calculates the tibia torsion (Figure 3.5). The latter two images form the ankle joint axis and the relative difference in the angle formed by the ankle joint axis and tibia plateau in the transverse plane, fitted during the post-processing, determines the torsion angle
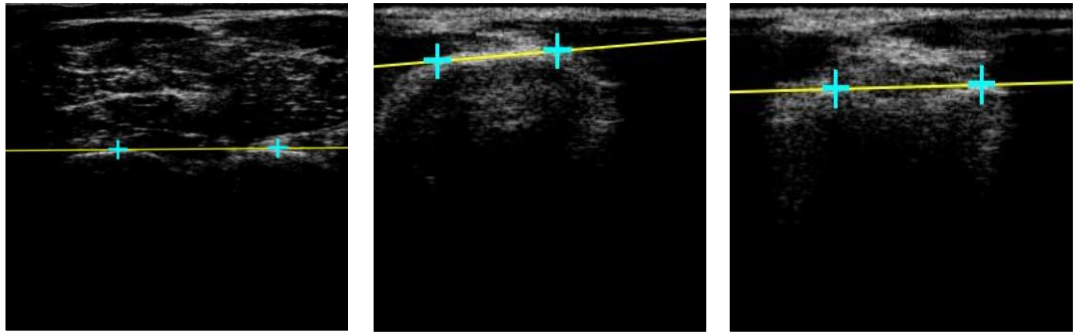
Figure 3.5. Left; posterior tibial plateau. Middle; distal tibia. Right; talus.

For the calculation of the KJC, one image is captured of the femoral trochlea notch (Figure 3.6). A single point is palpated on the image in the post-processing. The distance from the HJC to this point calculates the femur length.
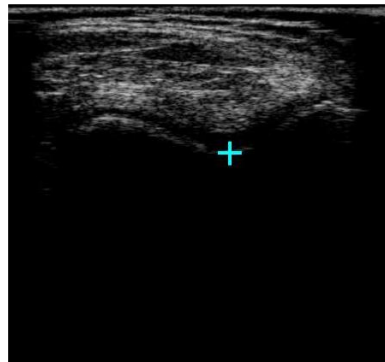
Figure 3.6. Femoral trochlea notch annotated with a single point at the deepest point.

The AJC is calculated by two images (Figure 3.7). A transverse image of the talus to calculate its mid-point and orientation. The second image is a longitudinal capture of the tibia-talus interface. A single point is then palpated to estimate the depth of the AJC which is then cross correlated with the mid-point of the talus to calculate the AJC.
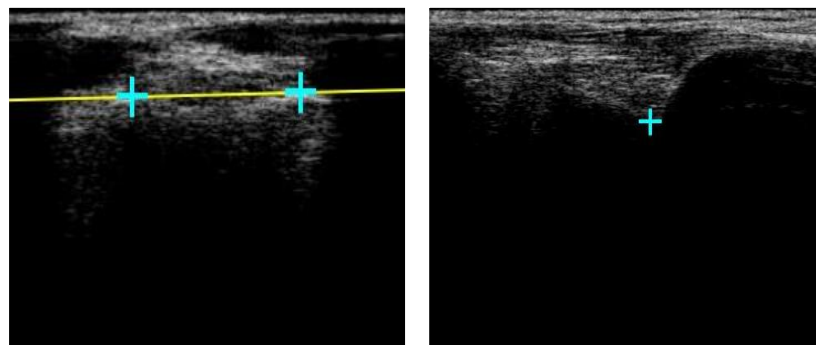
Figure 3.7. Left; talus. Right; tibia-talus interface.

The tibia length is calculated from the KJC to the AJC. Varus-valgus is calculated as the relative angle between the femur and tibia length vectors in the frontal plane. Flexion-extension is calculated as the relative angle between the femur and tibia length vectors in the sagittal plane.

For the generation of the variables in 3D space, the 2D image co-ordinates of the ultrasound image are converted into the 3D co-ordinate system of the ultrasound probe's rigid body cluster. Each pixel on the ultrasound image is displayed in the camera co-ordinate system. Once the landmark is identified on the ultrasound image during the acquisition, the pose of the two rigid bodies is captured and temporarily stored on the device. The 3D co-ordinates of all image points in the reference (tibia cluster) co-ordinate system is then calculated. This allows small movements of the subject without compromising the calculations, if the tibia cluster is not adjusted. Phantom tests

3.2.2 Phantom tests

Inter and intra-operator tests with the system took place with measurements conducted on a phantom (Aesculap, Tuttlingen). This was to test the resolution of the NDI and ultrasound system and assess the repeatability of the measurements in absence of movement or soft tissue artefacts. The phantom, as shown in Figure 3.8, consists of two hard plastic segments which are attached with a one degree of freedom joint which is adjusted to mimic the varus-valgus angle. At the proximal end of the longer (femur) segment is a sphere which mimics the femur head and an offset which mimics the femur neck. This can also be adjusted to alter the neck angle. Towards the distal end of the longer segment is a raised block with two landmarks used to mimic the condyles of the femur. At the centre is the one degree of freedom joint which also features a raised notch which is represents the femur trochlea notch. At the proximal end of the small segment (tibia), is another raised block with two landmarks to mimic the tibia plateau. And the same feature is found at the distal end for measurement of the distal tibia and ankle joint.

An inclinometer (Digi-Pas® DWL-80E, SD ±0.1°) measured the angles at which the phantom was manually set and was considered the gold standard for these tests. Four operators were asked to measure the phantom at -15°, -10°, -5°, 0°, 5°, 10° and 15° (-ve valgus, +ve varus) for a mimicked left leg. On the final repeat for each

angle, one operator evaluated the same set of images three times in the post-processing step, outputting five data sets for each angle. This quantified two elements of variability; the identification of the landmarks on the phantom and, the geometric evaluation of the ultrasound images. Three additional operators conducted one complete measurement of the phantom at the seven chosen angles.
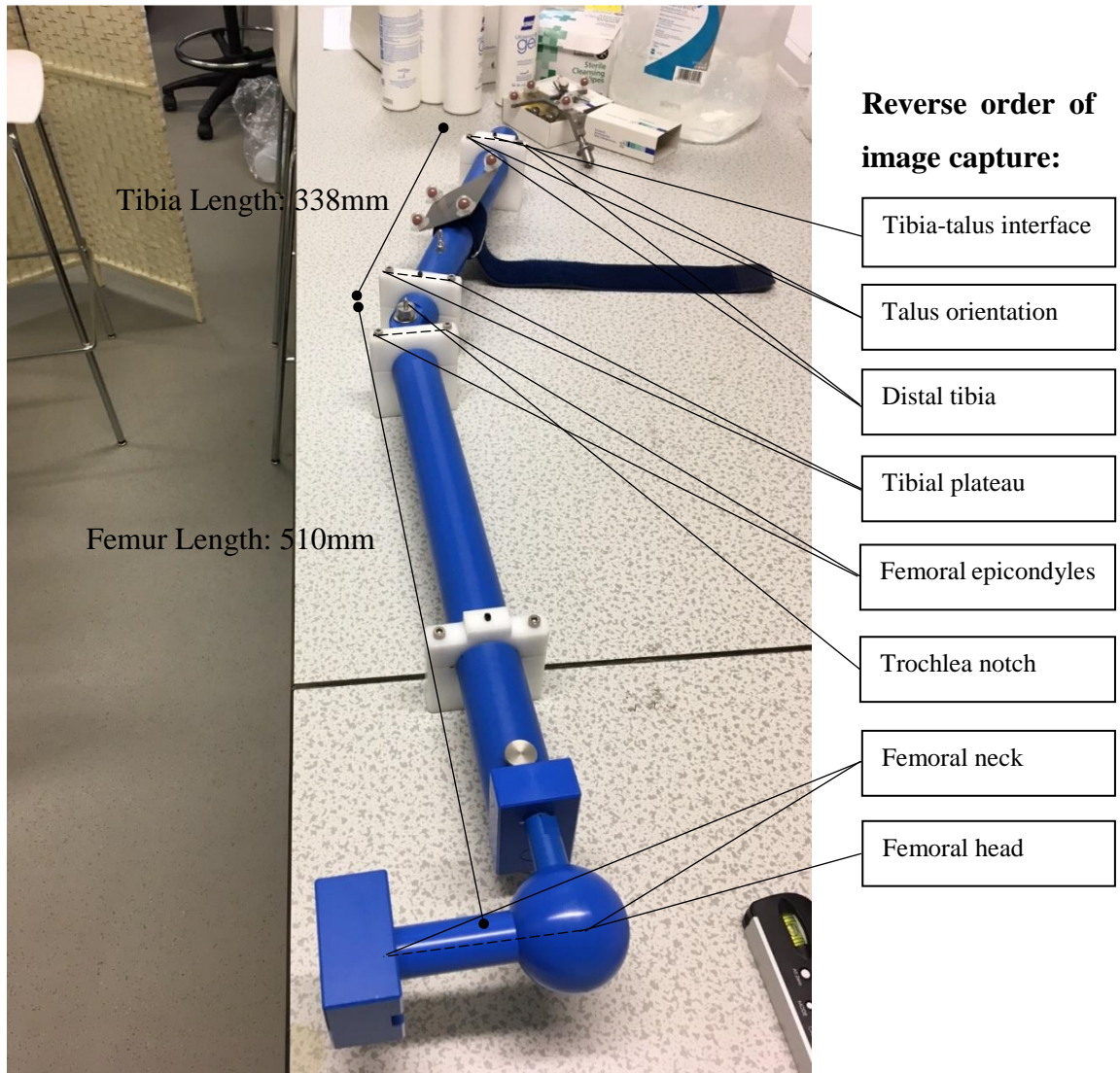
Figure 3.8. Landmarks needed for full analysis of the phantom, shown at 23° varus for a 'left' leg.

With respect to the images gained from the phantom, Figure 3.9 shows an example of an image gained from a spherical femur head, like the phantom used in the study. A very defined curvature is detected by the ultrasound.

Figure 3.9. Measurement of the phantom femur head and evident absence of soft tissue artefacts.

3.2.3 Subject tests

The University of Sheffield Ethics committee approved this study. For the inter-operator analysis, the reliability of the measurements was assessed having three operators (OP001, OP002 and OP003) repeating all the measurements three times on three young (age 27.7±1.5) healthy male subjects (S001, S002 and S003) of different body sizes (BMI: 19.9 kg/m², 29.9 kg/m² and 26.2 kg/m², respectively). The experiments were repeated on both legs in standing and supine positions. Supine examination took place across a bed and footrest, with the posterior knee exposed. Standing examination was conducted asking the subjects to keep their feet just over shoulder width apart. All image captures were performed in the same order for standing and supine analysis, as previously described, on both legs. A power analysis based on the data form the inter-operator analysis showed that to achieve a power greater than 0.8 with a SD of 1°, a sample size of at least 6 subjects was needed for the intra-operator reliability analysis. To this purpose, OP001 conducted the same experiments on six further young healthy subjects (4 males, 2 females, age 27.5 ± 4.5 y.o., and BMI 21.4 ± 4.0 kg/m^2).

3.2.4 Statistics

Statistical analysis was performed using SPSS (IBM Corp., Armonk, New York). For phantom measurements, inter and intra-operator analysis was performed by assessing the mean and standard deviation (SD) of all variables at each angle. Bland-Altman analysis was performed to interpret the level of agreement between the

true and measured value of all variables. Comparisons were initially tested for normality (Shapiro-Wilk test).

For analysis on healthy subjects, the mean and SD was calculated in both supine and standing positions. Inter-operator reliability was assessed using a two-way random effects model. The intraclass correlation coefficient (ICC) with 95% confidence intervals (CI) was computed across the three operators for all the variables in the standing and supine positions. For this analysis, subject legs were not considered individually. To complement these results, a randomised one-way analysis of variance (ANOVA) was used to determine whether there were significant differences between the mean standard deviations of the three operators (alpha level set at 0.05 for all tests).

3.3 Results

3.3.1 Phantom tests

The OrthoPilot provided highly repeatable measurements when used on a phantom (Figure 3.8) with small measured differences between the operators. The inter-operator study showed that varus-valgus measurements were slightly over estimated, with a mean error of $0.4°\pm0.3°$. Flexion-extension (set at $0°$) and the remaining variables were slightly underestimated ($-0.5°\pm0.1°$). Femur and tibia torsion values (set at $37°$ and $89°$ respectively) were consistent across all operators ($34.8°\pm0.5°$ and $87.3°\pm0.6°$ respectively). Femur and tibia measurements (actual lengths 510mm and 338mm respectively) were consistent for all operators, with a slightly higher range for the femur lengths over the 7 measurements of the phantom ($506mm\pm1.1mm$ and $337mm\pm0.7mm$ respectively).

Intra-operator varus-valgus measurements were also slightly over estimated, with a mean error $0.3°\pm0.2°$. Flexion-extension was underestimated ($-0.7°\pm0.3°$) and similarly, the remaining variables were also underestimated. Femur and tibia torsion values were $35.0°\pm0.5°$ and $86.0°\pm0.7°$ respectively. Femur and tibia lengths showed consistency and were $508mm\pm1.4mm$ and $335mm\pm0.6mm$ respectively.

For the variability in geometric evaluation, the highest error, albeit small, was shown for the segment length calculations with a standard deviation of $\pm0.6mm$ occurring in six out of the fourteen measurements (femur and tibia). In the remainder,

it was 0mm. For the varus-valgus, flexion-extension, femur and tibia torsion angles, the largest SD was ±0.2°, with an average of ±0.1°.

Figure's 3.10, 3.11 and 3.12 shows Bland-Altman plots for all variables and visually interprets the comparison in bias between inter and intra-operator results. The bias is measured from the zero line (dashed) to the mean line (solid) and indicates underestimation of the variable with respect to the true value if the mean is negative and overestimation if the mean is positive. It is shown from the Bland-Altman plots that there is little difference between the measurements when conducted by four operators or one. Underestimation of all variables with respect to the true value is shown both inter and intra-operatively.
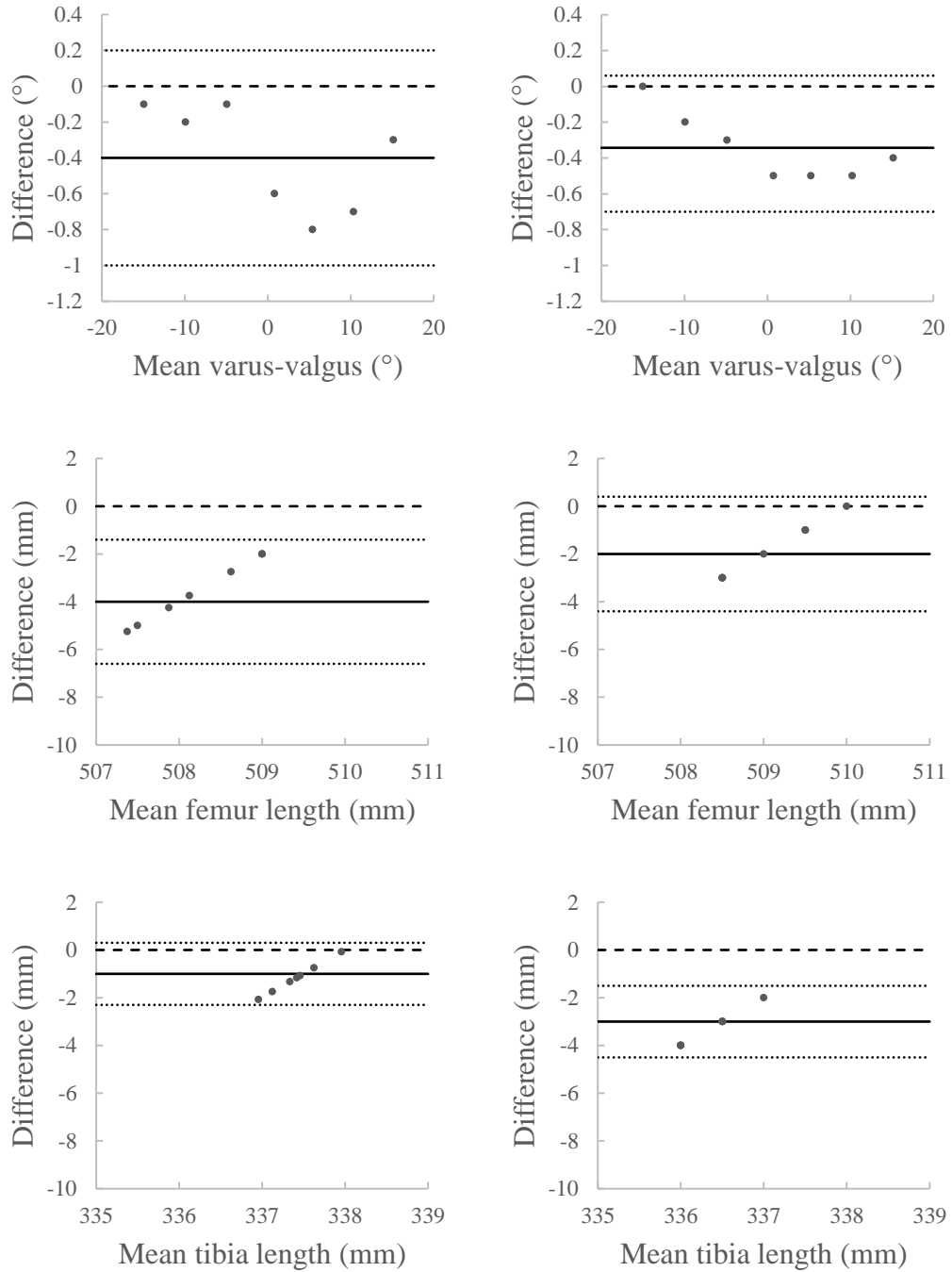
Figure 3.10. Inter (left) and intra (right) operator Bland-Altman plots of the difference between the measured and actual variable plotted against the mean of the measured and actual variable on the phantom. The mean (solid line), zero (dashed line) and limits of agreement at ±1.96SD (dotted lines) are shown.
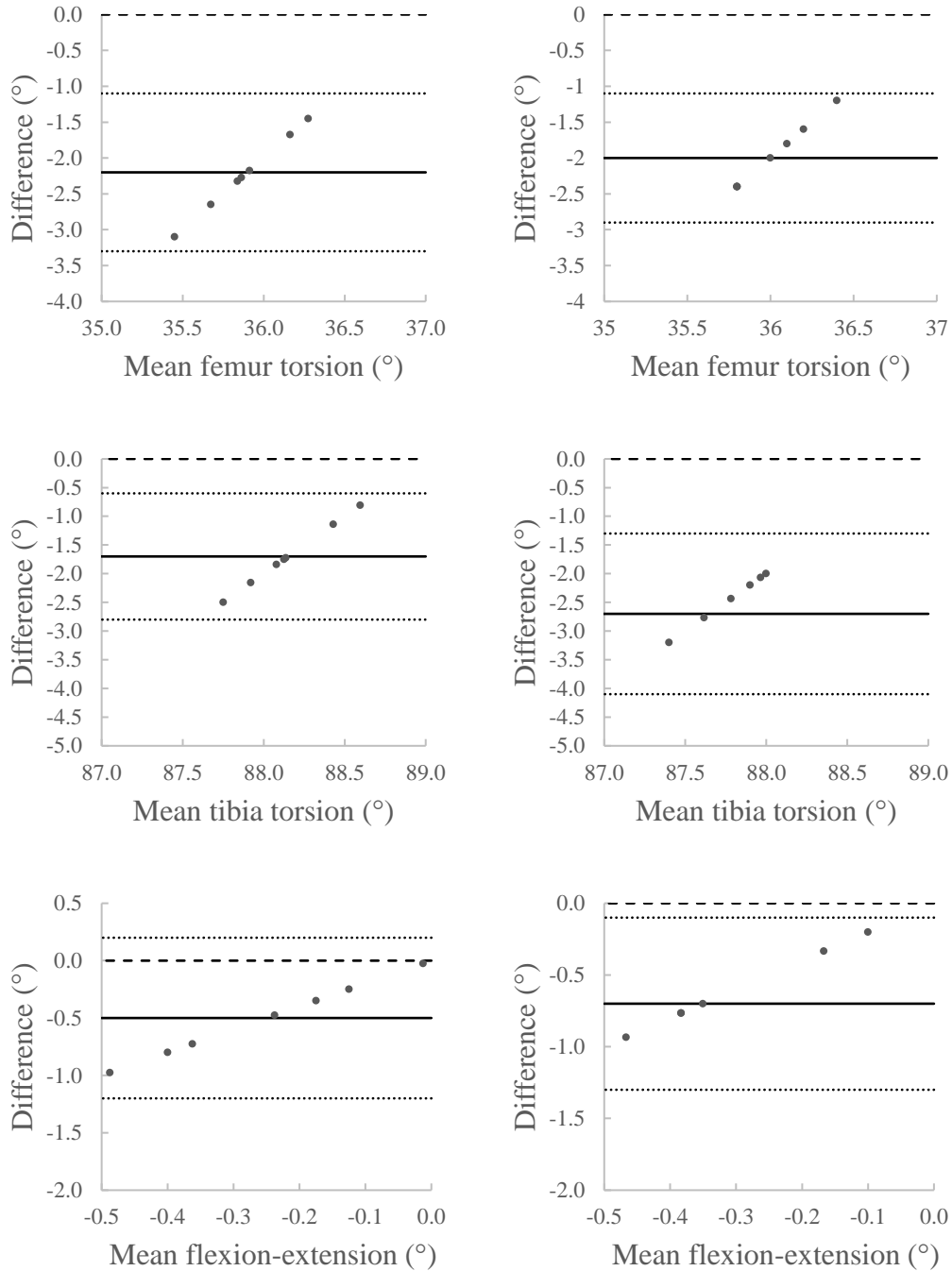
Figure 3.11. Inter (left) and intra (right) operator Bland-Altman plots of the difference between the measured and actual variable plotted against the mean of the measured and actual variable on the phantom. The mean (solid line), zero (dashed line) and limits of agreement at ±1.96SD (dotted lines) are shown.
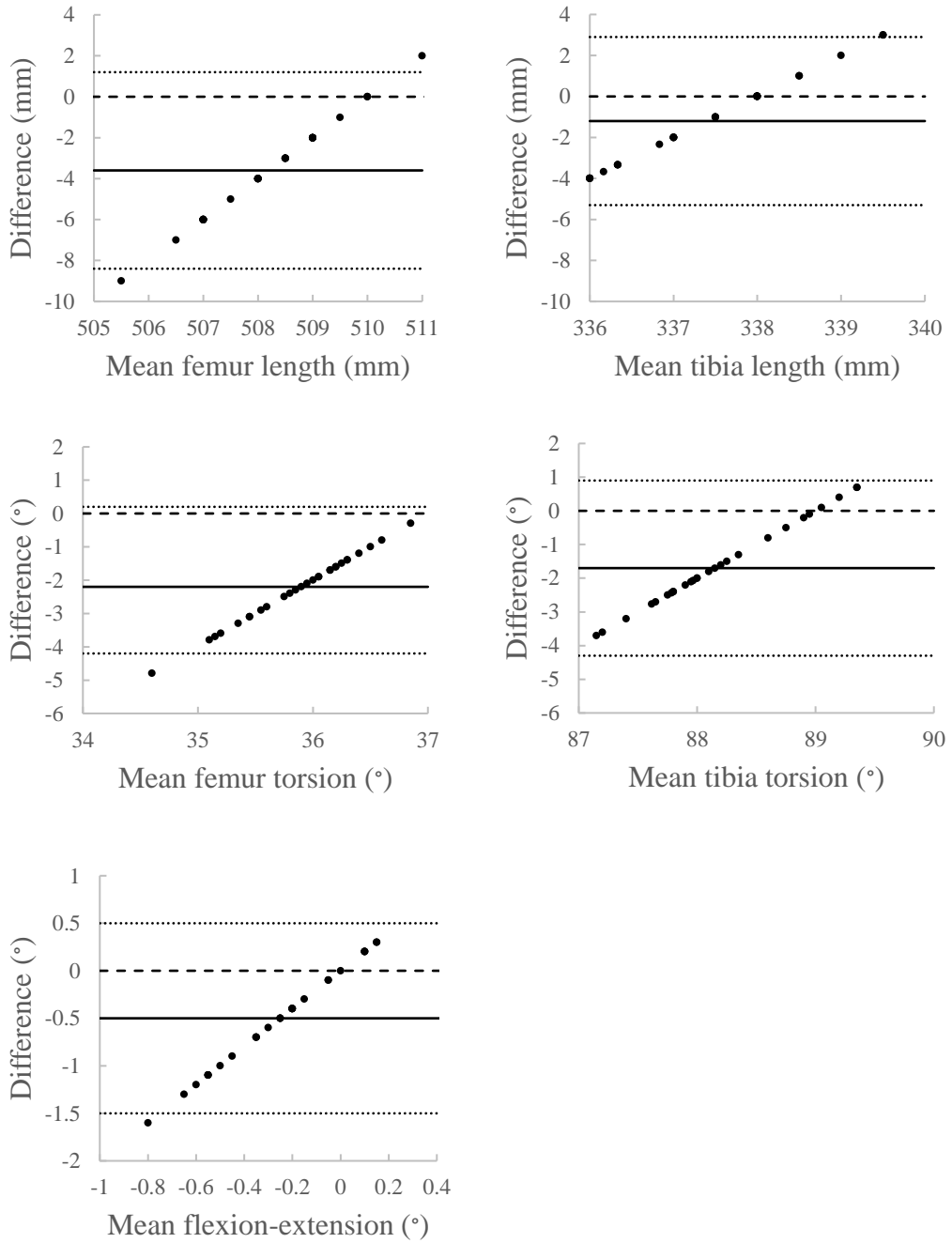
Figure 3.12. Inter operator Bland-Altman plots of the difference between the measured and actual variable plotted against the mean of the measured and actual variable on the phantom. The mean (solid line), zero (dashed line) and limits of agreement at ±1.96SD (dotted lines) are shown.

3.3.2 Subject tests

For all measures of length, in standing and supine, ICC values were > 0.99. For varus-valgus and flexion-extension, in standing and supine, ICC values were > 0.93. For measures of the torsions, except supine femur torsion measurements, the ICC drops to lower than 0.70 for the tibia torsion. For the ANOVA, all tests showed no significance between the standard deviations of each operator for all variables in supine and standing (p > 0.17). For the intra-operator results, varus-valgus and flexion-extension measurements was an average of 1° of SD across nine subjects (18 limbs) for OP001. The same results were observed also for OP002 and OP003, when looking at corresponding data from three subjects (6 limbs). The length measurements were also very consistent with few SD exceeding 5mm. For both femur and tibia torsions as measured by OP001 across nine subjects, the average SD was less than 4°. Many measurements, however, exceeded 5° of SD for OP002 and OP003.

Table 3.1. Individual and overall results for the three operators across *n* subjects (2*n* limbs) for all 6 variables in standing and supine positions.

Variable	Position	OP001 (*n*=9)	OP002 (*n*=3)	OP003 (*n*=3)	Average[¥] (*n*=3)	ICC (95% CI) [§] (*n*=3)	P-value[ɛ]
Varus (+ve)/	*Standing*	0.2 ± 3.2	0.1 ± 2.6	0.3 ± 3.2	0.2 ± 2.8	0.97 (0.86 – 0.99)	0.61
Valgus (-ve)(°)	*Supine*	1.1 ± 2.7	0.4 ± 1.8	0.0 ± 1.6	0.3 ± 1.8	0.93 (0.71 – 0.99)	0.63
Flexion (+ve)/	*Standing*	0.7 ± 6.2	4.2 ± 8.4	3.9 ± 8.5	3.6 ± 8.1	0.99 (0.97 – 0.99)	0.39
Extension (-ve)(°)	*Supine*	1.3 ± 3.4	1.8 ± 4.5	2.0 ± 4.0	1.7 ± 4.2	0.99 (0.97 – 0.99)	0.80
Femur Length	*Standing*	435 ± 31	457 ± 37	457 ± 35	456 ± 35	0.99 (0.99 – 1.00)	0.66
(mm)	*Supine*	439 ± 29	454 ± 34	456 ± 33	455 ± 33	0.99 (0.99 – 1.00)	0.49
Tibia Length	*Standing*	410 ± 27	426 ± 22	429 ± 23	428 ± 22	0.99 (0.98 – 0.99)	0.55
(mm)	*Supine*	406 ± 25	427 ± 21	424 ± 22	425 ± 21	0.99 (0.98 – 0.99)	0.17
Femur Torsion	*Standing*	32.7 ± 10.2	27.2 ± 16.0	36.5 ± 10.3	31.7 ± 12.2	0.68 (-0.09 – 0.95)	0.43
(°)	*Supine*	28.6 ± 9.6	25.0 ± 17.9	26.2 ± 12.0	26.2 ± 13.3	0.95 (0.78 – 0.99)	0.74
Tibia Torsion	*Standing*	30.9 ± 9.4	28.0 ± 6.9	28.2 ± 12.5	28.5 ± 10.4	0.69 (-0.61 – 0.96)	0.17
(°)	*Supine*	32.1 ± 8.5	32.4 ± 7.8	36.6 ± 8.6	33.5 ± 8.9	0.65 (-0.35 – 0.95)	0.78

Mean and SD of values measured by each operator over *n* subjects. [¥]Mean and SD across all operators for the same three subjects. [§]Inter-rater correlation coefficient (ICC) and 95% confidence intervals (CI). [ɛ]One-way ANOVA values.

Table 3.2. Differences between the measurements of each operator and the means for all the operators in the supine and standing position for the three subjects.

Supine

	S001	OP diff. from mean			S002	OP diff. from mean			S003	OP diff. from mean		
	OP Mean	OP 001	OP 002	OP 003	**OP Mean**	OP 001	OP 002	OP 003	**OP Mean**	OP 001	OP 002	OP 003
Varus/ Valgus (°)	**1.9±0.4**	-0.4	-0.1	0.4	**-1.6± 0.2**	0.1	0.1	-0.3	**0.5±0.6**	-0.4	-0.4	0.7
Flexion/ Extension (°)	**4.9±0.4**	0.4	-0.1	-0.3	**-3.7± 0.6**	0.4	0.3	-0.6	**4.1±0.2**	-0.1	-0.1	0.3
Femur Length (mm)	**501±0**	0	0	0	**430±1**	0	-1	0	**435±3**	-1	3	-2
Tibia Length (mm)	**454±1**	0	-1	1	**412±1**	1	0	0	**409±4**	0	-4	4
Femur Torsion (°)	**24.1± 2.5**	-8.0	-12.6	-12.0	**32.6± 3.1**	-1.3	-2.2	3.6	**11.1± 6.7**	-5.3	7.6	-2.2
Tibia Torsion (°)	**37.5± 4.8**	-5.3	4.1	1.2	**28.2± 2.5**	1.6	1.4	-2.9	**35.0± 8.5**	9.3	-2.0	-7.3

Standing

	S001	OP diff. from mean			S002	OP diff. from mean			S003	OP diff. from mean		
	OP Mean	OP 001	OP 002	OP 003	**OP Mean**	OP 002	OP 003	OP 001	**OP Mean**	OP 001	OP 002	OP 003
Varus/ Valgus (°)	**3.5±0.6**	0.4	0.4	-0.7	**-2.5± 0.3**	0.1	-0.4	0.2	**-0.4± 0.5**	-0.6	0.3	0.2
Flexion/ Extension (°)	**12.5±1.7**	1.9	-1.4	-0.5	**-5.8± 0.3**	0.1	-0.3	0.2	**4.2±0.6**	0.6	0.0	-0.5
Femur Length (mm)	**504±4**	3	-4	0	**430±2**	2	-1	0	**434±4**	3	1	-4
Tibia Length (mm)	**458±2**	0	2	-2	**412±2**	-2	2	-1	**414±2**	-1	2	0
Femur Torsion (°)	**40.1± 4.0**	3.9	0.1	-4.0	**32.5± 10.7**	-3.4	12.0	-8.5	**22.5± 1.8**	0.6	1.4	-2.1
Tibia Torsion (°)	**37.0± 5.4**	-6.1	4.2	2.0	**25.0± 4.3**	4.4	-0.1	-4.2	**23.7± 2.8**	-0.8	-2.3	3.1

The following bar charts in Figure's 3.13 and 3.14 summarise the inter-operator results for the right and left knee flexion-extension, femur and tibia torsion and femur and tibia lengths.
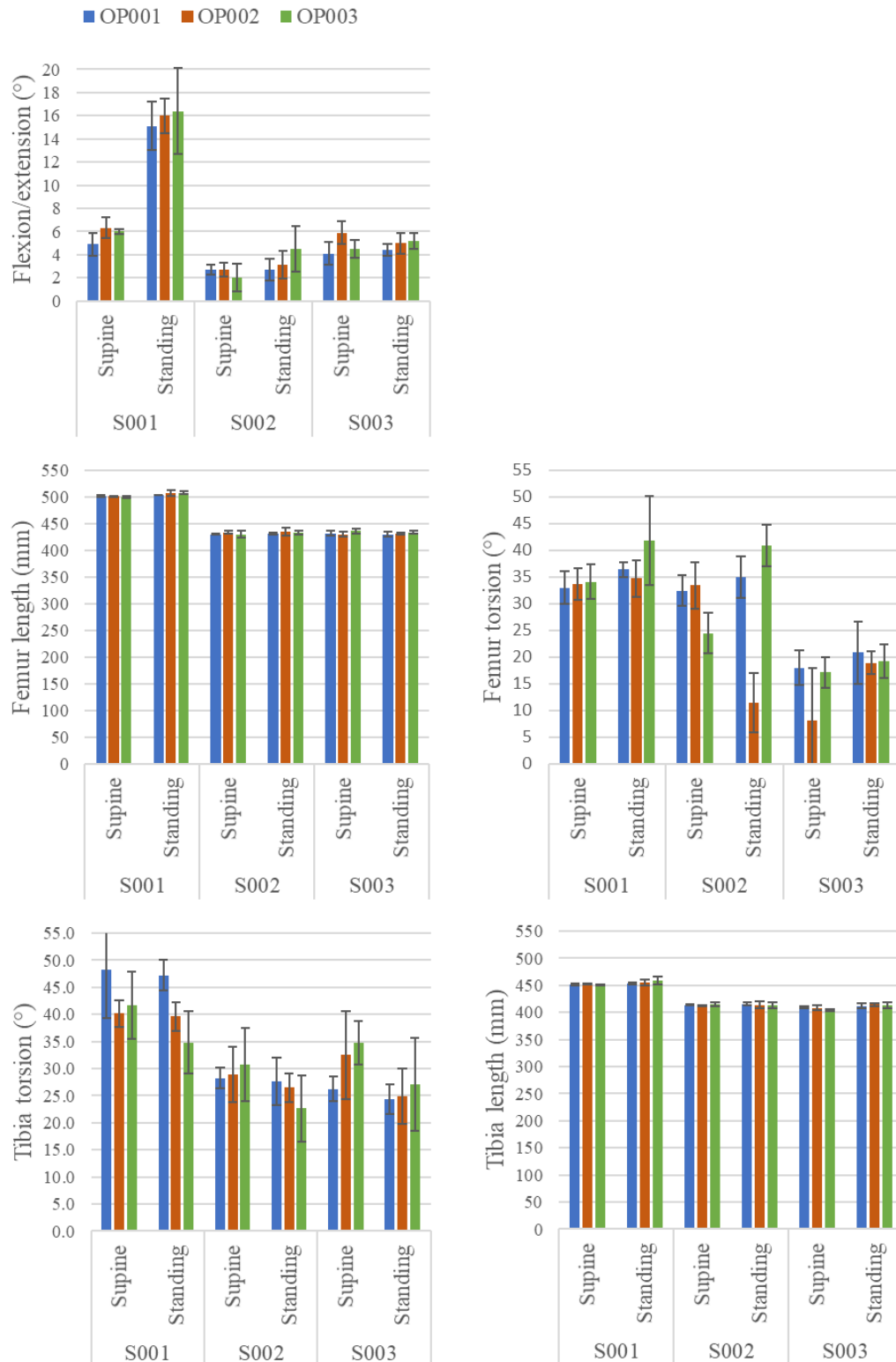
Figure 3.13. Right leg variables in supine and standing positions for the three operators and three subjects.
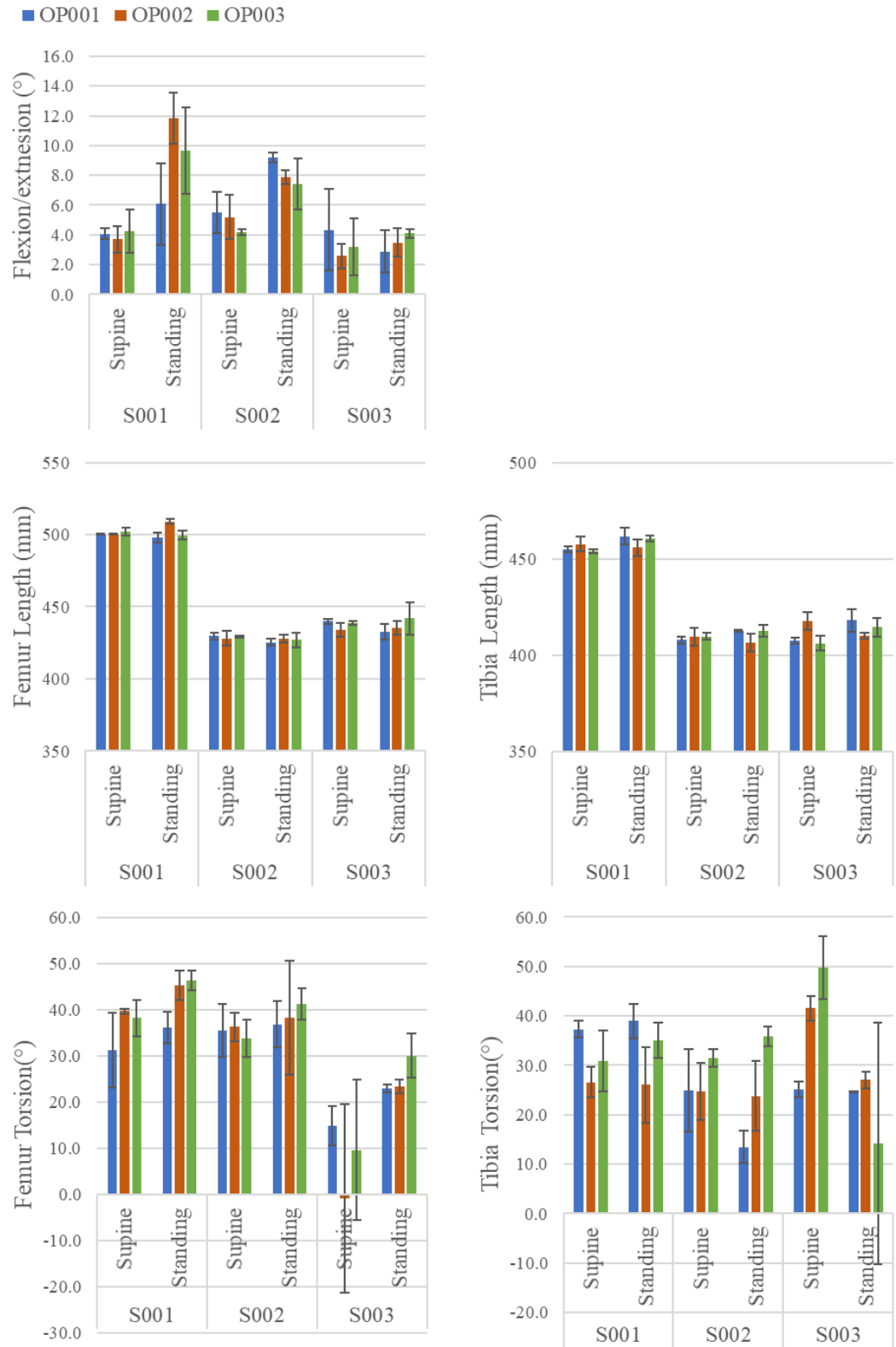
Figure 3.14. Left leg variables in supine and standing positions for the three operators and three subjects.

49

The right and left, supine and standing varus-valgus results are visualised below in Figure's 3.15 and 3.16 and show the difference in measurements between the operators for the three subjects.
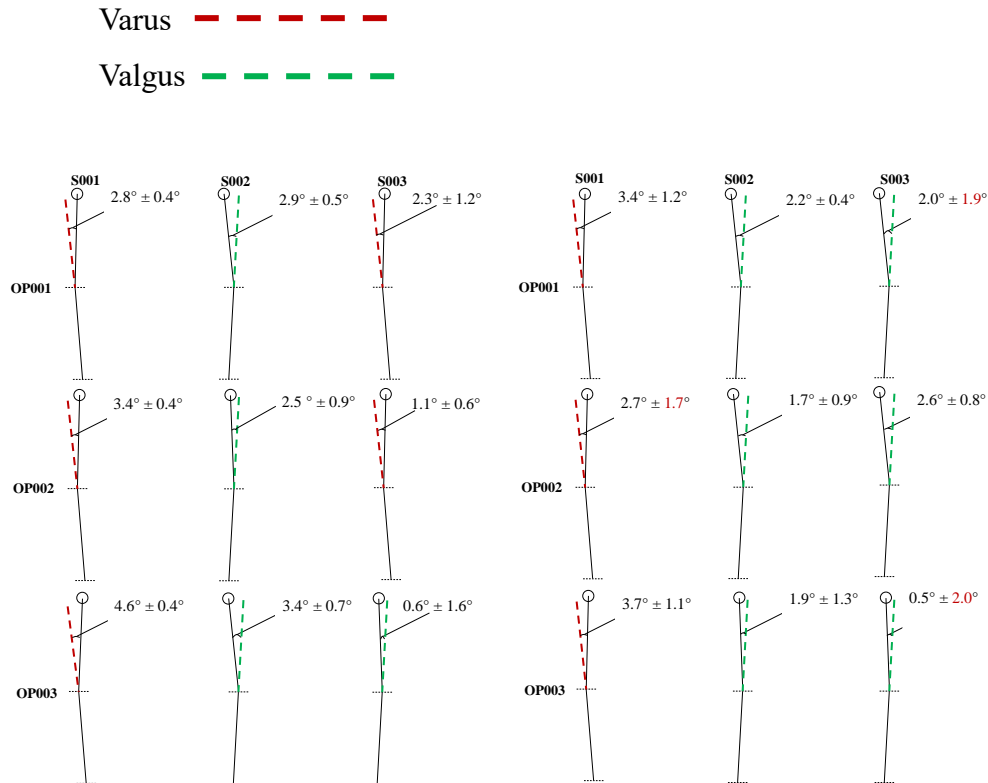
Figure 3.15. Standing varus-valgus results for each operator and subject for the left and right leg respectively. The red shows SD that is greater than 1.5°
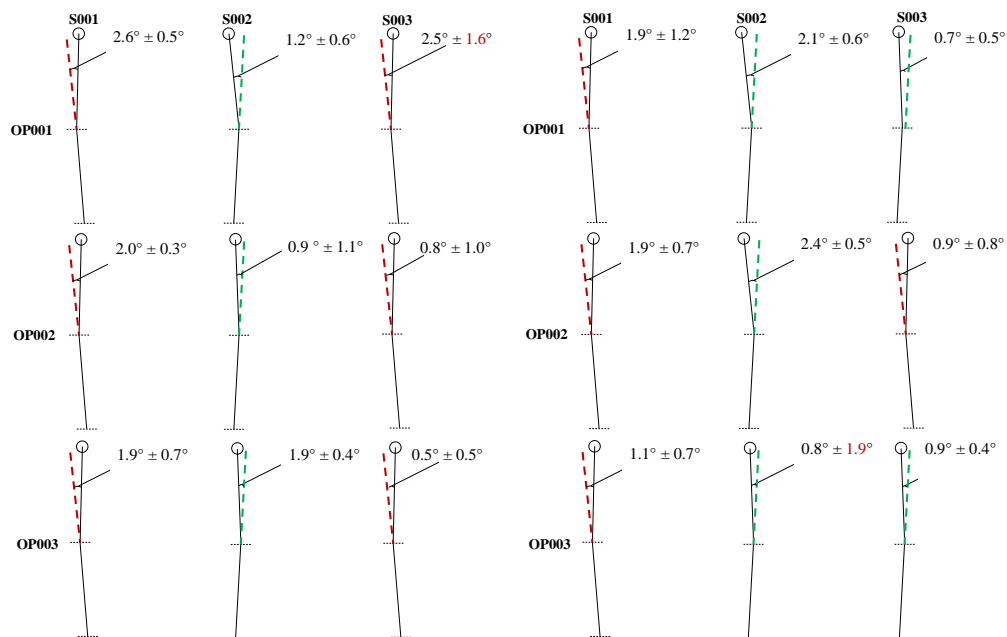
Figure 3.16. Supine varus-valgus results for each operator and subject for the left and right leg respectively. The red shows SD that is greater than 1.5°

50

3.4 Discussion

Pre-operative analysis of key lower extremity variables such as varus-valgus and femur torsion for TKA is vitally important for surgical planning (Gbejuade *et al.*, 2014; Nakano *et al.*, 2016). This part of the thesis aimed to assess the reliability and repeatability of an integrated ultrasound and motion capture system which could potentially be used as an alternative to invasive methods, such as full-length X-rays. In addition, its suitability to measure the anatomical variables of interest for surgical planning in standing (weight bearing) and supine (surgery like) positions was shown.

Reported results showed that the OrthoPilot can detect both joint angles and segment lengths when used on a phantom to within a reliable resolution. The results are comparable with length measurements performed by an author who compared four different measurement techniques (standard radiographs, CT scans, EOS-slow and EOS-fast) for length measurements with respect to a phantom of known dimensions (Escott *et al.*, 2013). EOS-slow and EOS-fast are two different acquisition procedures of approximately 8 seconds and 4 seconds respectively. EOS-slow measurements performed most accurately with an average 0.5% underestimation of the phantom length. In this study, the smallest and largest underestimation from the true value for the tibia and femur phantom measurements was 0.3% and 0.8% of their length, respectively. A key limitation of this part of the study, aiming at testing the resolution of the measurement devices, was that actual accuracy of the system was not quantified either on more realistic phantoms (e.g. adding silicon pads with plastic bones in water) or even better using alternative imaging systems (e.g. CT scans) on the healthy subjects. The main advantage of the phantom analysis, however, was the quantification of known angles and lengths regardless of the operator. This gave a great deal of confidence that the system was accurately measuring known parameters even if it was not comparable to subject measurements with respect to the anatomical features. For example, the images, overall, were not comparable to the subject measurements. The femur head was the only landmark which was comparable due to the curvature that could be easily detected. The other landmarks were distortions in the ultrasound image which were easily identifiable for the post-processing step but did not represent realistic human anatomy.

For lower limb segment length measurements on subject cohorts, few studies have been conducted using ultrasound (Terjesen *et al.*, 1991; Junk *et al.*, 1992). Most studies use conventional means such as radiographs or MRI (Leitzes *et al.*, 2005; Hinterwimmer *et al.*, 2008; Escott *et al.*, 2013; Lazennec *et al.*, 2016). Terjesen et al. however, showed that 95% of the ultrasound leg length measurements on 45 subjects were within 7mm of the radiographic measurements (Terjesen *et al.*, 1991). Their follow up study (Junk *et al.*, 1992) further emphasised the potential for ultrasound as a clinical tool with a study on 100 healthy subjects and showed that 95% of the differences for the length measurements between the two operators was less than 5mm. Similar repeatability values were found in this study, the average SD for both femur and tibia lengths over three repeats for all operators on both limbs was 3mm±2mm (with highest value being 11mm). Interestingly, the intra-operator results showed more spread for the tibia length measurements than across the four operators. The opposite was found for the femur measurements. The importance of leg length in TKA and THA is paramount, as bone is removed and replaced with an implant, careful consideration of the size and positioning of the implant is necessary in order for limb length to be sustained at the patients' pre-operative length (Pierrepont *et al.*, 2017).

For varus-valgus measurements on subject cohorts, standing radiographs, CT scans or MRI's are the most common choice for analysis, depending on availability. On patients, studies have taken place to determine whether such methods correlate with measurements taken intra-operatively, whereby surgeons have attempted to measure varus-valgus with a navigation system before proceeding with the surgery (Yaffe *et al.,* 2008). This study showed a large discrepancy between pre-operative standing radiographs and pre-operative navigation measurements (4.7°±2.9° difference) (Yaffe *et al.,* 2008). It was noted however, that the difference may have resulted from weight bearing against non-weight bearing analysis and its influence on lower limb kinematics which has shown to be significant (Brouwer *et al.*, 2003; Hunt *et al.*, 2008). Bellemans *et al.* (2012) investigated the HKA angle with full weight bearing radiographs on 250 males and 250 females, a considerably larger cohort than this study. Their varus-valgus measurements performed on young, healthy subjects suggested a certain degree of varus deformation is more likely than neutral alignment (average of 1.9° in males and 0.8° in females) (Bellemans *et al.*, 2012), which is consistent with the values found in this study (average of 0.2° and 0.3° in standing and

supine, respectively). For the inter-operator standing results compared to the supine, as shown in Figures 3.15 and 3.16, it was found that 4/18 results had a SD of greater than 1.5° compared to 2/18 for the supine results. This emphasises the current difficulties in performing the measurements in standing compared to supine. For example, the measurement of the femur trochlea notch in the standing position was the most problematic point and is a single measurement which influences both the femur length and the varus-valgus values. This is due to the difficulty in imaging the trochlea notch anteriorly, capturing an imaging beneath the knee cap. This can be avoided by imaging the posterior of the knee only. Peak error was less than 2.0° in all cases and with a typical mechanical alignment threshold of $0 \pm 3°$ for TKA surgery, this is an acceptable level of error.

Although the knee flexion-extension angle may not immediately seem like an important parameter in the context of surgical planning, it has actually been shown that it affects the varus-valgus when analysed on cadavers in the frontal plane (Hauschild *et al.*, 2009). This might have indeed affected some of the results of this study, where a larger knee flexion of ≈15º was observed, on average, by all operators for subject S001 in the standing position, as shown in Figure 3.13 and 3.14. Whilst this angle was surprisingly large, it was double checked with a goniometer, which provided consistent findings. Hauschild *et al.* (2009) showed that with increasing amounts of flexion, the reliability of the measurements decreases significantly compared to extended measurements. Therefore, controlling for the flexion-extension when measuring the varus-valgus is important. Further studies should investigate this observation more thoroughly in a patient cohort. The high variability shown for subject S001 in Figure 3.13 and 3.14 for both legs, conveys the need for standardising the standing position to avoid measuring the subjects in different poses. The measurement process that was implemented meant that the subject was measured in supine and standing in a random order. As there were three repeats for each operator, this meant a lot of changing between standing and supine which may have led to different standing poses between repeats and therefore the high variability. As a result, the peak error was 5°. Lower variability was found in the supine due to its inherently easy pose to adopt for the subject and analyse as an operator.

For torsion measurements, Kulig *et al*. (2010) validated an ultrasound graphic tilting method based on the use of an inclinometer attached to an ultrasound probe.

This technique highly correlates with MRI data for measurements of the femur torsion (Kulig *et al.*, 2010). Another author used a similar technique and found much higher inter-operator reliability for the tibia torsion measurements (ICC > 0.84) than those found in this study (Hudson *et al.*, 2006). Both studies showed average tibia torsions which were comparable to our findings, but their femur torsion measurements are considerably lower. The CI values in this study, conversely, portrayed a lack of inter-operator reliability. The negative CI values suggest an intra-operator variability which exceeds the inter-operator variability. Peak errors for the torsion measurements were also quite significant, with the highest at 20°. This is much higher than what would be considered clinically useful. A reason for this inconsistency, especially for the tibia torsion, is likely due to the measurements needed for its calculation. Three images are needed, the tibia plateau and two for the ankle joint axis. This dependence on three images, compared to two for the femur torsion potentially increased the variability between the operators. Further studies are needed to fully elucidate this aspect. Table 3.2 shows large differences between each operator compared to their overall mean for subject 2 in the standing position for the femur torsion. Differences were found for each subject, but this was the largest instance and up to 12° of variability between operators. The most likely cause of this was the high BMI of the subject (29.9kgm^{-2}) which made the standing measurements challenging. Further measurements on a larger cohort would be needed to verify this.

The above results are likely linked to one of the main limitations encountered in this study, which was the difficulty in the ultrasound image capturing associated with the application of pressure along the entire surface of the probe, especially in the standing position. This means that capturing the desired anatomy can be more challenging compared to supine measurements as you cannot rest the probe on the subject which assists image capture. For subjects which have low BMI (S001) this is not much of a concern. However, as tissue artefacts increase, optimal ultrasound image generation might become a problem, possibly causing restrictions in the systems capability for high BMI individuals, as also suggested by the error for the femur torsion measurements in S002. Imaging the femur neck orientation for example, required an equal pressure distribution over a relatively large probe face (90mm length). This point ties in with operator experience and possible varying interpretations of the ultrasound images (Smith and Finnoff, 2009). OP003 had been properly trained

and went through various sessions to familiarise themselves with the procedures, but their knowledge and experience with ultrasound was lower than the other operators Also, all the images were captured without any adjustment of the ultrasound parameters between trials or operators. Altering the ultrasound settings and using a smaller probe in the standing position might have led to even better results. It must also be emphasised however, that there was difficulty in measuring some of the points in the standing position and this was potentially pushing the system beyond what it was originally designed for.

The subject cohort size for this study was small, which of course does not allow for generalisation about the changes observed between the supine and standing positions. The subject cohort was also healthy, which meant conditions for measurements with ultrasound are easier than that of a patient population. For example, a cohort of patients requiring total knee arthroplasty will potentially suffer from osteoarthritis which may impact the quality of the images due to bone deterioration. A patient cohort may also be overweight or obese meaning the use of ultrasound becomes considerably more challenging. This could be overcome through allowed changes in the ultrasound parameters which the OrthoPilot system did not permit. Further investigation into this will be needed. Conclusions are therefore limited to the reliability and feasibility of the proposed approach. According to the reported results, especially for length, varus-valgus and flexion-extension measurements, these can be deemed satisfactory.

For certain measurements, improvements could be adopted. For example, the knee joint centre was measured from a single point and anteriorly (problematic in the standing position). This could be improved through analysing the femoral condyles and fitting a cylinder to measure the knee joint rotation axis and corresponding centre. This will be discussed in more detail in Chapter 5. What may be more beneficial in general, is a portable ultrasound system which can be used in a more flexible manner, and not reliant on a device used mainly for aiding orthopaedic surgeries, which is the main use of the OrthoPilot. Such a system is currently not established for LLA measurements but is in development for measurements of pelvic tilt with respect to the anterior pelvic plane. This measurement aids decision making in total hip replacement surgeries and is currently measured through invasive methods. This topic will be discussed in detail in Chapter 4.

Chapter IV

Non-invasive measurements of pelvic tilt

This chapter investigates the reliability of several experimental methods for the measurement of pelvic tilt. These were performed in parts by an ultrasound smart system, and an infrared stereophotogrammetric motion capture system. This chapter aims to show that several methods for measuring pelvic tilt, in different positions, can be fast and informative, which could potentially enhance the pre-operative planning stage of hip replacement surgeries.

4.1 Introduction

Pelvic tilt indicates how inclined the acetabulum is with respect to the femoral head and is therefore considered a crucial parameter in THA. Accurately assessing this angle is therefore an essential part of pre-operative planning in THA.

A commonly used method in pre-operative planning of pelvic tilt is the use of sagittal plane radiographs (DiGioia *et al.*, 2006; Philippot *et al.*, 2009; Taki *et al.*, 2012; Kanawade *et al.,* 2014; Tamura *et al.,* 2014; Tamura *et al.*, 2015, 2017; Ranawat *et al.*, 2016; Uemura *et al.*, 2017). This is the current clinical gold standard due to its availability and simplicity of analysis in terms of annotating the radiographs, however, its invasiveness associated to the use of X-Rays is a substantial draw back.

When PT is measured during a surgery, accurate measurements are essential for PT to act as a reference for the acetabular inclination. Intra-operative CT-based navigation has been shown to be equal in accuracy when compared to freehand surgery (Martin and von Strempel, 2006). Irrespective of surgical experience, CT-based navigation has shown to be accurate (Iwana *et al.*, 2013). Other methods have included the use of a pointer, or ultrasound (Hasart *et al.*, 2008). These techniques measure a set of landmarks, typically different from the radiographic measurements, to define a plane which helps orientate the implant as accurately as possible. This parameter is

called the Lewinnek plane, or the anterior pelvic plane (APP), and was previously described in Chapter 2 in Figure 2.4.

In their original paper, Lewinnek et al. (1978) suggested to use a zero PT angle, i.e. to make the APP coincide with the coronal plane, when referencing the implant position. However, using the information from standing radiographs to reference an implant insertion while lying might be inaccurate (Lazennec *et al.*, 2011). Real-time measurements of the APP during surgery are essential for ideal cup orientation (Philippot *et al.*, 2009).

Whilst many alternative methods have been shown and compared here for PT and APP measurements, very few have been adopted for pre-operative planning alternatives, with lower limb X-rays and CT scans still preferred as the THA planning methods. Ultrasound, as it has already been introduced into intra-operative scenarios, seems like the most promising alternative theoretically (Parratte *et al.*, 2008). Motion capture has been used in clinical settings for the past few decades. Gait analysis has become a collective part of clinical checks and a tool used in aiding the understanding of diseases associated with musculoskeletal defects (Wren *et al.*, 2011). Therefore, it is also a useful instrument in which other measurements for pre-operative purposes could be made. Accordingly, the following sections include a series of experimental methods which non-invasively measure the APP and PT in healthy subjects with the use of ultrasound and motion capture systems. It is broken down into two core sections:

1. The ultrasound experiments consisted of assessing the reliability of an integrated motion capture and ultrasound system (*smart system*; including an ultrasound device, smart phone and surface tablet) which allow real time measurements of the APP.
2. The motion capture experiments consisted of several different pilot measurement techniques to quantify the APP and PT through palpable, external landmarks.

4.2 Methods

4.2.1 Integrated *smart system*

The *smart system* consists of one surface tablet, one smart phone and an ultrasound device (Telemed – Echo Blaster 128) with an attached 9-MHz linear probe. The surface tablet shows the real time ultrasound image and interface for the processing of the measurements. The smart phone uses its light to detect the pose of two, pre-calibrated rigid bodies, with four reflective markers on each. One rigid body is attached to the ultrasound probe, and the other is used as a reference and is fixed in the proximity of the subject (Figure 4.1). Measurements were performed with an ultrasound probe and ultrasound gel for optimal image generation. The positions of the rigid bodies were recorded when the landmarks were located. Once the three positions (ASIS and PS ultrasound images shown in Figure 4.2) were measured, the system returned to the first ultrasound image for evaluation. Each identified landmark was marked on the image by one operator (same operator as the physical measurements) for all measurements, and the pelvic tilt and sagittal balance was calculated and shown in real time. The process and calculations for measuring the pelvic tilt with the smart system have been previously described (Martin, 2016).
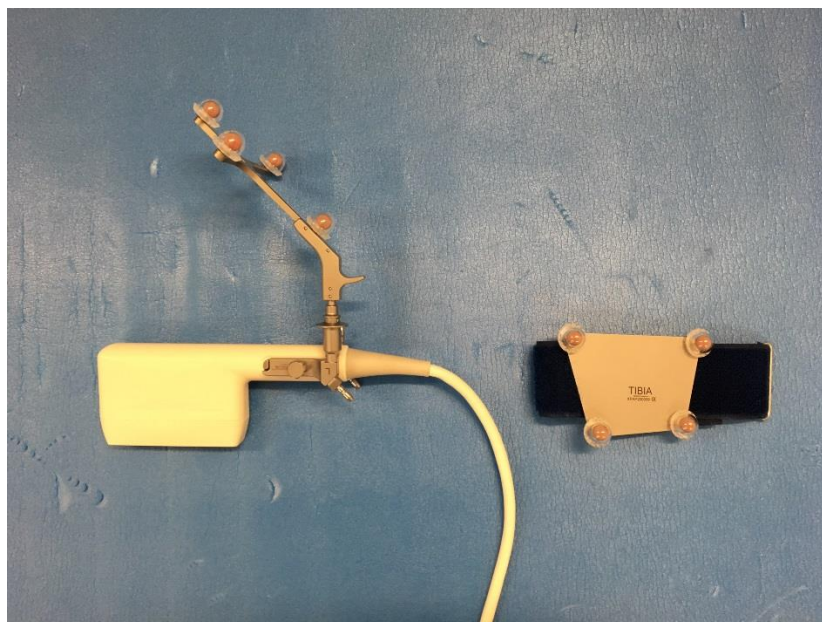
Figure 4.1. On the left is the ultrasound probe and attached is a cluster of markers used to track the probe position and transform the ultrasound co-ordinates into the global reference frame. On the right is the reference cluster.
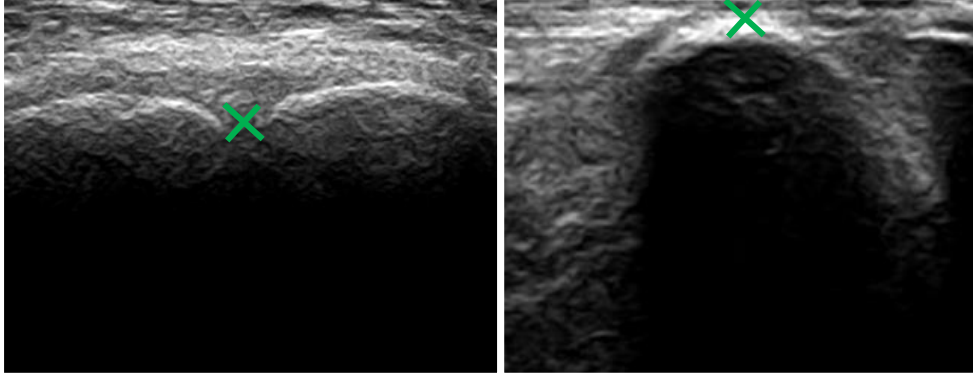
Figure 4.2. Pubic symphysis (left) and anterior superior iliac spine (right). The green crosses mark the positions of interest for the PT calculations.

In brief, to calculate PT, the APP is calculated first. This is defined with two vectors ($\vec{a}$ and $\vec{b}$) calculated from measuring the location of the RASIS, LASIS and PS bony landmarks:

$$\vec{a} = \overrightarrow{LASIS} - \overrightarrow{PS} \qquad (3.1)$$

$$\vec{b} = \overrightarrow{RASIS} - \overrightarrow{PS} \qquad (3.2)$$

The cross product of the two vectors is taken to generate a vector perpendicular to the APP at the PS:

$$\vec{c} = \vec{a} \times \vec{b} \qquad (3.3)$$

The dot product of the newly calculated vector and the vector defined by gravity, $\vec{z}$, is calculated which generates an angle $\tilde{\beta}$:

$$\tilde{\beta} = arccos \frac{\vec{c}.\vec{z}}{|\vec{c}|.|\vec{z}|} \qquad (3.4)$$

The pelvic tilt is then calculated between the APP and the gravity vector:

$$\tilde{\alpha}_{PT} = 90 - \tilde{\beta} \qquad (3.5)$$

It was hypothesised that the probe angle might affect PT measurements. To test this hypothesis, the effect of changes in the probe angle (with respect to contact with the skin) on the PT estimates were quantified with one operator measuring the pelvic tilt and sagittal balance of one healthy, male subject (age: 29, BMI: 26.5kgm^{-2}) at three probe angles (0°, 30° and 60°), at the PS landmark, three times at each angle in supine position. The probe angle was not considered at the two ASIS landmarks as their identification was deemed standardised at a consistent angle. The probe angle was monitored in real time using an inclinometer (Digi-Pas® DWL-80E, SD ±0.1°), and

verified after the acquisitions using a synchronised motion capture system (Vicon, Oxford, T160 series, 10 cameras). The angles were expressed in the same reference system as the smart system, by using the pre-calibrated rigid bodies.
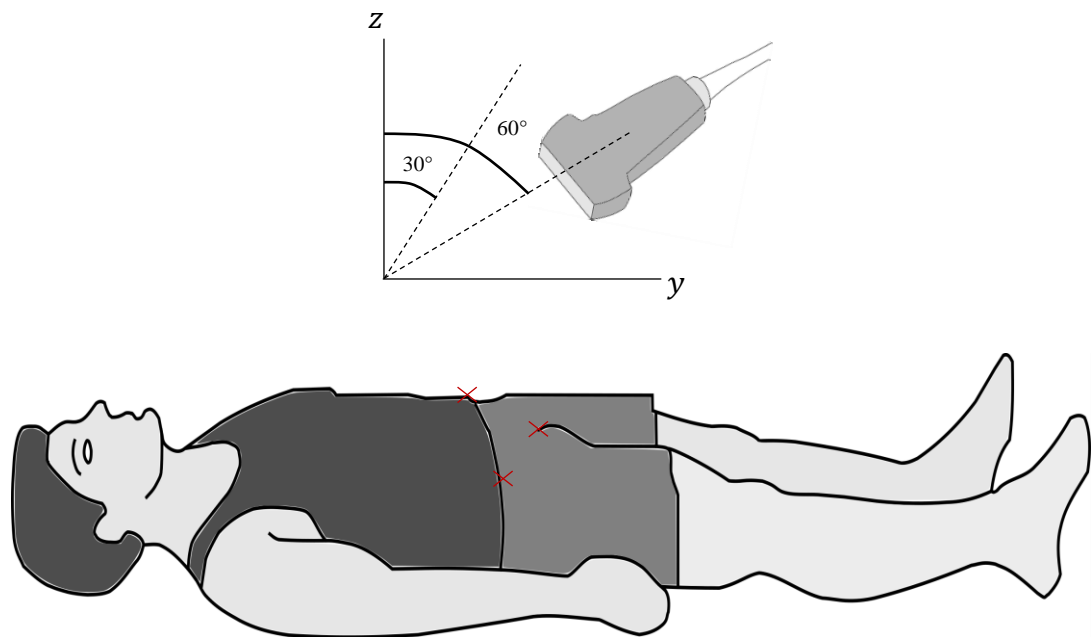
Figure 4.3. Sensitivity of measurements with respect to the angle of the probe at 0° (perpendicular), 30° & 60° (as shown in the plot) in the y-z plane. The red 'x's indicate the three landmarks needed for the APP calculation.

A resolution test was then performed to determine the minimum detectable changes in pelvic tilt. To perform this, the bed was initially tilted by 1°, and the same subject previously described was measured three times, with the probe kept perpendicularly (optimum theoretical angle). This was repeated at 2°, 3° and 8°. The results were then analysed by assessing the means of the pelvic tilt measurements at each angle and quantifying the differences between the inclined value and 0°. The pelvis was assumed to remain completely rigid during the incline.
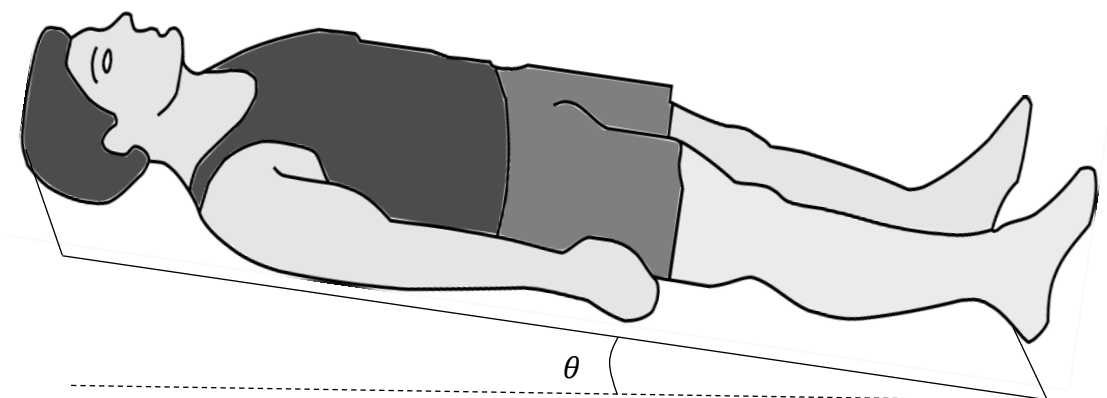
Figure 4.4. Changes in bed angle to measure the minimum detectable change of the pelvic tilt when slanted by known angles.

Repeatability and accuracy tests were performed after the previous trials to try and determine the cause of the significant variation in the measurements and validity of the measurement process. Accuracy measurements involved the use of a flat surface, which would theoretically produce 90° PT angles. The hypothesis was that freehand measurements with the smartphone would produce more variability than if it were fixed onto a tripod. Three locations were marked and then scanned in the same manner as the subject measurements. In the post-processing step, the most superficial and central location on the ultrasound image was marked on each ultrasound image. Repeatability was assessed by performing eight measurements with the smart phone freehand and fixed at bed angles of 0° and 5°. Mean and standard deviations were reported for all measurements. The accuracy was calculated as the difference between the surface measurements and the inclinometer value.

4.2.2 Motion capture measurements of the anterior pelvic plane

For the motion capture measurements of PT with reference to the APP (Figure 4.5), the previously described Vicon system was used to capture the location of three retroreflective markers attached to a wand, see Appendix section B. This was used to identify the three landmarks (RASIS, LASIS and PS) directly via palpation. Firstly, a resolution test was performed with the wand to test the minimum detectable change of the motion capture system. This involved palpating the surface of a physiotherapy bed, which was considered rigid for this purpose. 0°, 1°, 2°, 3° and 5° were implemented and theoretically would produce "PT" angles of 90°, 91°, 92°, .93° and 95° respectively with respect to the global co-ordinate system of the motion capture system. All angles were found accurately (mean difference and SD of 0.0° ± 0.3° between known angle and calculated angle).
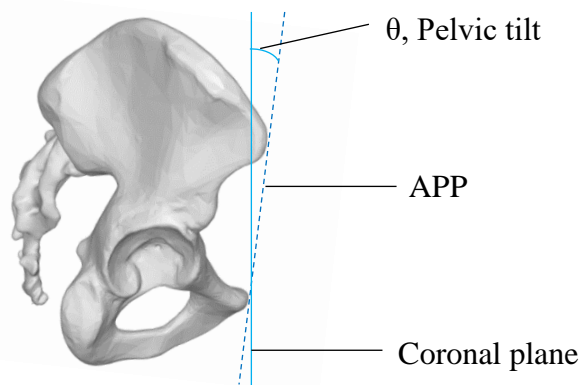
Figure 4.5. Sagittal view of the plane formed by the two anterior superior iliac spines and the pubic symphysis. In this schematic, the angle is slightly anterior.

Validation of this protocol consisted of measuring the APP at two supine angles, 0° and 5°. This implemented change in bed angle should theoretically produce a 5° change in the APP. The two ASIS landmarks were identified by the operator and palpated with the tip of the wand. The PS landmark was self-palpated by the participant. All participants (male: 2, female: 2, age: 26.8±3.2, BMI: 20.5kgm^{-2}±2.9kgm^{-2}) underwent strict instruction for identifying the PS landmark beforehand. If the participant found its identification challenging through touch, then ultrasound was used to help find the landmark and then removed prior to the measurements. The PS landmark was palpated first so that the subject was not rushing during the palpation, and verbal confirmation of its identification was made before the trial recording started. The wand was then handed to the operator who palpated the two ASIS landmarks. The subject was asked to lie comfortably and still, keeping their feet pointing upwards throughout. This was repeated three times at each bed angle and the subject was kept in place during the angle change. The pelvis was assumed to remain completely rigid during the incline.

Three male subjects (age: 21.0±3.1, BMI: 21.2kgm^{-2}±1.6kgm^{-2}) were then measured in supine and standing positions with the palpation conducted in the same way as previously stated. For the standing measurements, the subjects were asked to stand with their arms across their chests, after the self-palpation of the PS landmark, to keep their feet point forward and to remain as still as possible throughout.

The PT is calculated, initially in the same way as the ultrasound smart system for the APP measurements by defining the cross product from the two vectors defined in equations 3.1 & 3.2. Two planes are then needed and are defined in the global co-ordinate system by:

$$XY = [0,0,1] \qquad (3.6)$$

$$XZ = [0,1,0] \qquad (3.7)$$

Where XY and XZ are the required planes for calculating the PT in the supine and standing positions respectively. The angle between the vector z and the respective plane is the PT.

4.2.3 Motion capture measurements of the superior iliac spines

Pelvic tilt in this section is described in two ways. Firstly, with reference to the iliac spine height difference (Figure 4.6), and secondly by the plane formed by the four superior iliac spines (Figure 4.7). This method does not require the palpation of the awkward PS landmark but instead utilises the palpable posterior superior iliac spines and the previously used anterior superior iliac spines. Three measurements were gained from this technique. Two side specific measurements, as shown in Figure 4.6, for the left and right iliac spine height differences and one measurement of the angle of the plane formed by the four landmarks with respect to the transverse plane, shown in Figure 4.7. The latter measurement is used routinely in gait analysis for the quantification of the pelvis orientation from skin markers (Perrott *et al.*, 2017).
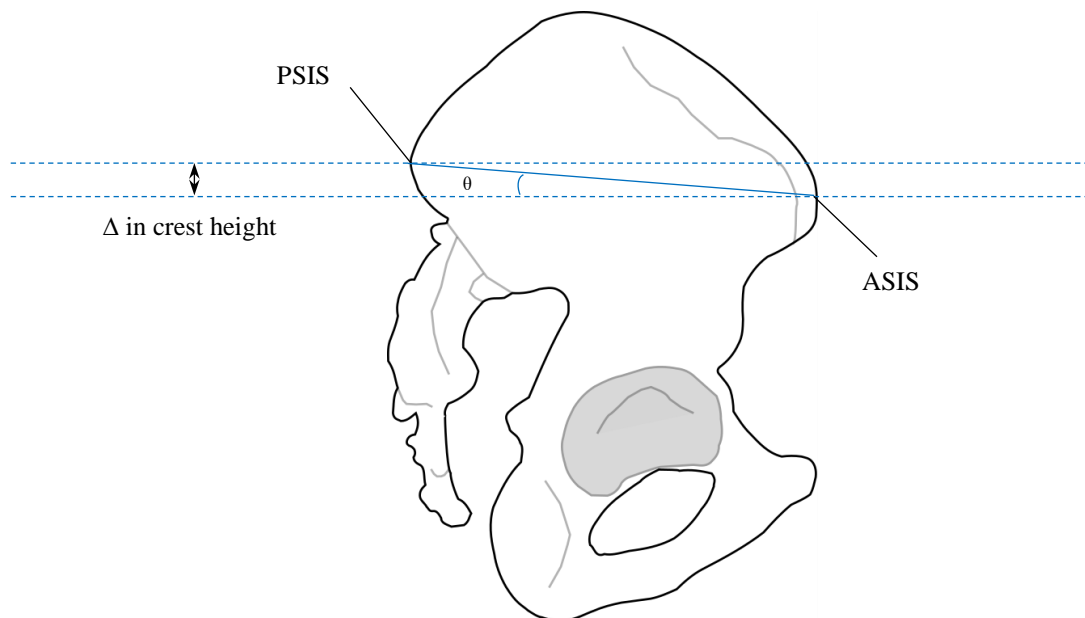
Figure 4.6. Sagittal plane view of the pelvis. The difference in the height of most posterior point (PSIS) and most anterior point (ASIS) of the pelvis is shown. Theta represents the PT measured from this method and in this example, the pelvis is anteriorly tilted.
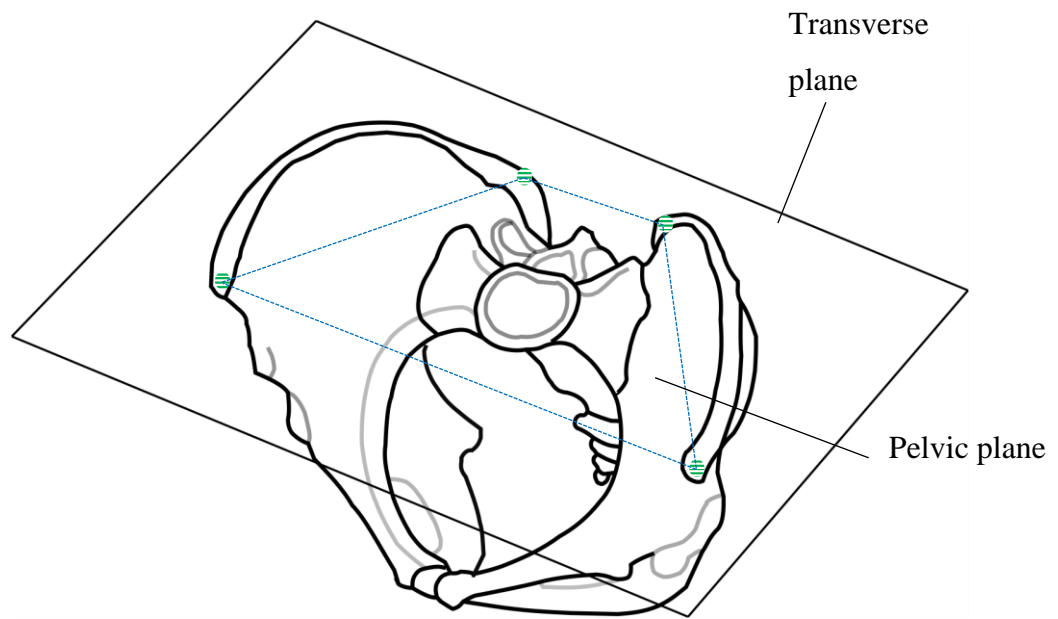
Figure 4.7. Transverse plane and pelvic plane (formed by the right and left anterior and posterior iliac spines). The angle between the two planes in the sagittal plane is the pelvic tilt. The angle between the two planes in the frontal plane is the pelvic obliquity.

Like the APP measurements, these trials were also conducted with a palpating wand. Validation of this protocol consisted of measuring three male subjects (age: 21.0±3.1, BMI: 21.2kgm^{-2}±1.6kgm^{-2}) in a level and tilted sitting position. The four landmarks were palpated in a level position and then the chair was manually tilted by a known quantity (4°). Subject positioning was controlled by setting the knee and hip angle at 90° and 100° respectively at the level position. Subjects were asked to keep their feet pointing forward and were outlined to standardise their positioning for each repeat. For the chair tilt, subjects were asked to extend their knees whilst plantar flexing their feet to lift the chair, which enabled enough room for two wooden blocks to be slid under the chair legs. A marker cluster was placed on the lower back to construct a local co-ordinate system to compensate for any slight movements of the subject during measurements. The accuracy was quantified by calculating the change in pelvic tilt between the two positions and comparing it to the real value of the change in chair angle. This process was repeated three times for the three subjects. The pelvis was assumed to remain completely rigid during the incline.

The main experiments consisted of quantifying the difference in pelvic tilt between the supine and standing positions for the same three subjects. For the supine position, a mesh gridded bed was used to have access to the posterior landmarks. A custom designed alignment device enabled control in subject positioning. Subjects were asked to relax, cross their arms against their chest and keep their feet pointing

upwards, minimising any external rotation. For the standing position, subjects crossed their arms against their chest and stood with their feet shoulder width apart and pointing forward. The local cluster for these measurements was placed laterally on the iliac crest as the lower back could not be utilised when the subject was supine. Palpation of the four landmarks took place in the supine position and then immediately in standing. This was repeated three times with a rest in between each repeat. Written, informed consent was obtained from each subject prior to the experiment.

For processing the PT measurements with respect to iliac crest height difference, the calculations were performed in a similar fashion to Gajdosik *et al.* (1985) and visually shown in Figure 4.6. In brief, it follows a trigonometric calculation as:

$$sin\theta = \frac{side\ opposite}{hypotenuse} \qquad (3.8)$$

where side opposite was the height difference between the PSIS and the floor and the ASIS and the floor, and the hypotenuse was the distance between the PSIS and ASIS (Gajdosik *et al.*, 1985).

For processing the PT measurements with respect to the anterior and posterior superior iliac spines, a mid-point of the PSIS landmarks was initially calculated. This allowed the calculation of a pelvic plane based on the two ASIS landmarks and the mid-PSIS landmark. From here, the calculations were the same as those for the APP measurements. An angle close to 90° meant the pelvic plane was almost coincident with the transverse plane of the subject as shown in Figure 4.7.

4.2.4 Post-processing

Motion capture data were processed in MATLAB and Nexus 2 (Vicon, Oxford, UK). The calculations performed to determine the wand tip were performed in MATLAB. The MATLAB interface within Nexus 2 meant certain processes could be streamlined, such as determining which frames each of the landmarks were being palpated between, as shown in Figure 4.8. For the APP motion capture measurements, each trial had three stable periods, meaning 6 frames were identified for these periods. For the chair tilt experiments, four landmarks were recorded (left and right anterior and posterior iliac spines) in separate trials, and finally, for the supine and standing measurements, five landmarks were recorded (left and right anterior and posterior iliac

spines and pubic symphysis) in separate trials. The mean x, y and z co-ordinates for each period was then carried forward for the calculations of the pelvic tilt.
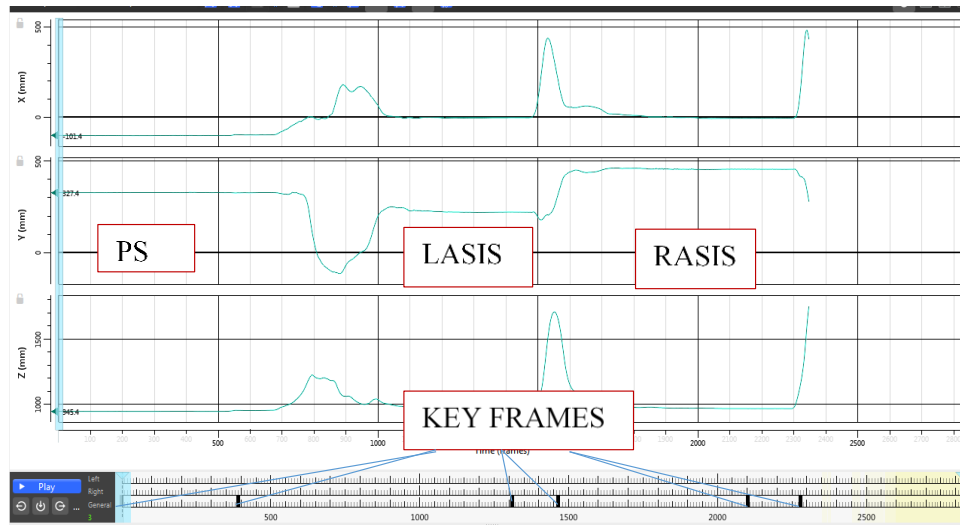
Figure 4.8. Example of the palpating periods for the APP motion capture measurements (three landmarks) and order, and the frames chosen to extract the wand tip co-ordinates from the trials in Nexus.

4.2.5 Statistics

Mean and standard deviations were recorded for all measurements.

4.3 Results

For all the measurements, an angle of greater than 90° was considered posterior PT and less than 90° was considered anterior PT.

4.3.1 Integrated motion capture and ultrasound results of APP

For the one subject measured, the mean and SD of the PT with respect to changing the angle of the probe (0°, 30° and 60°) at the PS landmark were 89.1°± 4.0°, 95.1°±7.3° and 80.9±7.0° respectively.

Fixed and freehand measurements performed with the smartphone showed equal repeatability with standard deviations of 2.1° or less. 4.3° and 1.9° differences were found for an incline of 5° for fixed and freehand measurements respectively. The results are shown in Table 4.2.

Table 4.2. Fixed and freehand smartphone measurements at 0° and at a 5° incline (for a targeted difference in angle of 5°).

Bed Angle	0°		5°		Difference (°)
	Mean (°)	*SD (°)*	*Mean (°)*	*SD (°)*	
Fixed	92.7	2.1	97.0	1.3	**4.3**
Freehand	94.6	1.8	97.5	1.4	**1.9**

Four initial angles were imposed to the bed, 1°, 2°, 3° and 8° (maximum safe angle). The mean and SD of the PT at each angle respectively on the one subject measured were 89.9°±1.7°, 92.7°±2.8°, 92.1°±2.8° and 103.2°±2.7°. From these initial results, a minimum of 5° was imposed on the bed angle when testing the PT accuracy of further subjects.

4.3.2 Motion capture results of APP

For the measurements performed on the bed surface, the mean and SD of the "PT" from the imposed angles (0°, 1°, 2°, 3° and 5°) were 90.3° ± 0.1°, 90.8° ± 0.0°, 91.7° ± 0.1°, 92.8°±0.1° and 95.2°±0.2° respectively.

Differences in PT from an imposed bed angle of 5° ranged from 3.5° up to 7.9°. All results are shown in Table 4.3.

Table 4.3. Difference in PT from imposed bed inclination of 5° (for a targeted change in PT of 5°).

Bed Angle	0°		5°		Difference (°)
	Mean (°)	*SD (°)*	*Mean (°)*	*SD (°)*	
S001	97.5	0.6	105.4	0.7	**7.9**
S002	94.8	1.1	102.3	0.3	**7.5**
S003	96.1	1.6	101.0	1.2	**4.9**
S004	91.9	1.3	95.4	0.5	**3.5**

The mean and standard deviation for the supine and standing PT measurements are shown in Table 4.4. Differences of 54.1°, 52.4° and 10.3° between the two positions were found for subjects 1, 2 and 3 respectively.

Table 4.4. Differences in PT from measurements in supine and standing.

Position	Supine		Standing		Difference (°)
	Mean (°)	*SD (°)*	*Mean (°)*	*SD (°)*	
S001	104.0	10.9	158.1	53.0	**54.1**
S002	94.4	0.6	146.8	25.4	**52.4**
S003	96.3	4.0	106.6	17.7	**10.3**

4.3.3 Motion capture results of the superior iliac spines measurements

There were small differences in all subjects between the left and right sides, less than 3° in 5/6 cases. The largest difference found was in standing for S002 (7.9°) however, the measurements were accompanied with very large SD (11.5° and 11.9° for the right and left side respectively). All subjects showed anterior changes when in the standing position compared to supine on both left and right sides (range: -9.2° to -15.6°).

Table 4.5. Differences in PT between the left and right sides, and, supine and standing, measured from the superior iliac spine height difference.

| Position | | Supine | | Standing | | Differences (°) | | | |
| | | | | | | Left/right | | Supine/standing | |
		Mean (°)	SD (°)	Mean (°)	SD (°)	Supine	Standing	Left	Right
S001	Right	78.2	1.6	93.8	0.9	2.1	0.9	-14.4	-15.6
	Left	80.3	3.3	94.7	0.7				
S002	Right	83.5	4.1	94.1	11.5	1.9	7.9	-10.6	-16.6
	Left	85.4	6.1	102.0	11.9				
S003	Right	84.4	3.6	96.7	4.2	2.9	-1.2	-13.3	-9.2
	Left	86.3	2.1	95.5	1.8				

The accuracy of the PT measurements showed significant variation in most subjects as shown in Table 4.6. Subjects S001 and S003 showed low SD and good accuracy with PT changes of -2.3°±3.2° and -3.1°±3.3° respectively. S002 had significant variation with a standard deviation of ±13.1°.

Table 4.6. Mean difference in PT between level and tilted (-4°) sitting positions (for a targeted change in PT of 4°).

| | PT Difference | |
	Mean (°)	SD (°)
S001	-2.3	3.2
S002	-1.7	13.1
S003	-3.1	3.3

The difference in PT between supine and standing was then quantified with all results shown in Table 4.7. Subjects S002 and S003 both showed posterior changes of 7.2° and 2.1° respectively. Subject S001 showed an anterior change of -7.3°.

Table 4.7. Difference in PT from between supine and standing positions.

| Position | Supine | | Standing | | Difference (°) |
	Mean (°)	SD (°)	Mean (°)	SD (°)	
S001	101.9	2.1	94.6	0.7	-7.3
S002	98.3	0.7	105.5	10.1	7.2
S003	96.1	3.2	98.2	5.2	2.1

4.4 Discussion

Pre-operative planning of pelvic orientation for implant positioning in total hip arthroplasty is important for implant longevity and most critically, patient satisfaction (Hassan *et al.*, 1998). This part of the thesis aimed at assessing the differences in PT measurements between supine and standing positions. This was performed after developing several non-invasive experimental pilot protocols with ultrasound and motion capture systems. This section reflects on the results obtained the ultrasound experiments and two motion capture protocols.

4.4.1 Integrated ultrasound and motion capture system

Ultrasound has been used extensively in a clinical setting for a wide range of applications (Mozaffari and Lee, 2017). Its role in determining segment orientation, specifically for pre-operative planning in arthroplasty interventions is much less common and a recent development (Greatrex *et al.*, 2017). The recent progress of a portable, integrated ultrasound and motion capture system has opened up the opportunity to replace conventional X-ray methods of PT measurements with ultrasound (Martin, 2016). The major advantage of this system is its potential to measure subjects in many different postures. However, whilst it has been shown to be accurate and repeatable on a phantom, measurements within healthy and osteoarthritic populations have been less promising (Martin, 2016; Kochman *et al.*, 2017; Marques *et al.*, 2018). This part of the chapter aimed at sourcing the errors within subject measurements on healthy participants.

The first measurements quantified the change in PT with adjustments in the probe angle at the PS landmark. Due to the anisotropic properties of ultrasound, the probe angle was considered to affect the measurements. The PS landmark is often not measured at a perpendicular orientation due to its sensitive location. The results from this experiment, conducted on one subject, showed an extreme range in measurements at 30° and 60° probe angles and slightly less perpendicularly. It is not known at what angle previous studies. performed their measurements for the PS landmark, but it cannot be suggested whether the probe angle adversely affects the PT measurements (Kochman *et al.*, 2017; Marques *et al.*, 2018). Hence, further investigation is needed on the sensitivity of probe angle on PT measurements. With restrictions on access to

the raw data, co-ordinates of the three landmarks could not be accessed which would provide crucial information for determining the variability of the landmark with respect to the probe position.

The second batch of tests examined whether freehand or fixed measurements with the smart phone impacted the PT calculations. Optimising the position of the smart phone as it captured the position of the two rigid bodies was hypothesised to improve the results. For these experiments, to reduce the potential error obtained from subject measurements, a physiotherapy bed was used as a phantom. This enabled a repeatable environment and isolation of the measurement process. During normal use (free hand measurements) the results on a flat plane at 0° and tilt of 5° were consistent with previous phantom measurements (Martin, 2016). Low standard deviations for both freehand and fixed smartphone measurements showed that this factor did not adversely affect the PT measurements. However, the difference between the mean value of the fixed and freehand measurements at 0° was 1.9°. This is relatively large compared to the 0.5° difference found at the 5° incline. Therefore, the measurements performed were precise but not accurate compared to the inclinometer values.

The third set of experiments consisted of measuring the resolution of the system within a subject cohort as this has not been previously performed. This consisted of detecting the minimum change of the PT measurements in supine when implementing known bed angles. It was found that a change in bed angle of 8° was detectable whereas angles up to 3° showed no differences. However, the mean and standard deviation of the measured PT from the one subject measured at 3° and 8° was 92.1°±2.8° and 103.2°±2.7°. This shows considerable variation in the measurements between the largest bed inclinations. A 10° change was observed as oppose to a 5° change. After this set of experiments, it was decided that a full-scale investigation into the PT differences between the supine and standing positions would not produce clinically meaningful results.

All measurements with the smart system were analysed by one operator who annotated the ultrasound images in real time. Comparisons between and within different operators were not performed which limits the interpretation of the results. However, the simplicity of the annotation and interpretation of the three ultrasound images meant this part of the post-processing was not considered to be a large

contributing factor to the variability of the results. It is likely similar inconsistency would have been found if the physical measurements were performed by more than one operator (Kochman *et al.*, 2017; Marques *et al.*, 2018). Kochman *et al.* (2017) found large differences in PT between supine, standing and sitting, outside of the ranges found in the literature. Marques *et al.* (2018) found large differences in PT measurements between operators for the same healthy participants. In standing and supine, the largest differences between operators were 15.6° and 12.6° respectively (Marques *et al.*, 2018). This amount of variation would not be clinically meaningful in measuring the PT and requires improvements in the precision of the experimental procedure. Considering also that participants were healthy subjects with low BMI ($23.0 kgm^{-2} \pm 1.3$ kgm^{-2}, n=12), subjects in a patient cohort requiring THA would be significantly higher and most likely average $> 30 kgm^{-2}$ (Marques *et al.*, 2018). Increases in BMI will raise the difficulty in obtaining reliable measurements with ultrasound, therefore initially, it is essential that consistency within and across operators is found in a healthy cohort. Accuracy in a patient population would also need to be eventually quantified. In this experiment, the measurements were found to be similarly variable within one operator, therefore performing more trials with other operators was not conducted.

4.4.2 Motion capture measurements of the anterior pelvic plane

The inaccuracies and unidentifiable errors of the ultrasound experiments led to a protocol development using a high-resolution motion capture system. Motion capture systems are used for a wide variety of applications, including within clinical settings to conduct various experiments for aiding disease diagnosis and rehabilitation (Wren *et al.*, 2011). This makes it suitable to develop new protocols to potentially integrate into pre-operative planning routines, which, for knee and hip arthroplasty patients, is typically utilised (Stief *et al.*, 2014, 2018; Bloomfield *et al.*, 2018). The APP is considered crucial in pre-operative planning as previously described, therefore a non-invasive protocol was developed to reliably and accurately measure this parameter.

An initial set of resolution experiments were performed to test the minimum detectable change on a phantom with the palpating wand. This was performed

accurately as the phantom was inclined at several different angles, all of which were detected by the motion capture system, as expected.

The first batch of subject measurements consisted of measuring the accuracy within a small cohort. Like the ultrasound measurements, the subjects were measured in a level supine position and at an inclination of 5°, and the subject did not stand between measurements. The range across the four subjects was from 3.5° to 7.9°. The range is almost as much as the amount of imposed inclination. Whilst this range is quite large, a small batch of subject measurements were performed to quantify the standing and supine PT differences.

Inconsistencies were found in the measurements which showed very high standard deviations in the standing position. Whilst strict instruction was given on the palpation of the PS landmark, it was conducted by the subject which is a potential limitation. It could not be verified in real-time whether the same point was palpated precisely, only verbal confirmation that they were ready for the trial to commence, having found the landmark, was performed. However, the supine measurements showed more consistency across the three repeats with standard deviations much less than the standing measurements. For S002, these were comparable to the accuracy experiments which showed low SD for all subjects. The supine and standing measurement, which were conducted alternatively between repeats, potentially had an impact on the PT measurements. This was performed to vary the measurement procedure to see whether repositioning of the participant adversely impacted the results. Due to the large variation in all results however, whether standing up and then going back to supine had an influence on the measurements could not be quantified. Though it may be the reason for the greater SD found in subjects S001 and S003 in the main experiments.

Few studies have attempted to measure the APP in a similar, non-invasive method to that discussed here. One study used a digitising robotic arm to palpate the three bony landmarks (Mayr *et al.*, 2005). Measurements were performed on a large cohort of 120 subjects including 30 healthy individuals, in both supine and standing positions. Within the healthy group, the mean PT angle in the supine position was 95.2°±2.7° compared to 95.1°±2.4° in this study. The much smaller sample size must be considered when making this comparison, for example for the measurements at the

5° inclination, the SD across the 4 subjects almost doubles to 4.2°. The greater spread questions whether the values at 0° are truly representative of the measured precision. An old study measured the APP using a custom made inclinometer and pressed it against the anterior pelvis (Anda *et al.*, 1990). They showed comparable results to those found by Mayr *et al.* (2005) but showed no difference in pelvic orientation between supine and standing positions. Non-invasive measurements of the APP seem to contrast to those who have quantified positional changes of the pelvis with conventional methods (X-rays, MRI, CT). For example, standing pelvic radiographs performed one author showed a mean anterior PT pf 4.68° ± 0.68° which is low, and similar to those found here and in other literature (Blondel *et al.*, 2009). In this paper however, supine analysis was not performed. One study retrospectively analysed the PT measurements of THA patients who had supine, standing, and sitting positions analysed, with CT for the former and radiographs for the two latter measurements (Pierrepont *et al.*, 2017). Their study highlighted the importance of individual consideration in THA as extreme ranges in all positions was observed across the subject population.

For these measurements, certain limitations were difficult to remove from the experimental setup. Subject movement and controlling the position of the pelvis is very difficult to account for and even subtle re-adjustments may have impacted the measurements. Another limitation was the identification of the pubic symphysis landmark which proposed more difficulty than the ASIS landmarks. Each subject was asked to self-palpate the PS landmark, meaning accurate measurements cannot be confirmed. Even after strict instruction, how much the subjects pressed on the soft tissue for example, could not be quantified.

4.4.3 Motion capture measurements of the superior iliac spines

Using the PSIS and ASIS landmarks instead of the PS landmark to quantify PT was appealing due to their relative ease of palpation. The PS landmark is in a region which may cause discomfort to some subjects; therefore, this alternative was also advantageous in that respect. It is not a novel method for measuring the pelvic inclination as it is commonly used in gait analysis from the measurement of skin markers on the four superior iliac spines (Perrott *et al.*, 2017). However, measurements in several static positions have not been quantified to the best of my knowledge.

From the measurements of PT with respect to the height difference of the anterior and posterior superior iliac spines on the left and right sides respectively, it was shown that the difference between the left and right side was small in all cases except for S002 on the right-hand side (7.9° difference in the standing position). All other measurements were below 3° and not meaningful due to the errors shown in some cases, especially for S002 were high standard deviations were found. Determining where this error came from is difficult, as there are several potential sources. Although a specific subject group was chosen (low BMI, healthy adult males), there was still potential error in the palpation of the landmarks. Even when chosen for reducing the soft tissue artefact error, palpation can still be a problem, and the posterior superior iliac spines have shown to be challenging to identify and in cases, not clinically reliable for measurements in various positions (Cooperstein and Hickey, 2016). Quantifying the impact of posture between repeats is also challenging, as the subjects were measured alternately from lying to standing. This was performed to vary the experimental process and not have subjects lying or standing for extended periods of time, which could lead to discomfort and posture changes.

Measuring the accuracy of the technique was found to be problematic, and not repeatable even though a standardised protocol was followed. The action of tilting the chair with the subject in place should have theoretically tilted the pelvis by four degrees and this change should have been detected in the calculations. The error in palpating the landmarks as well as the potential error in subject movement is likely to be equal or greater than the tilted angle. Determining a minimum detectable change would have been difficult as angles much larger than the one chosen would put the participants in uncomfortable positions which would compromise the protocol.

For the differences in PT between supine and standing, small differences were found in the PT angle between the two positions ($< 8°$). This is comparable to literature which in several cases found differences of less than 10°. For example, a mean posterior change of -7.2° (range: -10.7° to 3.3°) and -6.9° $\pm$ 5.7°, respectively have been found previously (Tamura *et al.,* 2014; Uemura *et al.*, 2017). These two studies, however, were conducted in a patient population for individuals about to undergo THA, therefore comparisons should be treated with caution. A study conducted on healthy participants was performed and found a mean anterior change in PT of 1° $\pm$ 4.6° (Mayr *et al.*, 2005). This was measured with respect to the APP, however. The

small change suggests that regardless of what is used as a reference for measuring the pelvic tilt, the change between supine and standing is relatively small compared to the changes found from sitting to standing or sitting to supine. Two out of the three subjects showed a posterior change in PT in these experiments. As it was a proof of concept study with a small sample size, the results must be treated with caution, as large SD exist within the subject measurements in some cases.

Overall, it seems that the most variation was shown in the standing measurements. This was potentially down to the posture adopted by the subject which may have changed between repeats even though foot positioning and upper body posture was standardised. Position was less of a problem in supine due to the alignment device used and relative ease of remaining stationary. The supine position is also problematic however, with pelvic posture likely to change between each repeat. The mesh gridding of the bed to allow access to the PSIS landmarks presented a small amount of discomfort that may have influenced the results. This was minimised as much as possible with the use of the alignment device which meant only the pelvis and lower back were exposed to the mesh. The palpation of the rear landmarks was not rudimentary, as it required both palpation as well as making sure the wand markers were visible to the motion capture system. Low-lying cameras meant this was feasible, but the set up involved trial and error to achieve the least marker occlusion. It was also only practical to perform the experiments with two people, as checking in real-time that the markers were visible to the cameras streamlined the experimental procedure. This degree of effort in attaining data may not be best suited for a large sample size or within a clinical setting where time is valuable. Therefore, from an experimental point of view, using the PS landmark for measuring the PT would be more convenient. However, from this set of experiments, using motion capture in this manner also does not currently provide a reliable framework for measuring the PT with respect to the APP.

Trying to quantify pelvic tilt with ultrasound and motion capture experiments to potentially aid pre-operative planning for THA is challenging, with proof of concept approaches showing no valid reason for further study at this stage. The use of *smart system* for APP measurements with ultrasound were found to be unreliable, with root causes not determined for the spread of the results having performed various assessments of the system. The use of a palpating wand and motion capture did not

lead to improvements when identical measurements were performed as to those with the *smart system* for APP measurements. Asking the subject to perform palpation of the PS landmark on themselves may have been the main reason for this. Quantification of PT from other landmarks on the pelvis were also deemed unreliable in their measurements. Controlling the pelvis for movement in general and particularly when imposed inclinations of the subject were conducted were expected to be the main cause of unreliability.

However, ultrasound use for the development of lower limb alignment measurements, crucial for pre-operative planning in TKA, has shown promise in Chapter 3. Chapter 5 evaluates ultrasound as a tool for image based musculoskeletal modelling. Briefly, the experiments involved the reconstruction of ultrasound images from sequences of 2D scans to 3D volumes through a synchronised motion capture and ultrasound setup.

Chapter V

3D ultrasound methods for image-based personalisation of musculoskeletal models

This chapter investigates the use of ultrasound and motion capture as a tool for image based musculoskeletal modelling, potentially replacing current techniques based on MRI. This chapter used a Python based package (Py3DFreeHandUS) for the motion capture and ultrasound data processing developed by Dr. Francesco Cenni. The musculoskeletal modelling was performed with help from Erica Montefiori.

5.1 Introduction

Musculoskeletal (MSK) modelling has been an increasingly popular aid in the analysis of human movement within the biomechanics community. Its inception was almost 30 years ago when its importance was initially conceived (Delp *et al.*, 1990) as a tool to quantify muscle and joint forces, which cannot be directly measured, but have a high potential to help the diagnosis and rehabilitation of musculoskeletal and neurodegenerative diseases.

Currently, to build a personalised MSK model, gait analysis and imaging data are combined to drive and scale the models. Typically, gait analysis provides the kinematic data from the marker set which is used to compute joint angles. Imaging data is used to gain subject specific anatomical features, such as bone geometries, muscle volume, and muscle paths and soft tissue volume. While certainly informative, MRI scans are time-consuming, cumbersome to the patient and relatively costly.

As shown in previous chapters, a valid method for low cost imaging is ultrasound. Ultrasound is typically performed in 2D which limits its use in terms of gaining volumes. One solution for this is to combine the imaging method with a motion capture system for 3D reconstructions. The combined motion capture and

ultrasound systems shown in the previous chapters were not flexible for experiments outside of their intended purpose. For example, measurements were restricted to lower limb alignment, torsion and segment lengths with OrthoPilot, and pelvic tilt with the *smart system*.

The enabling of 3D reconstructions of subject anatomy provides information that can be compared to segmented MRI scans. The potential to reduce the dependency of MRI scans in the production of MSK models with 3D ultrasound is appealing as the experiments can be performed in conjunction with gait analysis as portable ultrasound systems now exist at relatively cheap prices.

One of the main benefits of image-based musculoskeletal models is that they are characterised by higher fidelity to the anatomy and consequently provide an improved estimate of the joint centres and functional axes. This is indeed critical in gait analysis, especially for what concerns the hip joint centre (HJC). Historically, the HJC is calculated by regression equations, derived from skin marker locations, or through functional calibration techniques (Bell et al. 1989; Leardini et al. 1999; Harrington et al. 2007; Fiorentino et al. 2016). The error associated with HJC mis-location has been found to be significant in gait analysis (Stagni *et al.*, 2000). More recently, other authors attempted to estimate the HJC with an US based approach (Peters *et al.*, 2010; Upadhyaya *et al.,* 2015).

Upadhyaya *et al.* (2015) performed several functional tasks with the ultrasound device attached to the proximal femur. The femur was tracked, and bone depth was registered for each task and the main output was tissue thickness measured at each time point. A reduction in error of the HJC location using the registered bone position compared to a motion capture algorithm was found for the four participants.

Another study measured the HJC directly with motion capture and ultrasound by scanning key landmarks of the femoral head (Peters *et al.*, 2010). They validated their experiments with MRI scans by measuring the inter-HJC distance for both methods. The mean difference between the two methods was 4mm ± 2mm. The same method used in their study is performed in this chapter for HJC calculation. A follow up study was performed on cerebral palsy subjects which clinically tested their measurement technique in a patient population (Peters *et al.*, 2012). Whilst not validated against MRI scans, they performed an extensive comparison study against

regression, functional and fitting techniques for HJC calculations. They showed that Harrington's regression equations were most similar to their ultrasound measurements and concluded these would be most appropriate for HJC determination in a young cerebral palsy cohort (Harrington *et al.*, 2007; Peters *et al.*, 2012). The gold standard was 3D ultrasound and therefore the study was looking for an approach which could produce similar accuracies (Peters *et al.*, 2012). Functional tasks within the young, cerebral palsy cohort, performed less well. Therefore, due to the ease of regressive approaches, it was concluded that Harrington's equation was suitable in a cerebral palsy cohort, but 3D ultrasound is still considered the most accurate technique compared to MRI.

Defining the knee joint axis with ultrasound was first performed by Passmore et al., who used the most posterior points of the femoral condyles to define the knee joint axis (Passmore and Sangeux, 2016). These measurements were compared to three functional calibration techniques for defining the knee joint axis of rotation. Whilst being repeatable landmarks to scan, accuracy of the measurements was not conducted in the study and it was a relatively small cohort. A follow up study was conducted on a young cohort with lower limb torsional deformities (Passmore *et al.*, 2018). Their ultrasound condylar measurements, and three other methods for knee joint axis calculation were compared to EOS measurements of the lower limb, which was used as a gold standard. The difference between the knee joint axis measured from ultrasound and the EOS was 1°±4°. This was the most accurate method compared to the other measurement techniques. The same author conducted a literature review on ultrasound and MSK modelling work, including their own studies, which highlighted the flexibility and impact ultrasound can potentially have on subject specific modelling (Passmore *et al.*, 2017). Their work included subject specific modelling of muscle-tendon properties as well as the previously mentioned bone geometry work. This has been an area of interest due to the evidence of improved accuracy in muscle force prediction from incorporating subject specific muscle-tendon data into the models (Passmore *et al.*, 2017).

Another study has also utilised combined ultrasound and motion capture techniques to track the motion of the greater trochanter during gait and simultaneously compensate for soft tissue artefact (Jia *et al.*, 2017). Currently, and debatably their main limitation is the fact that they only compensate the soft tissue artefact for one

skin marker out of the entire gait protocol. Whilst being able to do this accurately, it is not clinically meaningful until more soft tissue artefact of the lower limb is accounted for, especially for a single segment, such as the femur.

In summary, this chapter builds on previous knowledge of 3D ultrasound techniques in the context of pre-operative planning and MSK modelling. It has been shown that accurate measurements can be conducted with this technique. Whilst the knee and hip joints have been previously analysed, the ankle, to the best of my knowledge has not been investigated in this context for implementation into musculoskeletal models. And further, a combination of the lower limb joints has not been analysed with respect to their impact on joint axis calculations in MSK models. Therefore, the aim of this chapter was to propose a method for lower-limb joint axis calculation through geometric fittings of segmented surfaces captured by an ultrasound and motion capture setup to reduce the dependency of MRI in MSK models.

5.2 Methods

5.2.1 Configuration

An ultrasound system (Telemed Echo Blaster 128 and linear probe, LV7.5/60/128Z-2, Lithuania) and a 10-camera motion capture system (Vicon T160 series, Oxford, UK) were digitally synchronised (0.010s delay). A custom designed marker cluster (Matijevich *et al.,* 2018), shown in Figure 5.1 was 3D printed (EOS Formiga P100, Munich, Germany) and attached to the ultrasound transducer. To gain the 2D ultrasound image pixels in 3D space, the location of the ultrasound image was transformed into the global reference frame. The transformations and rotations between the probe reference frame and ultrasound image were known for every time point. The ultrasound images and each pixel could then be transformed into the global co-ordinate system. DICOM sequences and c3d files were exported for the ultrasound and motion capture data respectively.
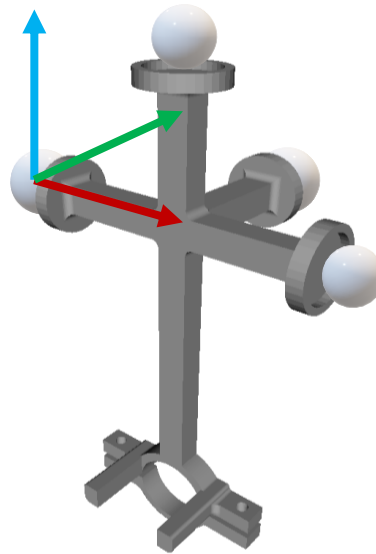
Figure 5.1. Custom marker cluster for attachment to ultrasound probe. The reflective markers form a reference system for the tracking of the ultrasound probe (Matijevich *et al.,* 2018) . Translation and rotations from the ultrasound image origin to the cluster origin are known from the external measurements.

5.2.2 Calibration

Although accurate measurements from the probe reference frame origin to the ultrasound image origin were known, a calibration procedure was undertaken as a check for these values. This was performed in a way similar to one study which scanned the bottom of a water bath (Single-wall calibration method) with an

ultrasound probe in a variety of orientations and motions (Prager *et al.*, 1998). A clear line is produced when scanning the phantom floor, as shown in Figure 5.2. To calculate the transformation matrix from the probe reference frame to the ultrasound reference frame, six parameters (three translations, three rotations) are needed from the transformation matrix, $^{R}T_P$, as shown in Equation 5.1:

$$\begin{pmatrix} x \\ y \\ 0 \\ 1 \end{pmatrix} = {}^{C}T_T\,{}^{T}T_R\,{}^{R}T_P \begin{pmatrix} s_x u \\ s_y v \\ 0 \\ 1 \end{pmatrix} \tag{5.1}$$

Where $^{T}T_R$ and $^{C}T_T$ are known at all time points as the transformations from the probe cluster reference frame to the global and from the global to the phantom reference frame respectively. s_x and s_x are the pixel to millimetre ratios. u and v are the pixel image co-ordinates. x and y are the co-ordinates of the ultrasound image in 3D space. To solve for $^{R}T_P$, two points are chosen on each ultrasound image which allows the calculation of an equation of a line for every frame.

Line detection is performed automatically with a line detection algorithm (Hough transform). This means an overdetermined problem needs to be solved to calculate the six parameters of $^{R}T_P$ and this is performed using the Levenberg-Marquardt optimisation algorithm. For a successful calibration, the probe needs to be moved extensively in various orientations to avoid repeat positioning.

Figure 5.2. Co-ordinate systems of the global, probe, ultrasound and phantom reference frames. Example of the line generated in the ultrasound images during calibration is shown on the right (Cenni *et al.*, 2016).

5.2.3 Reconstruction

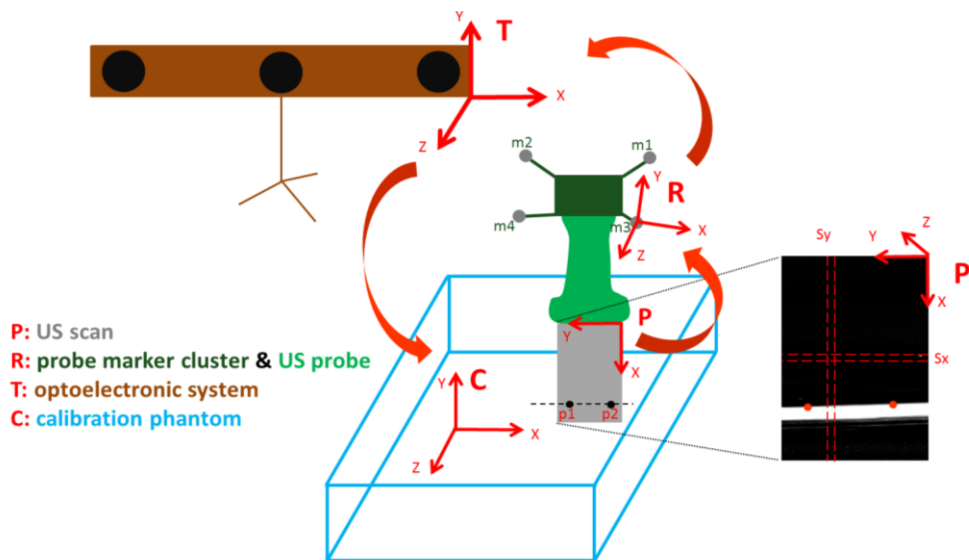To reconstruct the 2D ultrasound images into 3D volumes, Py3DFreeHandUS, an open source package developed in Python and specifically for this task was used and adapted for the purposes of this chapter (Cenni *et al.*, 2016). In brief, a 3D voxel array is constructed containing the grey values of the repositioned pixels from the ultrasound images. The voxel array is a parallelepipedon and is the smallest possible reconstruction containing all the ultrasound images from the sequence of realigned scans. Gap filling was performed through the voxel nearest neighbour (VNN) algorithm which assigns the same grey value to the gap nearest the closest voxel. From here, MeVisLab (MeVis Medical Solutions AG, Bremen, Germany) was used to check the quality and alignment of the voxel array and once suitable, exported as a DICOM sequence for segmentation and volume calculation. A custom workflow, as shown in appendix section A was used for the segmentation and volume calculations in MeVisLab.

5.2.4 Phantom measurements

Point measurements were performed to see whether the setup could accurately measure a known point in 3D space. This was performed by scanning a wand tip (the same wand previously described in Chapter 4) within a water bath which is known in global space from three external markers and calculating the distance between the real value and the calculated global co-ordinates from the ultrasound image. This was repeated three times for the same distance in two sessions.

Measurements were conducted on a plastic natural cast phantom femur (3B Scientific® GmbH, Hamburg, Germany) with no mimicking soft tissue to see whether the femur head and condyles could be reconstructed accurately. A laser scanner (FARO Edge ScanArm HD, Lake Mary, Florida) was used to measure its dimensions at a resolution of 0.1mm. This was considered the gold standard for the following measurements, which compared the ultrasound reconstructions of the phantom to the laser scanned model.

The femur was submerged in a water bath and securely fastened. The first ultrasound measurement consisted of a medio-lateral scan of the posterior condylar region. The probe was positioned longitudinally, and a freehand scan over the posterior medial and lateral condyles was performed in one sweep at 15Hz. The

condyles were then reconstructed into a 3D volume through segmentation having followed the previously described reconstruction process. An extra step involved exporting the reconstruction in DICOM format for processing in ITK-SNAP to reconstruct the 3D volume to allow the export of the volume in a stereolithography file format for further processing (Yushkevich *et al.*, 2006). The reconstruction was performed semi-automatically. A cylinder was then attached to the condyles in the same way as currently implemented in musculoskeletal models for the calculation of the knee joint axis in subject specific models (Yin *et al.*, 2015; Montefiori *et al.*, 2019). This involved highlighting the proximal curvature of the posterior condylar region in MeshLab, as shown in Figure 5.7 (Cignoni *et al.*, 2008). The cylinder was calculated from the data points obtained from the highlighted surfaces by a Gauss-Newton non-linear least squares approximation in MATLAB. The cylinder radius calculated from the reconstructed ultrasound images was compared to the cylinder attached to the laser scanned model.

Secondly, a transverse, proximal to distal scan of the femur head was conducted at 15Hz. This allowed the calculation of the femur head size from the reconstructed ultrasound images which was compared to the laser scanned femur head. The calculation was estimated through a spherical regression approximation calculated in MATLAB which fits a sphere to a series of data points obtained from the bone surface in MeshLab through a similar highlighting process as performed for the femur condyles. This highlighting included the outer circumference of the reconstructions, eliminating the main body and flat surfaces at the beginning and end of the reconstructions. Five repeats of the ultrasound scans were performed in two sessions and mean and standard deviations for the radii were used for the statistical comparisons. This process will indicate whether the ultrasound reconstructions can accurately measure realistic bone geometries in the absence of soft tissue artefacts.

Figure 5.4. Laser scanned model femur, proximal to distal sweep over the femur head and lateral to medial sweep of the posterior femur condyles.

5.2.5 Subject measurements

One healthy female subject (age: 29, BMI: 18.7kgm^{-2}) signed informed consent and agreed to participate in the pilot experiments whereby a series of ultrasound measurements were conducted on the lower limb. The subject had an MRI consisting of 5 transverse e-THRIVE 3D gradient echo sequences with 3 mm slice thickness at the pelvis, knee and ankle and 5mm slice thickness for the femur and tibia shafts. Gait analysis (Vicon, AMTI) was also performed which consisted of five natural walking trials. The MRI segmentations for the purpose of this pilot were considered the gold standard for measurement comparisons.

Ultrasound measurements of the lower limb were conducted at each joint for both legs. A proximal to distal 'sweep' of the ultrasound probe over the femur head, lateral to medial sweep over the posterior femur condyles and a proximal to distal sweep over the talar dome were performed for defining the joint axis of the hip, knee and ankle respectively. Figure 5.5 shows the areas 'swept' of each joint with the ultrasound probe. The speed of the sweeps was estimated to be 20mm/s, as calculated from a condylar sweep (longest sweep performed). This resulted in a series of ultrasound images which could be reconstructed into 3D space. The images were processed in the ways previously performed on the phantom and their geometries were segmented. A sphere was fitted to the femur head, and a cylinder was fitted to the curvature of the posterior femur condyles and talar dome for both legs. The fittings were compared to the same fitting procedure conducted on the segmented MRI. The difference in radius of the cylinders were calculated to provide the accuracy of the measurements.

A subject-specific model for the subject was built from the MRI scans, and the kinematics and kinetics from the gait analysis were used to drive the model in OpenSim (Delp *et al.*, 2007). The fittings for each joint were inputted into the model for output comparison between the ultrasound joint axis and MRI joint axis. The kinematics and joint contact forces (JCF) were calculated for three gait trials. The mean and SD were reported.
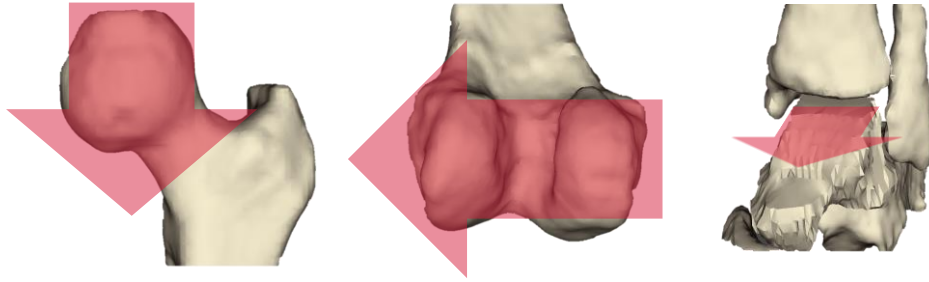
Figure 5.5. Proximal to distal sweep of the femur head (left), lateral to medial sweep of the posterior femur condyles (middle), proximal to distal sweep over the talar dome (right).

Two operator dependent post-processing steps were conducted in the femur phantom and subject trials and only the first step was used for the bottle measurements. The first is the segmentation of the object. This was standardised through segmenting the objects every five slices to reduce the time taken for segmentation. This meant segmentation times of approximately 5 minutes instead of up to 25-30 minutes. This time was considered important to keep low due to the processing of large numbers of trials. The second operator dependent step is the highlighting of the bone structures of the segmented ultrasound images for the geometric fittings. This involved selecting a portion of the segmented reconstructions and eliminating parts of the surface which will have a negative effect on the cylindrical fitting.
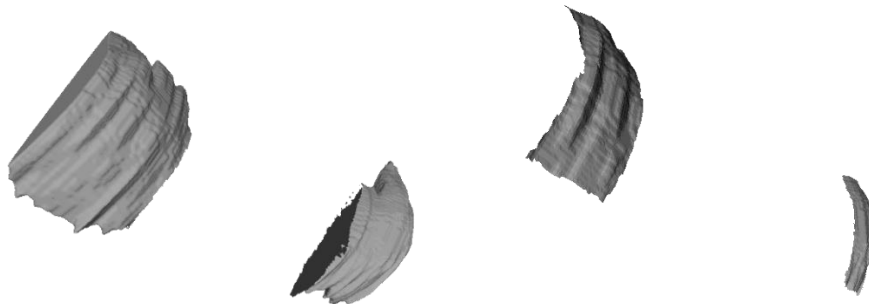
Figure 5.6. Original reconstructions of the lateral and medial condyles from the ultrasound segmentation (far left and middle left respectively). Final highlighted portion of the lateral and medial condylar surfaces (middle right and far right respectively) used for the cylinder fitting calculation.

Removing sections which are not critical is relatively subjective, meaning differences between different operators needs to be quantified. In brief, once the key curvature was highlighted and cropped, as shown in Figure 5.6, small sections of the final reconstructions (middle right and far right condyles in Figure 5.6) which did not follow a uniform curvature, was removed in a "clean-up", as it was assumed the distal

femur followed a uniform curvature. This was performed in the same manner as what is currently applied to processing the segmented MR-images.

Marker clusters and infrared cameras

Scanning area of femoral condyles (above) and resulting images (one slice, below)

Segmented femur and knee joint axis estimation from curvature of femoral condyles
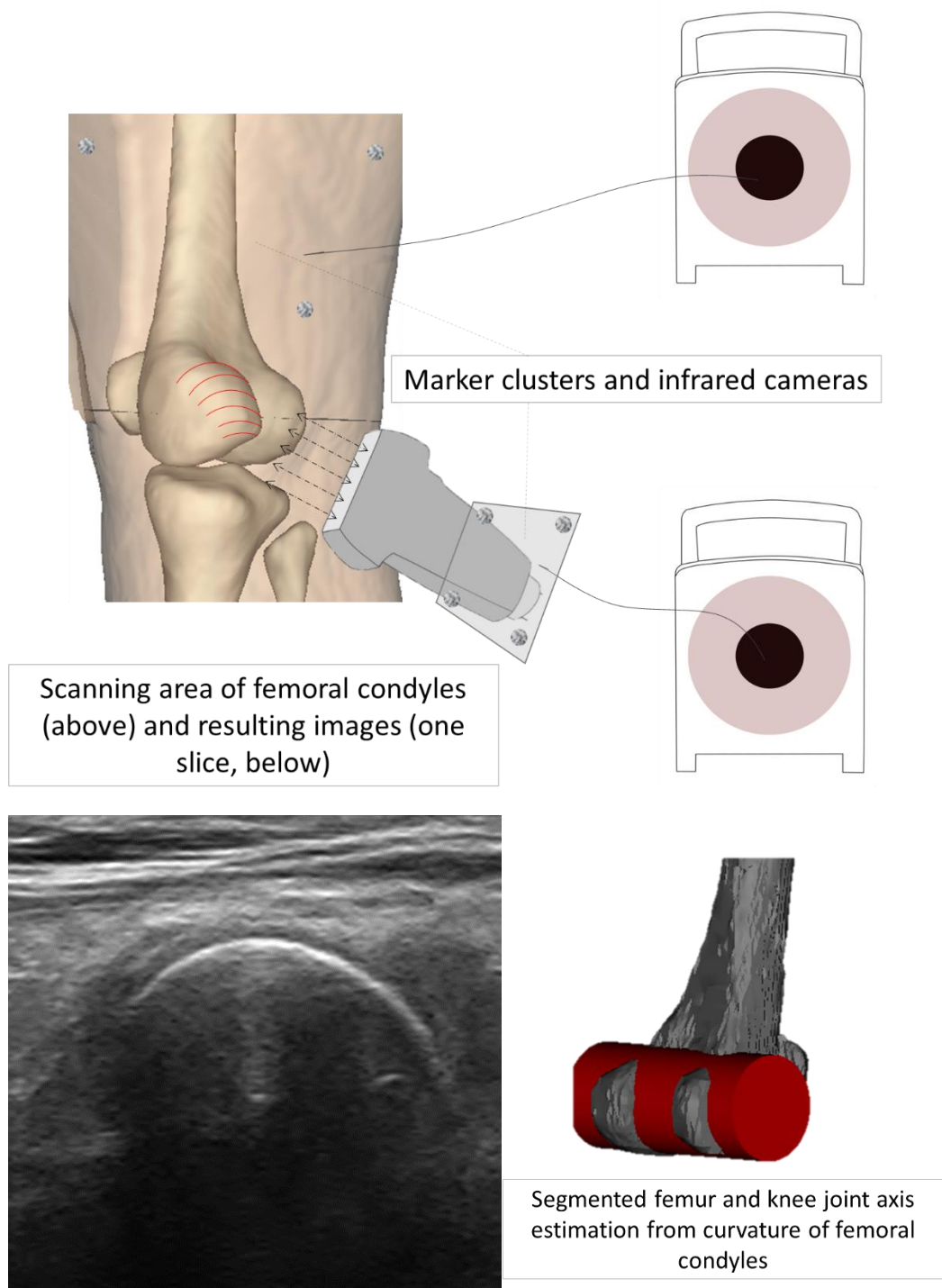
Figure 5.7. Schematic of the experiment performed for the scanning of the femoral condyles and segmented MRI with a cylinder fitted to the curvature of the condyles.

5.3 Results

5.3.1 Phantom measurements

Point detection with the ultrasound probe showed accuracy measurements under 10mm from the detectable wand tip. Table 5.1 shows the mean and standard deviation of the measurements.

Table 5.1. Accuracy of wand tip measurements from ultrasound scans conducted in two sessions. The mean of the differences is specified.

	Accuracy	
	Mean (mm)	*SD (mm)*
Session 1	8.2	1.1
Session 2	8.9	0.1

Next, radii measurements were performed on a femur phantom in the absence of any soft tissue artefact. For the cylinder fitting, 3/5 and 4/5 trials were successful in session 1 and session 2 respectively. The cylinder fitting of the phantom measurements overestimated the radii by 1.6mm in the two sessions with a peak error of 1.3mm. For the sphere fitting, 4/5 and 3/5 trials were successful in session 1 and session 2 respectively. Sphere fitting of the femur head overestimated the radii by 0.7mm and 0.2mm in the two sessions respectively with a peak error of 1.2mm. Table 5.3 shows the mean and standard deviations of the measurements.

Table 5.3. Accuracy of cylinder and sphere radius calculations from the reconstruction of the femur condyles and femur head respectively of a phantom femur conducted in two sessions.

	Femur Condyles (r=18.8mm)				**Femur Head (r=22.8mm)**			
	Mean (mm)	*SD (mm)*	**Accuracy (mm)**	**% Error**	*Mean (mm)*	*SD (mm)*	**Accuracy (mm)**	**% Error**
Session 1	20.4	1.2	**1.6**	**8.5**	23.5	1.9	**0.7**	**3.1**
Session 2	20.4	0.4	**1.6**	**8.5**	23.0	1.5	**0.2**	**0.9**
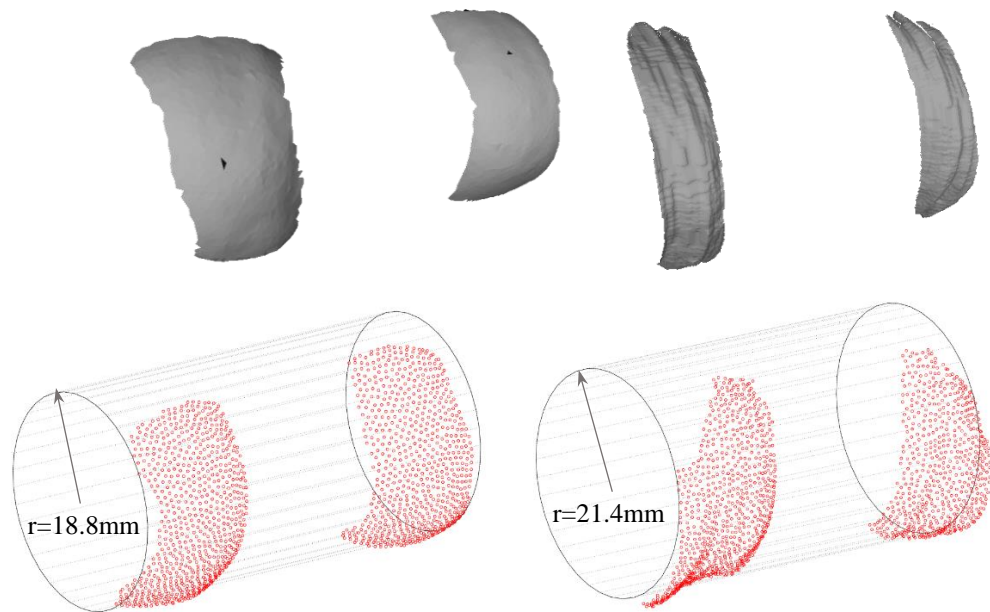
Figure 5.10. Cylinder fitting of the posterior femoral condyles from the laser scanned phantom (left column) and cylinder fitting of the reconstructed ultrasound scans (trial 1, session 1) of the phantom femur (right).
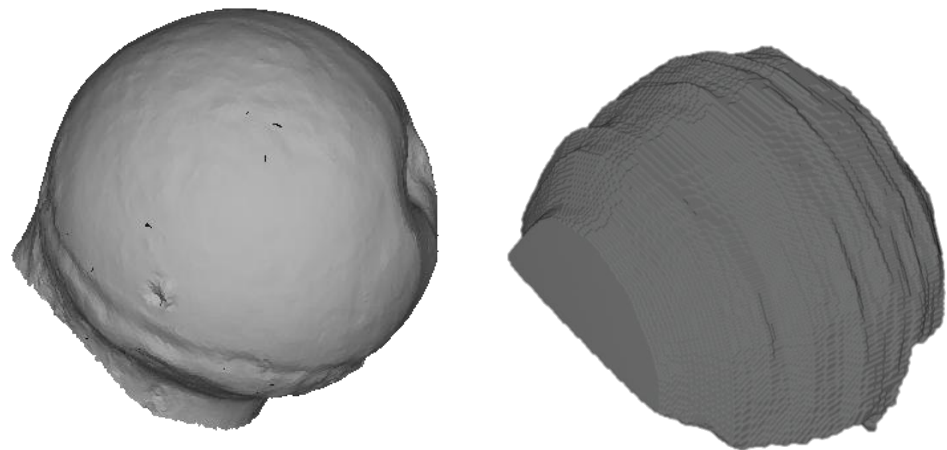
Figure 5.11. Laser scanned phantom femur head (left) and reconstructed femur head from the segmented ultrasound images (right).
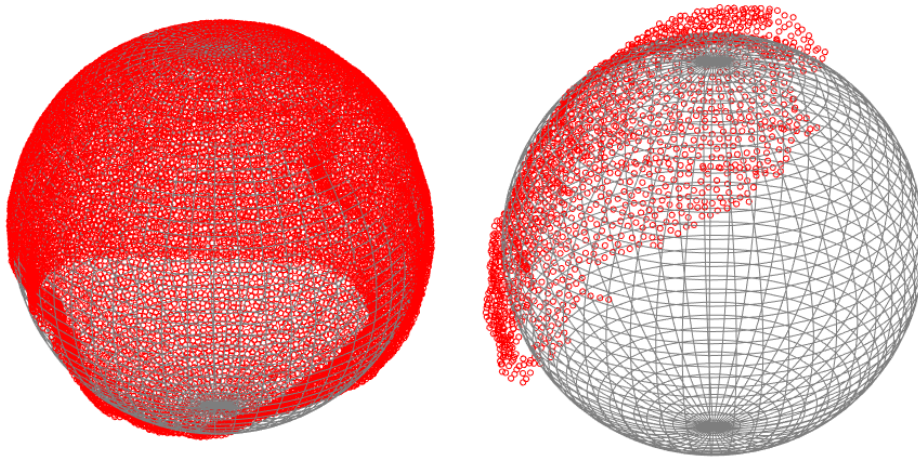
Figure 5.12. Sphere fitting (radius=22.8mm) to the laser scanned phantom (left) and sphere fitting (r=25.22mm) to the ultrasound reconstruction from trial 1, session 1. The red markers are the 3D locations of the mesh surface. The grey shell is the fitted sphere.

5.3.2 Subject measurements

The radii of the cylinders fitted to the posterior femur condyles were overestimated by 0.7mm and underestimated by 0.5mm for the left and right leg respectively with a peak error of 1.7mm. The radii of the spheres fitted to the femur head were underestimated by -4.1mm and -1.5mm for the left and right leg respectively with a peak error of 1.5mm. Table 5.4 shows the mean and standard deviations of the measurements.

Table 5.4. Accuracy of cylinder radius calculations from the reconstructed ultrasound images with respect to the MRI reconstructions of one subject for both legs.

| | Femur Condyles (Left: r=17.2mm, Right: r=18.3mm) | | | | Femur Head (Left: r=24.8mm, Right: r=23.3mm) | | | |
	Mean (mm)	*SD (mm)*	**Accuracy (mm)**	**% Error**	*Mean (mm)*	*SD (mm)*	**Accuracy (mm)**	**% Error**
Left	17.9	1.8	**0.7**	**4.1**	19.2	0.8	**-4.1**	**-16.5**
Right	17.8	1.2	**-0.5**	**-2.7**	23.3	0.3	**-1.5**	**-6.4**
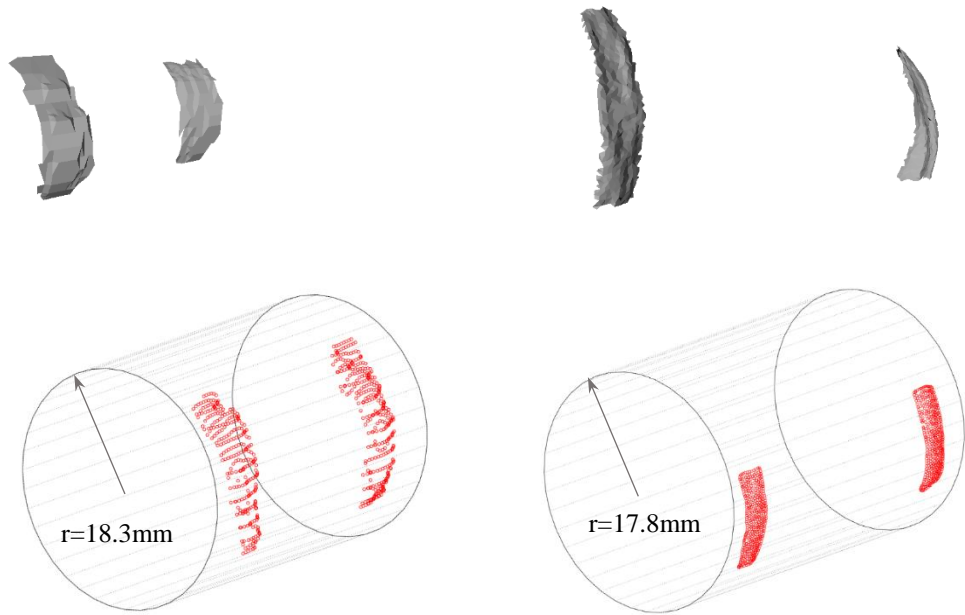
Figure 5.13. Difference between the MRI (top) and ultrasound (bottom) cylindrical fittings of the right posterior condyles.
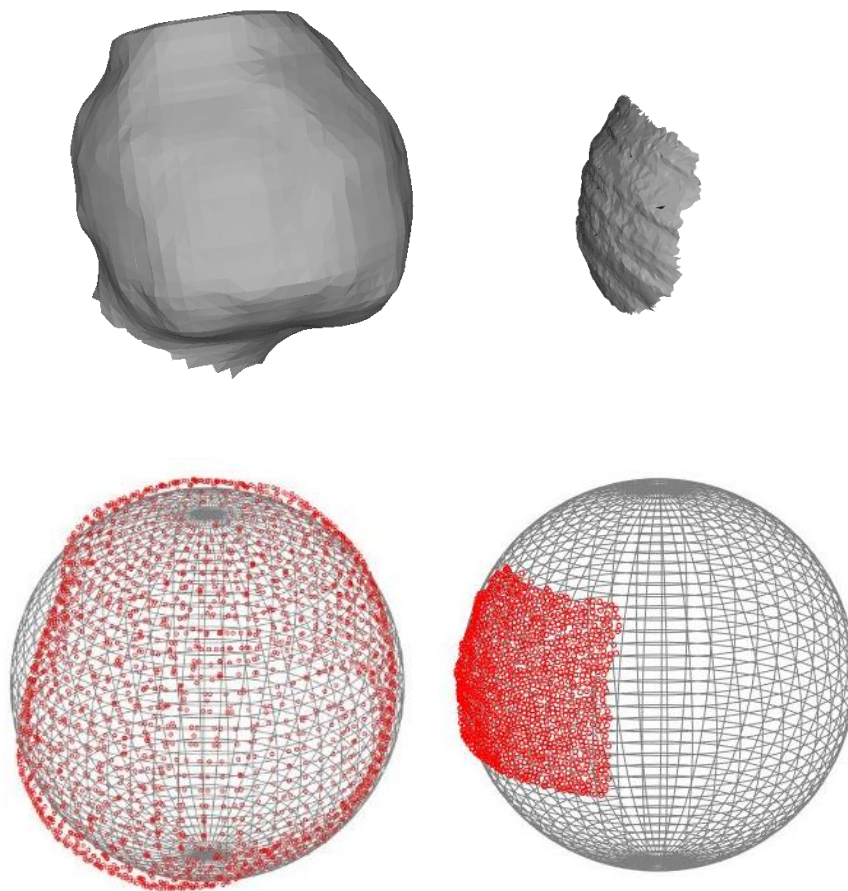
Figure 5.14. Difference between the MRI (left) and ultrasound (right) sphere fittings of the right femur head.

For the talus measurements, only one ultrasound trial was successfully segmented for the left foot. The radius for the cylinder attached to the ultrasound reconstruction was 24.9mm for the talar dome, an overestimate of 8.2mm compared to the MRI fitting (16.7mm).

For the outputs of the subject specific model, negligible differences were found between the MRI and US models for the hip and knee kinematics. A 12° difference was found over the entire gait cycle for the ankle joint kinematics. Negligible differences were found between the JCF at the knee. Differences of 0.40 body weight (BW) were found between the MRI and US simulations of peak JCF for the hip and ankle as shown in Figure 5.15. Figure 5.16 shows shifts in the kinematic curve at the ankle for manually implemented radii values and the resultant impact on the JCF at the ankle. Three shifts were implemented: +5mm, +10mm and -5mm from the original radii calculated from the US geometric fitting.
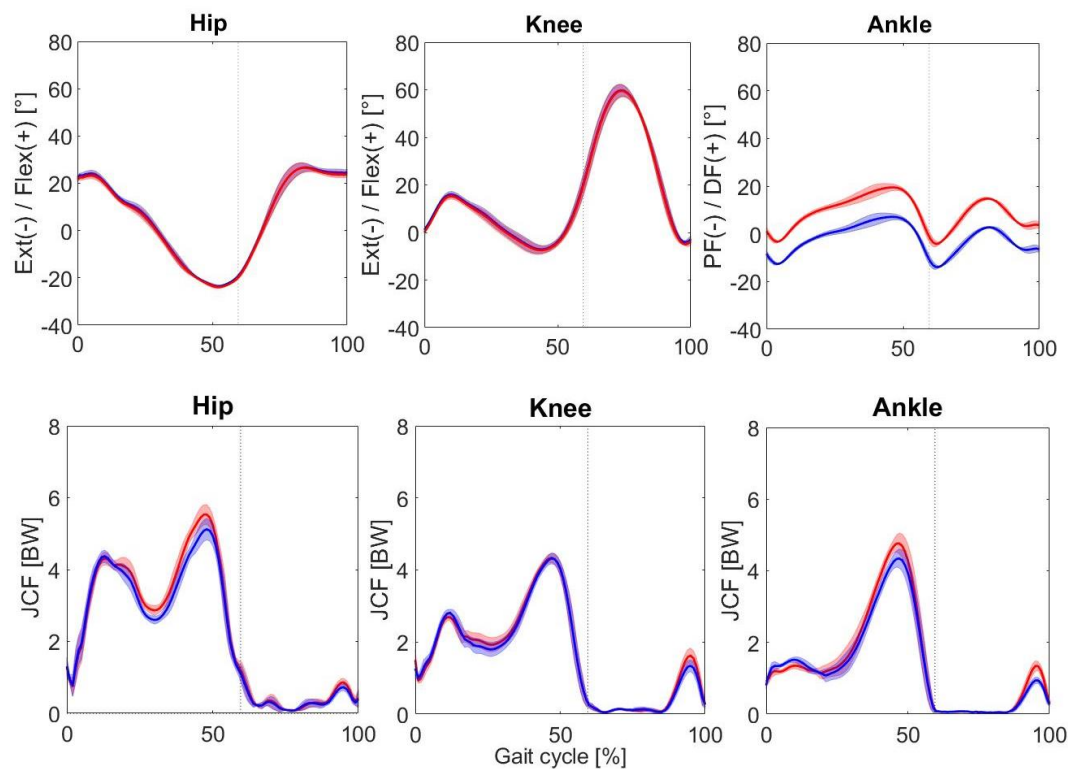
Figure 5.15. Mean and SD for the kinematics (top) and joint contact forces (bottom) using MRI (Blue) or US (Red) based joint axes estimates.
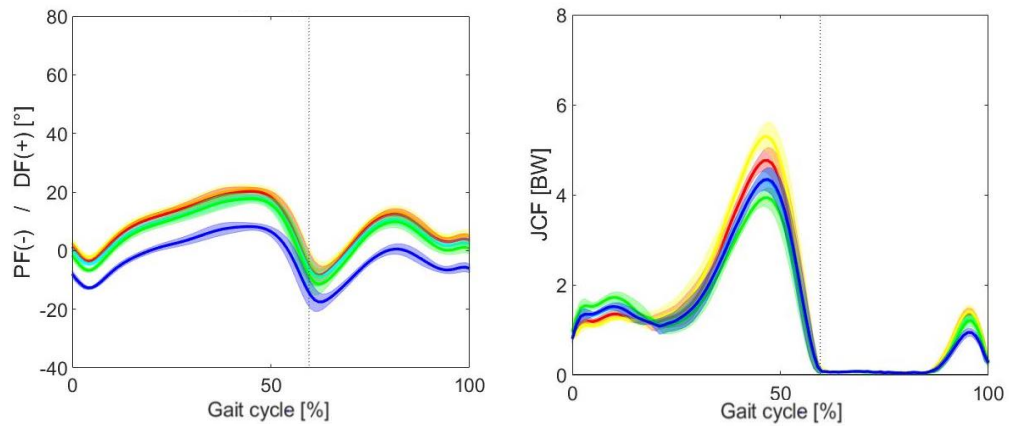
Figure 5.16. Mean and SD of the ankle kinematics (left) and resulting JCFs (right) from inputting different US talus radii with the original MRI (Blue), original US (Red), US (+5mm light blue), US (+10mm light green) and US (-5mm yellow).

5.4 Discussion

A protocol has been proposed which uses an open source package (Py3DFreeHandUS) to combine motion capture data with ultrasound data to reconstruct anatomical structures into three-dimensions. The aim of this proof of concept study was to partially replace the current techniques used to build musculoskeletal models from MR images with combined ultrasound and motion capture data.

5.4.1 Phantom measurements

Firstly, a wand tip was scanned with the ultrasound probe to see whether a known point in 3D space could be detected accurately. An accuracy of under 10mm was found in both sessions, which is less accurate than what reported in the literature of approximately 2mm (Cenni *et al.*, 2016). However, specifically identifying the wand tip with the ultrasound device may have been the main source of error. As the accurate location of the tip was identified on the ultrasound image as a single point, this may lead to a small error due to the subjectivity of the tips feature. The low SD of the measurements suggests consistency and in terms of accuracy, a slight offset is present during the processing and identification of the wand tip in the ultrasound images.

Measurements conducted on the femur phantom were performed to see whether realistic anatomical features without the interference of soft tissue artefact could be accurately determined. The first measurement consisted of reconstructing the posterior aspect of the femoral condyles such that a cylinder could be attached which in turn would define the knee joint axis of the phantom. Assumptions within the literature showing the knee joint axis of rotation moves about a cylindrical axis has been previously shown (Colle *et al.*, 2016; Renault *et al.*, 2018; Montefiori *et al.*, 2019). Cylinders can be predicted to a high degree of accuracy with small detected curvatures from least-squares algorithms and have shown to be robust in their estimation. This is shown by the measurements performed on the phantom, with cylinder radius calculations from the ultrasound reconstructions only slightly overestimating the cylinder fitted to the laser scanned phantom by up to 1.6mm±1.2mm on average in both sessions.

The second measurement consisted of reconstructing the femur head. Greater accuracy was observed for both sessions compared to the condyle measurements (less than 1mm of radii overestimation). A consequence of overestimating the measurements of the femur head was likely in the reconstruction process. Figure 5.17 shows the full curvature of the femur head could not be identified with ultrasound, which limits the segmentation process to approximately a hemisphere. This however, if accurately segmented is effective for the fitting of a full sphere and accurate calculation of the radius. The difference between the sphere fitting to the laser scanned femur (left) and fitting to a reconstructed trial (right) is shown in Figure 5.12 which displays that less structure in the reconstruction may lead to slight overestimations of the fitting.
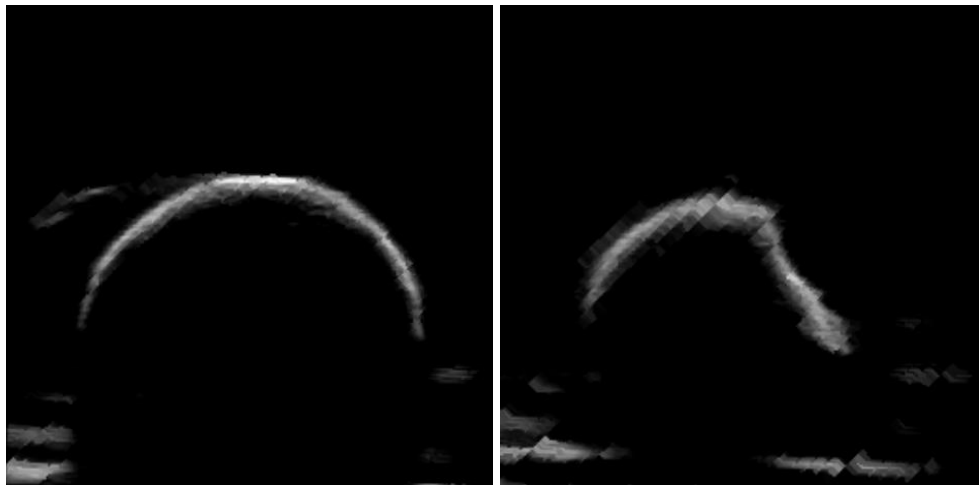
Figure 5.17. Best possible outline of the phantom femur head at its maximum diameter (left) and surface deformation on phantom (right).

Quantifying geometries such as the femoral head is extremely relevant in defining the rotation of the hip joint, and consequently the HJC of the subject. It is shown from non-image based methods, locating the HJC can be mis-calculated by up to 30mm (Sangeux, Peters and Baker, 2011). Being able to attach a sphere to reconstructed bone geometries from imaging methods allows a much greater accuracy of HJC calculation (Kainz *et al.*, 2015). The values quoted (SD < 2mm) here are well below those predicted by external anatomical landmarks and like accuracies shown by other image-based techniques. For example, Harrington et al. showed SD values of 7-8mm for HJC predictions (Harrington *et al.*, 2007).

A problem with the measurements on the femur head was an area of surface deformation which may have adversely impacted the segmentation process. This is

shown in the right image of Figure 5.11 which displays an indent in the femur head which could not be avoided in the scanning procedure. Tying to predict the curvature of the circumference may have introduced errors into the segmentation process and therefore estimation of the sphere. Whilst this deformation was not a problem when fitting a sphere to the laser scanned model, it may have had an impact in the ultrasound segmentation.

Overall, the accuracy shown in the phantom experiments meant that subject measurements were potentially feasible, and the pilot study was conducted.

5.4.2 Subject measurements

Accurately measuring the anatomy of the lower limb is essential for subject specific musculoskeletal models. Currently, internal anatomies, such as muscles and bones are dependent on gold standard imaging techniques such as MR imaging and CT-scans. Whilst this technique is non-invasive, it is expensive, meaning repeat measurements are problematic to obtain and the need for other, cheaper measurement methods is desirable. B-mode ultrasound has the potential to partially replace the need for MR-imaging due to its ability to detect various superficial anatomical features. One key part of subject specific modelling is the definition of the joint rotations of the hip, knee and ankle. This preliminary study focused on the knee joint only. This is currently defined as a one degree of freedom joint which rotates about an axis defined by a cylinder attached to the posterior condylar surface (Eckhoff *et al.*, 2005; Hancock *et al.*, 2013; Yin *et al.*, 2015; Renault *et al.*, 2018). This is the first time, to the best of the author's knowledge, that the same process has been attempted with 2D ultrasounds sequences reconstructed into 3D volumes.

The impact of geometric fitting for joint articulation on the prediction of joint kinematics is considered to be low due to the low sensitivity the knee joint axis has on musculo-skeletal models (Martelli *et al.*, 2015). For average standard deviations of 2.3mm in landmark identification of the medial and lateral epicondyles, Martelli et al. found a variation in knee axes orientation of less than 2°. This led to an average joint angle variation of 2.3° from the imposed uncertainties. It was shown that the joint co-ordinate definition has a large impact on the muscle force prediction within the model but low impact on joint contact forces. Whilst individual anatomical landmarks were not examined in this study, it is difficult to contrast whether geometric fitting of

surfaces would result in similar axis deviations and subsequent joint kinematics. However, one author studied the variation of geometric fitting to anatomical structures for ankle articulation (Hannah *et al.*, 2017). They fitted a cylinder to the ankle joint to represent the medio-lateral axis for dorsi/plantar flexion movement. They found a maximum 1.7° inter-operator (three operators, fitting a cylinder to three subjects, for three gait trials) variation for the medio-lateral axis measurement which is similar to other reported results (Martelli *et al.*, 2015).

The measurements performed showed high accuracy on both legs, with cylinder radii predictions from the ultrasound reconstructions overestimating the MRI fitted cylinders by only 2mm for both legs. For measurements on this scale, predictions under 5mm are highly desirable, and these measurements fall well under this mark. However, the standard deviation is perhaps larger than desirable, as the raw data suggests dispersion about the real value is like the calculated difference meaning single measurements should be considered with caution at this point. Determining what causes the lack of precision in the current measurements is a key next step. With respect to the impact this may have on the subject specific model, a sensitivity analysis should also be conducted for the impact of axis location in the model.

Geometric fitting of the posterior femoral condyles to define the flexion/extension axis of the knee is not a novel concept, and literature has shown its usefulness in several biomechanical fields, including musculoskeletal models and total knee arthroplasty interventions (Eckhoff *et al.*, 2007; Niki *et al.*, 2017). Furthermore, Eckhoff *et al.* (2007) found no differences between and within operators for posterior condyle cylinder attachments to 23 segmented CT scans of cadaver knees.
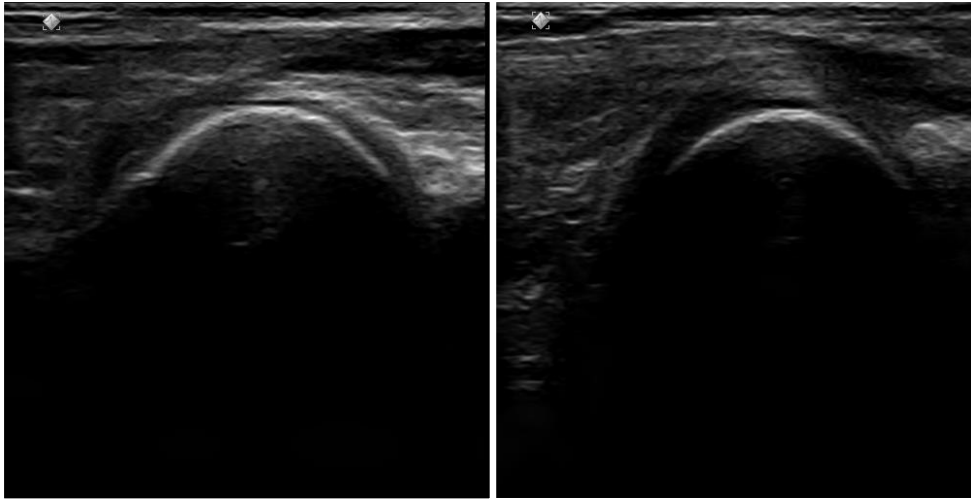
Figure 5.18. Lateral (left) and medial (right) femoral condyles at their greatest curvature during an ultrasound sweep of the posterior distal femur.

Marker based axis calculations are commonly used in gait analysis for the calculation of the knee flexion/extension axis. Specifically, the medio-lateral axis of the knee joint is calculated as a vector from the palpated medial and lateral epicondyles of the distal femur. For static measurements of the medio-lateral axis, one study has shown that marker based measurements varies considerably to gold standards (EOS radiographs) (Passmore *et al.,* 2018). The average difference in the static standing position between the measurement techniques for the knee flexion angle was 10°±11°. Their ultrasound measurements showed a much closer agreement to the reference of 1°±4° showing the effectiveness of ultrasound in young subjects with lower limb deformities.

For the femur head measurements, consistency was found and shown to be like other studies which quantified the HJC in a similar manner. For example, one study, which used a least-squares fitting approach to ultrasound reconstructions showed a median under estimation of the radius for her cohort of -2.5mm (intervals up to 3.5mm and down to -4.5mm) compared to MRI measurements (Peters *et al.*, 2012). It can be confidently stated that supine HJC measurements can be accurately measured with ultrasound.

This is the first time, to the best of my knowledge, the use of ultrasound for joint axis measurements for all lower limb joints has been used as inputs into a subject specific model. The results shown on the one subject analysed show small differences at each joint for the JCF with ultrasound slightly overestimating the JCF at all joints

by up to 0.75 BW. Figure 5.16 shows that the ankle JCF is sensitive to changes in the ankle joint kinematics. By implementing known changes in the model input (talus fitting radius), the model was sensitive to them. This shows that accuracy in measuring the talus radii is essential for future work.

The same two operator dependent stages as described in the phantom measurements were also present in the subject measurements. The first operator dependent stage was the segmentation of the 2D sequences of ultrasound images. Detecting and segmenting the curvature of the condyles was not considered to be subjective in interpretation due to the surface of the femur producing a bright, hyperechoic reflection. However, detecting the condyles, as they were emerging during the sweep was challenging in the segmentation process. This was not deemed problematic as it is not essential for last post-processing step of highlighting the condyle curvature. The second operator dependent stage was the mesh cleaning which involved removing parts of the segmentations not desirable for the cylindrical fitting. This was not quantified in terms of one operator assessing the same trial several times or across operators, but it should be a key point of investigation in the future for assessing the robustness of the workflow.

Figure 5.13 shows the difference between the cylinder attachment to the segmented MR-images (top) and segmented ultrasound images (bottom). As is clear, there is a difference in the amount of surface selected for the cylinder attachment, which was mainly down to the relatively small amount of selectable surface from the reconstructed ultrasound images. However, it is apparent that this has little impact on the results.

5.4.3 Current limitations

One of the assumptions behind this study was that there was negligible difference in the size of the medial and lateral condyles of the distal femur, which might affect the validity of the cylindrical fitting. One study conducted a rigorous analysis of the curvature of the condyles with the use of 16 laser scanned cadaver lower limbs. They measured the radius of the medial and lateral as 18.71mm±1.71mm and 20.33mm±1.80mm (Kosel *et al.*, 2010). However, a later study has found no differences in medial and lateral condyle radii (17.4mm±1.6mm and 17.3mm±1.4mm respectively) through a cylindrical fitting method conducted on 3D models

reconstructed from the CT scans of 122 knees (Niki *et al.*, 2017). Whilst these two studies oppose one another, overall, this was considered not to have an impact on the cylindrical fitting in this study but there is the potential this may adversely impact the results. This would currently be challenging with ultrasound, as its limited view of the posterior condyles limits the extent of the analysis which can be conducted, therefore MRI may be a better initial alternative. Other literature shows the knee to consist of two points of curvature, with differences in the radius of the condyles between anterior and posterior aspects of the distal femur (Pinskerova *et al.*, 2000). Therefore, this highlights the current relative simplicity of cylinder attachment to the posterior condyles, though the impact of this would need to be quantified.

The current method of gap filling for the voxel-array reconstruction, VNN, used in the data processing of this study is known for its fast implantation, but is less accurate than other methods (Rohling *et al.,* 1999). For these measurements, the longest reconstructions took 30 minutes (bottle scans and subject scans took approximately the same amount of time). When processing relatively large volumes, such as the posterior knee, it is undesirable to use an algorithm which takes in the order of hours to process. For the current overall method, it is realistic to conceive, from measurements to radii calculation, a total time of 2-3 hours.

The main disadvantage of the VNN algorithm is the "collage" artefact it presents in the gap filling process, which is mainly sensitive to tissue movements and instrument error (Rohling, Gee and Berman, 1999). It occurs due to a slice plane which intersects several ultrasound images. This was the main reason for discarding some of the trials, as the segmentation process was impeded due to the artefacts. Whilst present in most trials, rarely was it severe enough to affect the objectivity of the segmentation. Figure 5.19 shows the impact this has on the reconstruction.
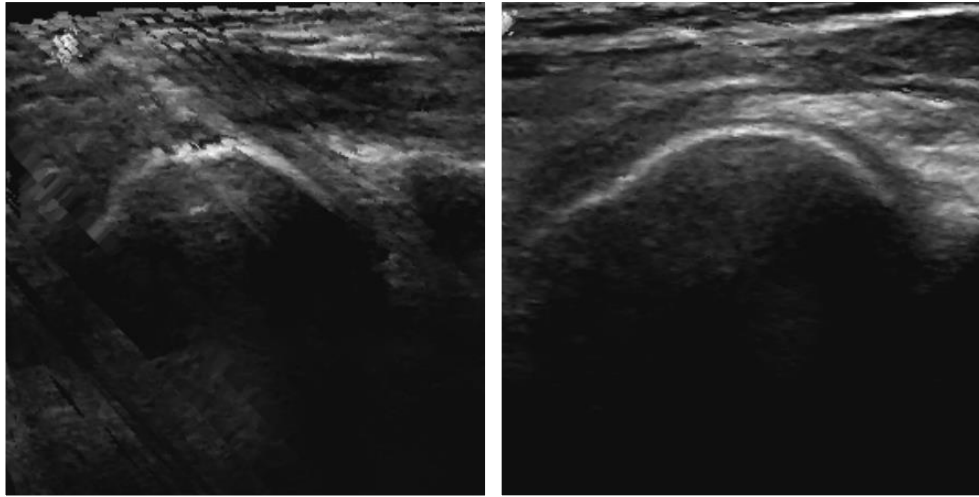
Figure 5.19. Severe (left) and minor (right) artefacts from VNN reconstructions. Left ultrasound slice is affected by the reconstruction, making segmentation challenging. Right ultrasound slice has minor distortion in the top right section but does not affect the segmentation process.

All motion capture data were filtered with a fourth order, low pass Butterworth filter at a cut off frequency of 5Hz as is common practice with kinematic marker trajectories. This minimised the instrumental noise which in some cases was apparent on the ultrasound probe's marker cluster. In all cases where the data filtering was not enough to smooth the data set, the trial was re-performed and, if significant artefacts were observed in the gap filling, trials were discarded.

Freehand ultrasound presents a flexible measurement method for the assessment of musculoskeletal parameters, but it doesn't come without disadvantages. The main disadvantage is the ability of the operator which will need at least a basic understanding in image optimisation and knowledge in the interpretation of the features of an ultrasound image. The scanning of bone, however, is probably the least susceptible anatomy to anisotropy during an ultrasound scan due to its high relative density difference compared to the surrounding tissue (muscles, tendons etc.). Manipulation and control of the ultrasound probe in a freehand sweep takes practice and the dependence of the measurement conducted in this study on the operator should be quantified. It also not known how much the speed of the acquisition impacts the reconstructions. An estimated speed has been given (20mm/s), though what may be interesting for future analysis is the sensitivity of sweep speed to the reconstructions. Whilst the measurements felt consistent, purposefully measuring slower and faster sweeps may determine whether acquisition speed adversely impacts the results or not at all.

One method for potentially improving image quality is to average image acquisitions gained to improve the smoothness of the bony surfaces which appear very clearly on the image. Smoothing from multiple images may allow for the 'cleaning' of images which were prone to being less distinct and subject to significant noise. This is a key disadvantage to ultrasound which is reliant on expertise in identifying distinguishing features on the image. If this dependency can be reduced by improving the image quality and contrast between certain features through averaging, the reliability of using ultrasound could be improved in this context.

The time required currently for going from the measurements to the final processed geometries is also relatively long. For a single trial, the experimental trial is very quick (<1 minute). For the initial post-processing (labelling the trial in Nexus) is also fast (<2 minutes) however the reconstruction into the relative co-ordinate system is currently time consuming (15 minutes) with room to be speeded up. The next processing step (reconstruction of the ultrasound images) takes up to 10 minutes. Then the segmentation and organisation of the DICOM file can take 15 minutes. The next step is the cleaning of the geometries (15 minutes). Following this is the geometric fitting of the geometries which is a further 5 minutes. Therefore, a total time of an hour per trial. This scaled up to several repeats over several joints makes this a time-consuming process.

Currently, only a small investigation into the impact of ultrasound on the musculoskeletal model has been performed which limits the interpretation of the results. A comprehensive validation will be needed including the sensitivity of single axis measurements on the outputs of the MSK model. Currently, the talus measurements inputted into the model is a single value as only one measurement was collected. An evaluation of whether the ankle can be considered for the ultrasound measurements needs to be performed through further investigation.

Alternatives to this current setup exist and could be considered viable alternatives in the future. Cenni *et al.* (2016) showed that similar accuracies in reconstruction and calculations can be obtained with an OptiTrack (OptiTrack, NaturalPoint, USA) system which reduces the need for an expensive motion capture system, which us beneficial for experiments using relatively small volumes.

To conclude, a promising pipeline for ultrasound measurements of lower limb joint axis has been developed and implemented into subject specific models. The next step will be for a significant validation of the measurement process on a healthy cohort. Another step will be the implementation of the hip and knee joint axis measurement techniques used in this chapter into the OrthoPilot device for potentially improving the accuracy of the system and therefore pre-operative planning measurements.

Chapter VI

Conclusion

In this chapter, an overview is given of the key work achieved, the novelty and the future of the research. In brief, the aim of the thesis was to establish non-invasive protocols for pre-operative planning in knee and hip surgeries. Several objectives included developing motion capture and ultrasound experiments for measurements of knee and pelvic alignment. The ultrasound measurements were also applied to the development of musculoskeletal models to reduce the dependency of MR-imaging.

6.1 Summary

Chapter 3 showed that pre-operative planning with the use of ultrasound and motion capture is practical, as performed with OrthoPilot for measurements of varus-valgus, flexion-extension, and femur and tibia lengths. Initial reliability was shown on a phantom which was followed by a small subject cohort. Supine and standing measurements were conducted which showed the flexibility of the measurement system unlike common alternatives (X-Ray, MRI, CT) which are typically limited to standing or supine positions. Three operators performed precise measurements of key lower limb parameters. For varus-valgus measurements, there was a maximum of one-degree difference between operators. For the segment lengths, there was less than 5mm difference for all measurements between operators. Femur and tibia torsions on the other hand, showed less precision in their measurements. All three operators exhibited the same imprecision in these measurements. Due to the small cohort, quantifying the differences between supine and standing can only be treated on individual cases and no population-based assumptions could be drawn from the results unlike that shown by other studies (Bellemans *et al.*, 2012).

The use of the *smart system* in Chapter 4 for pre-operative planning in hip arthroplasty operations was shown to be less feasible and quantification of potential errors in the measurement process did not get to the root cause of the variability. Equivalent measurements using only a motion capture system and palpating wand also

were deemed unsatisfactory and not fit for further development. The reasons for developing these methods were like the reasons discussed with respect to the OrthoPilot measurements due to their flexibility in subject positioning. The variability between sitting, supine and standing positions for measurements of pelvic tilt has been extensively investigated in the literature but often through invasive means (Philippot *et al.*, 2009; J. Lazennec *et al.*, 2015; Uemura *et al.*, 2017). The need for a non-invasive measurement method for pelvic tilt measurements is still desired.

Three-dimensional reconstructions of ultrasound images for joint axis calculation of the lower limb, as shown in Chapter 5 demonstrated feasibility for implementation into musculoskeletal models. Initial ultrasound trials on a femur phantom showed good accuracy of measuring the radii of the femur head and femur condyles with accuracies of less than 1mm for condyle reconstructions and less than 5mm for femur head reconstructions. For the one subject measured, a pipeline has been developed that allows for the calculation of knee and hip joint axis to be measured accurately with ultrasound with small impacts (less than one body weight of joint contact forces) on the musculoskeletal model outputs. The measurement of the ankle joint axis was less robust and subject to difficulties.

The scientific output from the thesis included publication of the work in Chapter 3 (Greatrex *et al.*, 2017). The work from Chapter 3 was also presented at the International Society of Biomechanics conference, 2017. The work from Chapter 5 resulted in a poster presentation at the Computer Methods in Biomechanics and Biomedical Engineering conference, 2019.

6.2 Main Limitations

One of the main limitations was the use of a phantom in absence of soft tissue for the initial accuracy measurements. This could have been assessed with the use of several cadaver limbs which would provide a realistic measurement process as the presence of soft tissue artefact greatly affects the operator's ability to distinguish key features. Comparisons could then have been assessed with MRI of the cadaver limbs.

The second main limitation was that the experiments were all performed on healthy subjects. Assessing a patient cohort would have tested the robustness of the protocols and assessed whether using ultrasound in patients with degenerative diseases

that affect bone geometries and are potentially higher BMI as a feasible approach for assessment in pre-operative planning.

6.3 Novelty

For the measurements of lower limb parameters with OrthoPilot, this was the first time several lower limb parameters such as varus-valgus and femur and tibia torsion, have been quantified in both supine and standing with the use of ultrasound. Varus-valgus has been quantified in supine and standing in the literature only with invasive techniques, such as lower limb radiographs, or lengthy imaging procedures like MRI (Brouwer *et al.*, 2003; Sabharwal and Zhao, 2008; Duffell *et al.*, 2014; Gbejuade *et al.*, 2014; Guggenberger *et al.*, 2014; Winter *et al.*, 2014). Chapter 3 and its related publication portray the potential of ultrasound in pre-operative planning with the use of an intra-operative aid. The flexibility to switch between pre-operative planning and surgical execution could streamline the overall procedure for the patient. Chapter 3 is the first step in achieving this aspiration.

Chapter 4 showed the need and challenges for a non-invasive measurement method for pre-operative planning in total hip arthroplasty. The measurements conducted were the first attempted in terms of using motion capture for pelvic tilt detection from several different sets of palpable landmarks on the pelvis in several positions. The development of the protocol was the first of its kind and sets out a process which can be developed and worked on for future testing. Measuring subjects in the supine position was found to be problematic compared to standing and sitting.

Chapter 5 quantified for the first time the impact of replacing all lower limb joint axes, typically gained from MRI, with ultrasound for inputs into musculoskeletal models. The differences quantified in the joint reaction forces at each joint were small. This was the first time, to the best of my knowledge, such a procedure has been performed. Though individually, for the hip joint for example, reconstructions of the femur curvature with ultrasound has been previously performed (Peters, Baker and Sangeux, 2010). Comparable accuracies were found in Chapter 5. For the knee joint axis, no other studies have been found which have reconstructed the posterior condyles with ultrasound. Whilst the ankle joint was less successful in ultrasound reconstructions, this was the first time this has been attempted as well.

6.4 Future Work

The OrthoPilot results represented the first step in crossing over pre-operative planning with the intra-operative procedure. This will need to be developed further through testing on a large patient cohort who will undergo knee surgery with the primary aim of quantifying the varus-valgus difference between supine and standing. This additional information for the surgeon will be a useful addition in potentially quantifying the best re-alignment angle for the prosthesis. The information gained from this thesis should also be tested with respect to improving the image acquisition protocol that is currently required with OrthoPilot. It is hypothesised that gaining 3D reconstructions of each joint, following a procedure like the one used in the final chapter of this thesis, will provide greater accuracy in lower limb parameter calculations.

The potential of ultrasound and its impact on musculoskeletal models has been explored at a pilot level. Undoubtedly, a crucial limitation of the study was that only one subject was tested, meaning a restricted conclusion could be made about the results. Therefore, the key next step will be a large validation study on healthy subjects. Moreover, the ultrasound measurements were only successfully performed in the supine position. Therefore, performing the measurements reliably and accurately in the standing position will also be a key point of investigation. This will then help with the proposed improvements to the OrthoPilot system.

References

Ala Eddine, T. *et al.* (2001) 'Variations of pelvic anteversion in the lying and standing positions analysis of 24 control subjects and implications for CT measurement of position of a prosthetic cup', *Surgical and Radiologic Anatomy*, 23(2), pp. 105–110. doi: 10.1007/s00276-001-0105-z.

Anda, S. *et al.* (1990) 'Pelvic inclination and spatial orientation of the acetabulum. A radiographic, computed tomographic and clinical investigation.', *Acta radiologica*, 31(4), pp. 389–394. doi: 10.3109/02841859009172013.

Archibeck, M. J. *et al.* (2016) 'Inaccuracies in the Use of Magnification Markers in Digital Hip Radiographs', *Clinical Orthopaedics and Related Research*. Springer US, 474(8), pp. 1812–1817. doi: 10.1007/s11999-016-4704-8.

Babazadeh, S. *et al.* (2013) 'The long leg radiograph is a reliable method of assessing alignment when compared to computer-assisted navigation and computer tomography', *Knee*. Elsevier B.V., 20(4), pp. 242–249. doi: 10.1016/j.knee.2012.07.009.

Beardsley, C., Egerton, T. and Skinner, B. (2016) 'Test–re-test reliability and inter-rater reliability of a digital pelvic inclinometer in young, healthy males and females', *PeerJ*, 4(2013), p. e1881. doi: 10.7717/peerj.1881.

Bell, A. L., Brand, R. A. and Pedersen, D. R. (1989) 'Prediction of hip joint centre location from external landmarks', *Human Movement Science*, 8(1), pp. 3–16. doi: 10.1016/0167-9457(89)90020-1.

Bellemans, J. *et al.* (2012) 'In Neutral Mechanical Alignment Normal for All Patients? The Concept of Constitutional Varus', *Clinical Orthopaedics and Related Research*, 470(1), pp. 45–53. doi: 10.1007/s11999-011-1936-5.

Bendaya, S. *et al.* (2015) 'Healthy vs. osteoarthritic hips: A comparison of hip, pelvis and femoral parameters and relationships using the EOS?? system', *Clinical Biomechanics*. Elsevier Ltd, 30(2), pp. 195–204. doi: 10.1016/j.clinbiomech.2014.11.010.

Blondel, B. *et al.* (2009) 'Pelvic tilt measurement before and after total hip arthroplasty.', *Orthopaedics & traumatology, surgery & research : OTSR*, 95(8), pp. 568–572. doi: 10.1016/j.otsr.2009.08.004.

Bloomfield, R. A. *et al.* (2018) 'Proposal and Validation of a Knee Measurement System for Patients with Osteoarthritis', *IEEE Transactions on Biomedical Engineering*, 9294(c), pp. 1–8. doi: 10.1109/TBME.2018.2837620.

Brouwer, R. W. *et al.* (2003) 'The whole leg radiograph: standing versus supine for determining axial alignment.', *Acta orthopaedica Scandinavica*, 74(5), pp. 565–8. doi: 10.1080/00016470310017965.

Cappozzo, a. *et al.* (1995) 'Position and orientation in space of bones during movement: anatomical frame definition and determination', *Clinical Biomechanics*, 10(4), pp. 171–178. doi: 10.1016/0268-0033(95)91394-T.

Cenni, F. *et al.* (2016) 'The reliability and validity of a clinical 3D freehand ultrasound system', *Computer Methods and Programs in Biomedicine*. Elsevier Ireland Ltd, 136, pp. 179–187. doi: 10.1016/j.cmpb.2016.09.001.

Chiari, L. *et al.* (2005) 'Human movement analysis using stereophotogrammetry', *Gait & Posture*, 21(2), pp. 197–211. doi: 10.1016/j.gaitpost.2004.04.004.

Chinnappa, J. *et al.* (2017) 'Predictors and Functional Implications of Change in Leg Length After Total Knee Arthroplasty', *The Journal of Arthroplasty*. Elsevier Ltd, 32(9), pp. 2725-2729.e1. doi: 10.1016/j.arth.2017.04.007.

Cignoni, P. *et al.* (2008) 'MeshLab: an Open-Source Mesh Processing Tool', *Eurographics Italian Chapter Conference 2008: Salerno, Italy*, pp. 129–136. doi: 10.2312/LocalChapterEvents/ItalChap/ItalianChapConf2008/129-136.

Colle, F. *et al.* (2016) 'Comparison of three formal methods used to estimate the functional axis of rotation: an extensive in-vivo analysis performed on the knee joint.', *Computer methods in biomechanics and biomedical engineering*. Taylor & Francis, 19(5), pp. 484–92. doi: 10.1080/10255842.2015.1042464.

Cooperstein, R. and Hickey, M. (2016) 'The reliability of palpating the posterior superior iliac spine: a systematic review', *J Can Chiropr Assoc*, 60(1), pp. 36–46. Available at: http://www.ncbi.nlm.nih.gov/pubmed/4807681.

Culliford, D. *et al.* (2015) 'Future projections of total hip and knee arthroplasty in the UK: results from the UK Clinical Practice Research Datalink', *Osteoarthritis and Cartilage*. Elsevier Ltd, 23(4), pp. 594–600. doi: 10.1016/j.joca.2014.12.022.

Deep, K. *et al.* (2016) 'A Comparison of Three Different Methods of Measurement of Knee Deformity in Osteoarthritis', *Journal of Orthopedics, Rheumatology and sports Medicine*, (January). doi: 10.19104/jorm.2016.107.

Deep, K., Eachempati, K. K. and Apsingi, S. (2015) 'The dynamic nature of alignment and variations in normal knees', *The Bone & Joint Journal*, 97-B(4), pp. 498–502. doi: 10.1302/0301-620X.97B4.33740.

Delp, S. L. *et al.* (1990) 'An interactive graphics-based model of the lower extremity to study orthopaedic surgical procedures', *IEEE Transactions on Biomedical Engineering*, 37(8), pp. 757–767. doi: 10.1109/10.102791.

Delp, S. L. *et al.* (2007) 'OpenSim: Open-Source Software to Create and Analyze Dynamic Simulations of Movement', *IEEE Transactions on Biomedical Engineering*, 54(11), pp. 1940–1950. doi: 10.1109/TBME.2007.901024.

DiGioia, A. M. *et al.* (2006) 'Functional Pelvic Orientation Measured from Lateral Standing and Sitting Radiographs', *Clinical Orthopaedics and Related Research*, 453(January), pp. 272–276. doi: 10.1097/01.blo.0000238862.92356.45.

Donati, M. *et al.* (2007) 'Enhanced anatomical calibration in human movement analysis', *Gait & Posture*, 26(2), pp. 179–185. doi: 10.1016/j.gaitpost.2007.04.009.

Duffell, L. D. *et al.* (2014) 'The knee adduction angle of the osteo-arthritic knee: A comparison of 3D supine, static and dynamic alignment.', *The Knee*. Elsevier B.V., 21(6), pp. 1096–100. doi: 10.1016/j.knee.2014.09.002.

Durandet, A. *et al.* (2013) 'Radiographic Analysis of Lower Limb Axial Alignments', *Proceedings of the*, II.

Eckhoff, D. *et al.* (2007) 'Difference between the epicondylar and cylindrical axis of the knee.', *Clinical orthopaedics and related research*, 461(461), pp. 238–44. doi: 10.1097/BLO.0b013e318112416b.

Eckhoff, D. G. *et al.* (2005) 'Three-dimensional mechanics, kinematics, and morphology of the knee viewed in virtual reality.', *The Journal of bone and joint surgery. American volume*, 87 Suppl 2(suppl_2), pp. 71–80. doi: 10.2106/JBJS.E.00440.

Escott, B. G. *et al.* (2013) 'EOS Low-Dose Radiography: A Reliable and Accurate Upright Assessment of Lower-Limb Lengths', *The Journal of Bone and Joint Surgery (American)*, 95(23), p. e183 1. doi: 10.2106/JBJS.L.00989.

Faria, R. *et al.* (2013) 'The EOS 2D/3D X-ray imaging system: a cost-effectiveness analysis quantifying the health benefits from reduced radiation exposure.', *European journal of radiology*. Elsevier Ireland Ltd, 82(8), pp. e342-9. doi: 10.1016/j.ejrad.2013.02.015.

Fiorentino, Niccolo M. *et al.* (2016) 'Accuracy of Functional and Predictive Methods to Calculate the Hip Joint Center in Young Non-pathologic Asymptomatic Adults with Dual Fluoroscopy as a Reference Standard', *Annals of Biomedical Engineering*, 44(7), pp. 2168–2180. doi: 10.1007/s10439-015-1522-1.

Fiorentino, Niccolo M *et al.* (2016) 'Gait & Posture In-vivo quanti fi cation of dynamic hip joint center errors and soft tissue artifact', *Gait & Posture*. Elsevier B.V., 50, pp. 246–251. doi: 10.1016/j.gaitpost.2016.09.011.

Folinais, D. *et al.* (2013) 'Measuring femoral and rotational alignment: EOS system versus computed tomography', *Orthopaedics & Traumatology: Surgery & Research*. Elsevier Masson SAS, 99(5), pp. 509–516. doi: 10.1016/j.otsr.2012.12.023.

Gajdosik, R. *et al.* (1985) 'Pelvic tilt. Intratester reliability of measuring the standing position and range of motion.', *Physical therapy*, 65(2), pp. 169–74. Available at: http://www.ncbi.nlm.nih.gov/pubmed/3969397.

Gbejuade, H. O. *et al.* (2014) 'Do long leg supine CT scanograms correlate with weight-bearing full-length radiographs to measure lower limb coronal alignment?', *Knee*. Elsevier B.V., 21(2), pp. 549–552. doi: 10.1016/j.knee.2013.05.009.

Goldstein, Z. H. *et al.* (2016) 'Perceived Leg-Length Discrepancy After Primary Total Knee Arthroplasty: Does Knee Alignment Play a Role?', *American journal of orthopedics (Belle Mead, N.J.)*, 45(7), pp. E429–E433. Available at: http://ovidsp.ovid.com/athens/ovidweb.cgi?T=JS&CSC=Y&NEWS=N&PAGE=fulltext&D=emexa&AN=616762516%0Ahttp://openurl.ac.uk/ukfed:uwe.ac.uk?sid=OVID:embase&id=pmid:28005109&id=doi:&issn=1934-3418&isbn=&volume=45&issue=7&spage=E429&pages=E429-E433&date=2016&titl.

Greatrex, F. *et al.* (2017) 'Reliability of an Integrated Ultrasound and Stereophotogrammetric System for Lower Limb Anatomical Characterisation', *Applied Bionics and Biomechanics*, 2017, pp. 1–8. doi: 10.1155/2017/4370649.

Guggenberger, R. *et al.* (2014) 'Assessment of Lower Limb Length and Alignment by Biplanar Linear Radiography: Comparison With Supine CT and Upright Full-Length Radiography', *American Journal of Roentgenology*, 202(2), pp. W161–W167. doi: 10.2214/AJR.13.10782.

Hagins, M. *et al.* (1998) 'Intratester and Intertester Reliability of the Palpation Meter (PALM) in Measuring Pelvic Position', *Journal of Manual & Manipulative Therapy*. Taylor & Francis, 6(3), pp. 130–136. doi: 10.1179/jmt.1998.6.3.130.

Hancock, C. W. *et al.* (2013) 'Cylindrical Axis, Not Epicondyles, Approximates Perpendicular to Knee Axes', *Clinical Orthopaedics and Related Research®*, 471(7), pp. 2278–2283. doi: 10.1007/s11999-013-2864-3.

Hannah, I. *et al.* (2017) 'Sensitivity of a juvenile subject-specific musculoskeletal model of the ankle joint to the variability of operator-dependent input', *Proceedings of the Institution of Mechanical Engineers, Part H: Journal of Engineering in Medicine*, 231(5), pp. 415–422. doi: 10.1177/0954411917701167.

Harrington, M. E. *et al.* (2007) 'Prediction of the hip joint centre in adults, children, and patients with cerebral palsy based on magnetic resonance imaging', *Journal of Biomechanics*, 40(3), pp. 595–602. doi: 10.1016/j.jbiomech.2006.02.003.

Hart, D. and Wall, B. F. (2004) 'UK population dose from medical X-ray examinations', *European Journal of Radiology*, 50(3), pp. 285–291. doi: 10.1016/S0720-048X(03)00178-5.

Hasart, O., Perka, C. and Tohtz, S. (2008) 'Comparison between pointer-based and ultrasound-based navigation technique in THA using a minimally invasive approach.', *Orthopedics*, 31(10 Suppl 1). Available at: http://www.ncbi.nlm.nih.gov/pubmed/19298038.

Hassan, D. M. *et al.* (1998) 'Accuracy of intraoperative assessment of acetabular prosthesis placement.', *The Journal of arthroplasty*, 13(1), pp. 80–4. doi: 10.1016/S0883-5403(98)90079-1.

Hauschild, O. *et al.* (2009) 'Reliability of leg alignment using the OrthoPilot system depends on knee position: A cadaveric study', *Knee Surgery, Sports Traumatology, Arthroscopy*, 17(10), pp. 1143–1151. doi: 10.1007/s00167-009-0825-x.

Herrington, L. (2011) 'Assessment of the degree of pelvic tilt within a normal asymptomatic population', *Manual Therapy*. Elsevier Ltd, 16(6), pp. 646–648. doi: 10.1016/j.math.2011.04.006.

Hicks, J. L. and Richards, J. G. (2005) 'Clinical applicability of using spherical fitting to find hip joint centers', *Gait and Posture*, 22(2), pp. 138–145. doi: 10.1016/j.gaitpost.2004.08.004.

Hinman, R. S., May, R. L. and Crossley, K. M. (2006) 'Is there an alternative to the full-leg radiograph for determining knee joint alignment in osteoarthritis?', *Arthritis Care and Research*, 55(2), pp. 306–313. doi: 10.1002/art.21836.

Hinterwimmer, S. *et al.* (2008) 'An MRI-based technique for assessment of lower extremity deformities-reproducibility, accuracy, and clinical application.', *European radiology*, 18(7), pp. 1497–505. doi: 10.1007/s00330-008-0896-y.

Hudson, D., Royer, T. and Richards, J. (2006) 'Ultrasound measurements of torsions in the tibia and femur.', *The Journal of bone and joint surgery. American volume*, 88(1), pp. 138–143. doi: 10.2106/JBJS.D.02924.

Hunt, M. A. *et al.* (2006) 'Foot rotational effects on radiographic measures of lower limb alignment', *Canadian Journal of Surgery*, 49(6), pp. 401–406.

Hunt, M. A. *et al.* (2008) 'Measures of frontal plane lower limb alignment obtained from static radiographs and dynamic gait analysis', *Gait & Posture*, 27(4), pp. 635–640. doi: 10.1016/j.gaitpost.2007.08.011.

Iwana, D. *et al.* (2013) 'Accuracy of angle and position of the cup using computed tomography-based navigation systems in total hip arthroplasty', *Computer Aided Surgery*, 18(5–6), pp. 187–194. doi: 10.3109/10929088.2013.818713.

Jia, R. *et al.* (2016) 'A computer-aided tracking and motion analysis with ultrasound (CAT & MAUS) system for the description of hip joint kinematics', *International Journal of Computer Assisted Radiology and Surgery*, 11(11), pp. 1965–1977. doi: 10.1007/s11548-016-1443-y.

Jia, R. *et al.* (2017) 'CAT & MAUS: A novel system for true dynamic motion measurement of underlying bony structures with compensation for soft tissue movement', *Journal of Biomechanics*. Elsevier Ltd, 62, pp. 156–164. doi: 10.1016/j.jbiomech.2017.04.015.

Junk, S. *et al.* (1992) 'Leg length inequality measured by ultrasound and clinical methods', *European Journal of Radiology*, 14(3), pp. 185–188. doi: 10.1016/0720-048X(92)90083-L.

Kainz, H. *et al.* (2015) 'Estimation of the hip joint centre in human motion analysis: A systematic review', *Clinical Biomechanics*, 30(4), pp. 319–329. doi: 10.1016/j.clinbiomech.2015.02.005.

Kanawade, V., Dorr, L. D. and Wan, Z. (2014) 'Predictability of Acetabular Component Angular Change with Postural Shift from Standing to Sitting Position', *The Journal of Bone and Joint Surgery-American Volume*, 96(12), pp. 978–986. doi: 10.2106/JBJS.M.00765.

van Kessel-Cobelens, A. M. *et al.* (2008) 'Pregnancy-Related Pelvic Girdle Pain: Intertester Reliability of 3 Tests to Determine Asymmetric Mobility of the Sacroiliac Joints', *Journal of Manipulative and Physiological Therapeutics*, 31(2), pp. 130–136. doi: 10.1016/j.jmpt.2007.12.003.

Kmita, A. and Lucas, N. P. (2008) 'Reliability of physical examination to assess asymmetry of anatomical landmarks indicative of pelvic somatic dysfunction in subjects with and without low back pain', *International Journal of Osteopathic Medicine*, 11(1), pp. 16–25. doi: 10.1016/j.ijosm.2008.01.003.

Kochman, A. *et al.* (2017) 'Application of Navigated Ultrasound for Assessment of the Anterior Pelvic Plane in Patients With Degenerative Hip Diseases', *Journal of Ultrasound in Medicine*, 36(7), pp. 1373–1380. doi: 10.7863/ultra.16.07016.

Kosel, J. *et al.* (2010) 'Anatomical Study of the Radius and Center of Curvature of the Distal Femoral Condyle', *Journal of Biomechanical Engineering*,

132(9), p. 091002. doi: 10.1115/1.4002061.

Kulig, K. *et al.* (2010) 'Measurement of femoral torsion by ultrasound and magnetic resonance imaging: concurrent validity.', *Physical therapy*, 90(11), pp. 1641–1648. doi: 10.2522/ptj.20090391.

Kurtz, S. (2005) 'Prevalence of Primary and Revision Total Hip and Knee Arthroplasty in the United States From 1990 Through 2002', *The Journal of Bone and Joint Surgery (American)*, 87(7), p. 1487. doi: 10.2106/JBJS.D.02441.

Kurtz, S. (2007) 'Projections of Primary and Revision Hip and Knee Arthroplasty in the United States from 2005 to 2030', *The Journal of Bone and Joint Surgery (American)*, 89(4), p. 780. doi: 10.2106/JBJS.F.00222.

Lang, J. E. *et al.* (2012) 'Magnitude of Limb Lengthening After Primary Total Knee Arthroplasty', *The Journal of Arthroplasty*. Elsevier Inc., 27(3), pp. 341–346. doi: 10.1016/j.arth.2011.06.008.

Lazennec, J. *et al.* (2015) 'Total Hip Prostheses in Standing, Sitting and Squatting Positions: An Overview of Our 8 Years Practice Using the EOS Imaging Technology', *The Open Orthopaedics Journal*, 9(1), pp. 26–44. doi: 10.2174/1874325001509010026.

Lazennec, J. Y. *et al.* (2011) 'Pelvis and total hip arthroplasty acetabular component orientations in sitting and standing positions: Measurements reproductibility with EOS imaging system versus conventional radiographies', *Orthopaedics and Traumatology: Surgery and Research*. Elsevier Masson SAS, 97(4), pp. 373–380. doi: 10.1016/j.otsr.2011.02.006.

Lazennec, J. Y. *et al.* (2015) 'Measuring extension of the lumbar–pelvic–femoral complex with the EOS® system', *European Journal of Orthopaedic Surgery and Traumatology*. Springer Paris, 25(6), pp. 1061–1068. doi: 10.1007/s00590-015-1603-8.

Lazennec, J. Y. *et al.* (2016) 'Do Patients' Perceptions of Leg Length Correlate With Standing 2- and 3-Dimensional Radiographic Imaging?', *The Journal of Arthroplasty*, 31(10), pp. 2308–2313. doi: 10.1016/j.arth.2016.03.065.

Leardini, A. *et al.* (1999) 'Validation of a functional method for the estimation of hip joint centre location', *Journal of Biomechanics*, 32(1), pp. 99–103. doi: 10.1016/S0021-9290(98)00148-1.

Leitzes, A. H. *et al.* (2005) 'Reliability and accuracy of MRI scanogram in the evaluation of limb length discrepancy.', *Journal of pediatric orthopedics*, 25(6), pp. 747–749. doi: 10.1097/01.bpo.0000173246.12184.a5.

Lewinnek, B. Y. G. E. *et al.* (1978) 'Dislocations after Total Hip Arthroplasties', *The Journal of Bone & Joint Surgery*, 60-A(2), pp. 217–220.

Liodakis, E. *et al.* (2011) 'Upright MRI measurement of mechanical axis and frontal plane alignment as a new technique: A comparative study with weight bearing full length radiographs', *Skeletal Radiology*, 40(7), pp. 885–889. doi: 10.1007/s00256-010-1074-2.

Maderbacher, G. *et al.* (2017) 'Presence of rotational errors in long leg radiographs after total knee arthroplasty and impact on measured lower limb and

component alignment', *International Orthopaedics*. International Orthopaedics, 41(8), pp. 1553–1560. doi: 10.1007/s00264-017-3408-3.

Malchau, H. *et al.* (2002) 'The Swedish Total Hip Replacement Register.', *The Journal of bone and joint surgery. American volume*, 84-A Suppl(Suppl 2), pp. 2–20. Available at: http://www.ncbi.nlm.nih.gov/entrez/query.fcgi?cmd=Retrieve&db=PubMed&dopt=Citation&list_uids=12479335.

Marques, C. J., Martin, T., Fiedler, F., *et al.* (2018) 'Intra- and Inter-rater Reliability of Navigated Ultrasound in the Assessment of Pelvic Tilt in Symptom-Free Young Adults', *Journal of Ultrasound in Medicine*. doi: 10.1002/jum.14581.

Marques, C. J., Martin, T., Kochman, A., *et al.* (2018) 'Pelvic Tilt Angle Differences Between Symptom-Free Young Subjects and Elderly Patients Scheduled for THA: The Rationale for Tilt-Adjusted Acetabular Cup Implantation', *The Open Orthopaedics Journal*, 12(1), pp. 364–372. doi: 10.2174/1874325001812010364.

Martelli, S. *et al.* (2015) 'Sensitivity of a subject-specific musculoskeletal model to the uncertainties on the joint axes location', *Computer Methods in Biomechanics and Biomedical Engineering*. Taylor & Francis, 18(14), pp. 1555–1563. doi: 10.1080/10255842.2014.930134.

Martin, A. and von Strempel, A. (2006) 'Two-year Outcomes of Computed Tomography-based and Computed Tomography Free Navigation for Total Knee Arthroplasties', *Clinical Orthopaedics and Related Research*, PAP(449), pp. 275–282. doi: 10.1097/01.blo.0000218738.69247.d8.

Martin, T. (2016) 'A Smart Device Based Measuring System for Pelvic Tilt Computation in Hip Arthroplasty', *PRZEGLĄD ELEKTROTECHNICZNY*, 1(3), pp. 28–31. doi: 10.15199/48.2016.03.06.

Matijevich, E. S., Branscombe, L. M. and Zelik, K. E. (2018) 'Ultrasound estimates of Achilles tendon exhibit unexpected shortening during ankle plantarflexion', *Journal of Biomechanics*. Elsevier Ltd, 72, pp. 200–206. doi: 10.1016/j.jbiomech.2018.03.013.

Mayr, E. *et al.* (2005) 'The frontal pelvic plane provides a valid reference system for implantation of the acetabular cup: spatial orientation of the pelvis in different positions.', *Acta orthopaedica*, 76(6), pp. 848–53. doi: 10.1080/17453670510045471.

Meijer, M. F. *et al.* (2016) 'Do CAS measurements correlate with EOS 3D alignment measurements in primary TKA?', *Knee Surgery, Sports Traumatology, Arthroscopy*. Springer Berlin Heidelberg, pp. 1–10. doi: 10.1007/s00167-016-4031-3.

Melhem, E. *et al.* (2016) 'EOS® biplanar X-ray imaging: concept, developments, benefits, and limitations', *Journal of Children's Orthopaedics*. Springer Berlin Heidelberg, 10(1), pp. 1–14. doi: 10.1007/s11832-016-0713-0.

Michaud, T. C. (2011) *Human locomotion: the conservative management of gait-related disorders*. Newton Biomechanics Newton, MA.

Montefiori, E. *et al.* (2019) 'An image-based kinematic model of the tibiotalar and subtalar joints and its application to gait analysis in children with Juvenile

Idiopathic Arthritis', *Journal of Biomechanics*. Elsevier Ltd. doi: 10.1016/j.jbiomech.2018.12.041.

Mozaffari, M. H. and Lee, W.-S. (2017) 'Freehand 3-D Ultrasound Imaging: A Systematic Review', *Ultrasound in Medicine & Biology*, 43(10), pp. 2099–2124. doi: 10.1016/j.ultrasmedbio.2017.06.009.

Mündermann, A., Dyrby, C. O. and Andriacchi, T. P. (2008) 'A comparison of measuring mechanical axis alignment using three-dimensional position capture with skin markers and radiographic measurements in patients with bilateral medial compartment knee osteoarthritis', *The Knee*. Elsevier B.V., 15(6), pp. 480–485. doi: 10.1016/j.knee.2008.07.002.

Nakano, N. *et al.* (2016) 'Coronal lower limb alignment in normal knees-A radiographic analysis of 797 normal knee subjects', *Knee*. Elsevier B.V., 23(2), pp. 209–213. doi: 10.1016/j.knee.2015.12.004.

Niki, Y. *et al.* (2017) 'Comparison between cylindrical axis-reference and articular surface-reference femoral bone cut for total knee arthroplasty.', *Knee surgery, sports traumatology, arthroscopy : official journal of the ESSKA*. Springer Berlin Heidelberg, 25(12), pp. 3741–3746. doi: 10.1007/s00167-016-4251-6.

Niu, K. *et al.* (2018) 'In situ comparison of A-mode ultrasound tracking system and skin-mounted markers for measuring kinematics of the lower extremity', *Journal of Biomechanics*. Elsevier Ltd, 72, pp. 134–143. doi: 10.1016/j.jbiomech.2018.03.007.

Oh, S.-K., Chung, S.-S. and Lee, C.-S. (2009) 'Correlation of Pelvic Parameters with Isthmic Spondylolisthesis', *Asian Spine Journal*, 3(1), p. 21. doi: 10.4184/asj.2009.3.1.21.

Parratte, S. *et al.* (2008) 'The use of ultrasound in acquisition of the anterior pelvic plane in computer-assisted total hip replacement: a cadaver study.', *The Journal of bone and joint surgery. British volume*, 90, pp. 258–263. doi: 10.1302/0301-620X.90B2.19950.

Passmore, E. *et al.* (2016) 'Measuring Femoral Torsion In Vivo Using Freehand 3-D Ultrasound Imaging', *Ultrasound in Medicine and Biology*, 42(2), pp. 619–623. doi: 10.1016/j.ultrasmedbio.2015.10.014.

Passmore, E. *et al.* (2017) 'Application of ultrasound imaging to subject-specific modelling of the human musculoskeletal system', *Meccanica*. Springer Netherlands, 52(3), pp. 665–676. doi: 10.1007/s11012-016-0478-z.

Passmore, E., Graham, H. K. and Sangeux, M. (2018) 'Defining the medial-lateral axis of the femur: Medical imaging, conventional and functional calibration methods lead to differences in hip rotation kinematics for children with torsional deformities', *Journal of Biomechanics*, 69, pp. 156–163. doi: 10.1016/j.jbiomech.2018.01.018.

Passmore, E. and Sangeux, M. (2016) 'Defining the medial-lateral axis of an anatomical femur coordinate system using freehand 3D ultrasound imaging', *Gait & Posture*, 45(February), pp. 211–216. doi: 10.1016/j.gaitpost.2016.02.006.

Perrott, M. A. *et al.* (2017) 'Comparison of lower limb and trunk kinematics between markerless and marker-based motion capture systems', *Gait and Posture*.

Elsevier B.V., 52, pp. 57–61. doi: 10.1016/j.gaitpost.2016.10.020.

Peters, A. *et al.* (2012) 'A comparison of hip joint centre localisation techniques with 3-DUS for clinical gait analysis in children with cerebral palsy', *Gait & Posture*. Elsevier B.V., 36(2), pp. 282–286. doi: 10.1016/j.gaitpost.2012.03.011.

Peters, A., Baker, R. and Sangeux, M. (2010) 'Validation of 3-D freehand ultrasound for the determination of the hip joint centre', *Gait & Posture*. Elsevier B.V., 31(4), pp. 530–532. doi: 10.1016/j.gaitpost.2010.01.014.

Petrone, M. R. *et al.* (2003) 'The Accuracy of the Palpation Meter (PALM) for Measuring Pelvic Crest Height Difference and Leg Length Discrepancy', *Journal of Orthopaedic & Sports Physical Therapy*, 33(6), pp. 319–325. doi: 10.2519/jospt.2003.33.6.319.

Philippot, R. *et al.* (2009) 'Pelvic balance in sagittal and Lewinnek reference planes in the standing, supine and sitting positions', *Orthopaedics & Traumatology: Surgery & Research*, 95(1), pp. 70–76. doi: 10.1016/j.otsr.2008.01.001.

Pierrepont, J. *et al.* (2017) 'Variation in functional pelvic tilt in patients undergoing total hip arthroplasty', *Bone & Joint Journal*, 99-B(2), pp. 184–191. doi: 10.1302/0301-620X.99B2.BJJ-2016-0098.R1.

Pietsch, M. *et al.* (2013) 'Patient-specific total knee arthroplasty: the importance of planning by the surgeon', *Knee Surgery, Sports Traumatology, Arthroscopy*, 21(10), pp. 2220–2226. doi: 10.1007/s00167-013-2624-7.

Pinskerova, V. *et al.* (2000) 'The shapes and relative movements of the femur and tibia at the knee.', *Der Orthopade*, 29 Suppl 1, pp. S3–S5. doi: 10.1007/PL00003679.

Prager, R. W. *et al.* (1998) 'Rapid calibration for 3-D freehand ultrasound', *Ultrasound in Medicine & Biology*, 24(6), pp. 855–869. doi: 10.1016/S0301-5629(98)00044-1.

Radtke, K. *et al.* (2010) 'Effect of limb rotation on radiographic alignment in total knee arthroplasties', *Archives of Orthopaedic and Trauma Surgery*, 130(4), pp. 451–457. doi: 10.1007/s00402-009-0999-1.

Ranawat, C. S. *et al.* (2016) 'Effect of Spinal Deformity on Pelvic Orientation from Standing to Sitting Position', *Journal of Arthroplasty*. Elsevier Ltd, 31(6), pp. 1222–1227. doi: 10.1016/j.arth.2015.11.035.

Renault, J.-B. *et al.* (2018) 'Articular-surface-based automatic anatomical coordinate systems for the knee bones', *Journal of Biomechanics*. Elsevier Ltd, pp. 1–8. doi: 10.1016/j.jbiomech.2018.08.028.

Robertsson, O. *et al.* (2001) 'The Swedish Knee Arthroplasty Register 1975-1997: An update with special emphasis on 41,223 knees operated on in 1988-1997', *Acta Orthopaedica Scandinavica*, 72(5), pp. 503–513. doi: 10.1080/000164701753532853.

Rohling, R., Gee, A. and Berman, L. (1999) 'A comparison of freehand three-dimensional ultrasound reconstruction techniques', *Medical Image Analysis*, 3(4), pp. 339–359. doi: 10.1016/S1361-8415(99)80028-0.

Rouhandeh, A. *et al.* (2014) 'Quantification of Soft Tissue Artefacts Using Motion Capture Data and Ultrasound Depth Measurements', 6(6), pp. 324–328.

Sabharwal, S. *et al.* (2007) 'Reliability analysis for radiographic measurement of limb length discrepancy: full-length standing anteroposterior radiograph versus scanogram.', *Journal of pediatric orthopedics*, 27(1), pp. 46–50. doi: 10.1097/01.bpo.0000242444.26929.9f.

Sabharwal, S. and Zhao, C. (2008) 'Assessment of Lower Limb Alignment: Supine Fluoroscopy Compared with a Standing Full-Length Radiograph', *The Journal of Bone and Joint Surgery-American Volume*, 90(1), pp. 43–51. doi: 10.2106/JBJS.F.01514.

Sangeux, M., Peters, A. and Baker, R. (2011) 'Hip joint centre localization: Evaluation on normal subjects in the context of gait analysis', *Gait & Posture*, 34(3), pp. 324–328. doi: 10.1016/j.gaitpost.2011.05.019.

Schiraldi, M. *et al.* (2016) 'Mechanical and kinematic alignment in total knee arthroplasty', *Annals of Translational Medicine*, 4(7), pp. 130–130. doi: 10.21037/atm.2016.03.31.

Sharma, L., Cahue, S., *et al.* (2003) 'Physical functioning over three years in knee osteoarthritis: Role of psychosocial, local mechanical, and neuromuscular factors', *Arthritis & Rheumatism*, 48(12), pp. 3359–3370. doi: 10.1002/art.11420.

Sharma, L., Dunlop, D. D., *et al.* (2003) 'Quadriceps strength and osteoarthritis progression in malaligned and lax knees.', *Annals of internal medicine*, 138(8), pp. 613–9. Available at: http://www.ncbi.nlm.nih.gov/pubmed/12693882.

Sharma, L. *et al.* (2010) 'Varus and valgus alignment and incident and progressive knee osteoarthritis', *Annals of the Rheumatic Diseases*, 69(11), pp. 1940–1945. doi: 10.1136/ard.2010.129742.

Shiers, L. G. P. (1960) 'Arthroplasty of the Knee: Interim Report of a New Method', *Journal of Bone & Joint Surgery, British Volume*, 42-B(1), pp. 31–39.

Skou, S. T. *et al.* (2014) 'Association of Knee Confidence With Pain, Knee Instability, Muscle Strength, and Dynamic Varus-Valgus Joint Motion in Knee Osteoarthritis', *Arthritis Care & Research*, 66(5), pp. 695–701. doi: 10.1002/acr.22208.

Smith, J. and Finnoff, J. T. (2009) 'Diagnostic and Interventional Musculoskeletal Ultrasound: Part 1. Fundamentals', *PM and R*. American Academy of Physical Medicine and Rehabilitation, 1(1), pp. 64–75. doi: 10.1016/j.pmrj.2008.09.001.

Specogna, A. V. *et al.* (2006) 'Radiographic Measures of Knee Alignment in Patients With Varus Gonarthrosis: Effect of Weightbearing Status and Associations With Dynamic Joint Load', *The American Journal of Sports Medicine*, 35(1), pp. 65–70. doi: 10.1177/0363546506293024.

Stagni, R. *et al.* (2000) 'Effects of hip joint centre mislocation on gait analysis results', *Journal of Biomechanics*, 33(11), pp. 1479–1487. doi: 10.1016/S0021-9290(00)00093-2.

Stief, F. *et al.* (2014) 'Effect of lower limb malalignment in the frontal plane

on transverse plane mechanics during gait in young individuals with varus knee alignment', *The Knee*. Elsevier B.V., 21(3), pp. 688–693. doi: 10.1016/j.knee.2014.03.004.

Stief, F. *et al.* (2018) 'Abnormal loading of the hip and knee joints in unilateral hip osteoarthritis persists two years after total hip replacement', *Journal of Orthopaedic Research*, 36(8), pp. 2167–2177. doi: 10.1002/jor.23886.

Taki, N., Mitsugi, N. and Mochida, Y. (2012) 'Change in Pelvic Tilt Angle 2 to 4 Years After Total Hip Arthroplasty', *Journal of Arthroplasty*. Elsevier Inc., 27(6), pp. 940–944. doi: 10.1016/j.arth.2011.10.003.

Tamura, S. *et al.* (2015) 'Hip range of motion during daily activities in patients with posterior pelvic tilt from supine to standing position', *Journal of Orthopaedic Research*, 33(4), pp. 542–547. doi: 10.1002/jor.22799.

Tamura, S. *et al.* (2017) 'Does Pelvic Sagittal Inclination in the Supine and Standing Positions Change Over 10 Years of Follow-Up After Total Hip Arthroplasty?', *The Journal of Arthroplasty*. Elsevier Ltd, 32(3), pp. 877–882. doi: 10.1016/j.arth.2016.08.035.

Tamura, S., Takao, M. and Sakai, T. (2014) 'Spinal Factors In fl uencing Change in Pelvic Sagittal Inclination From Supine Position to Standing Position in Patients Before Total Hip Arthroplasty', *Journal of Arthroplasty*. Elsevier Inc., 29(12), pp. 2294–2297. doi: 10.1016/j.arth.2013.11.014.

Terjesen, T. *et al.* (1991) 'Leg-length discrepancy measured by ultrasonography.', *Acta orthopaedica Scandinavica*, 62(2), pp. 121–4. doi: 10.3109/17453679108999237.

Thelen, T. *et al.* (2016) 'Normative 3D acetabular orientation measurements by the low-dose EOS imaging system in 102 asymptomatic subjects in standing position: Analyses by side, gender, pelvic incidence and reproducibility.', *Orthopaedics & traumatology, surgery & research : OTSR*. Elsevier Masson SAS, 103(2), pp. 209–215. doi: 10.1016/j.otsr.2016.11.010.

Uemura, K. *et al.* (2017) 'Change in Pelvic Sagittal Inclination From Supine to Standing Position Before Hip Arthroplasty', *The Journal of Arthroplasty*. Elsevier Ltd, pp. 1–6. doi: 10.1016/j.arth.2017.03.015.

Upadhyaya, S., Lee, W. and Joslin, C. (2015) 'Ultrasound and Mocap to improve non invasive hip joint center calculation', in *Medical Measurements and Applications (MeMeA), 2015 IEEE International Symposium on*, pp. 490–494. doi: 10.1109/MeMeA.2015.7145253.

Vanwanseele, B., Parker, D. and Coolican, M. (2009) 'Frontal knee alignment: three-dimensional marker positions and clinical assessment.', *Clinical orthopaedics and related research*, 467(2), pp. 504–9. doi: 10.1007/s11999-008-0545-4.

Vicon® (2002) 'Plug-in-Gait modelling instructions'. Oxford, UK: Vicon®612 Motion Systems, Oxford Metrics Ltd.

Whiteside, L. a and Arima, J. (1995) 'The anteroposterior axis for femoral rotational alignment in valgus total knee arthroplasty.', *Clinical orthopaedics and related research*, 77(321), pp. 168–72. Available at:

http://www.ncbi.nlm.nih.gov/pubmed/7497664.

Wiles, P. (1958) 'The surgery of the osteo-arthritic hip', *British Journal of Surgery*, 45(193), pp. 488–497. doi: 10.1002/bjs.18004519315.

Winter, A. *et al.* (2014) 'Pre-operative analysis of lower limb coronal alignment — A comparison of supine MRI versus standing full-length alignment radiographs', *The Knee*. Elsevier B.V., 21(6), pp. 1084–1087. doi: 10.1016/j.knee.2014.05.001.

Wren, T. A. L. *et al.* (2011) 'Influence of gait analysis on decision-making for lower extremity orthopaedic surgery: Baseline data from a randomized controlled trial', *Gait and Posture*. Elsevier B.V., 34(3), pp. 364–369. doi: 10.1016/j.gaitpost.2011.06.002.

Yaffe, M. A., Koo, S. S. and Stulberg, S. D. (2008) 'Radiographic and navigation measurements of TKA limb alignment do not correlate', *Clinical Orthopaedics and Related Research*, 466(11), pp. 2736–2744. doi: 10.1007/s11999-008-0427-9.

Yin, L. *et al.* (2015) 'Identifying the Functional Flexion-extension Axis of the Knee: An In-Vivo Kinematics Study', *PLOS ONE*. Edited by L. Ren, 10(6), p. e0128877. doi: 10.1371/journal.pone.0128877.

Yushkevich, P. A. *et al.* (2006) 'User-guided 3D active contour segmentation of anatomical structures: Significantly improved efficiency and reliability', *NeuroImage*, 31(3), pp. 1116–1128. doi: 10.1016/j.neuroimage.2006.01.015.

Appendix

A.   Free-hand US and motion capture bone segmentation walkthrough

This section is a guide for bone segmentation from ultrasound and motion capture data with a Python based package, Py3DFreeHandUS (https://github.com/u0078867/Py3DFreeHandUS) and MeVisLab (https://www.mevislab.de/mevislab).

Step 1. Installation

Install Py3DFreeHandUS package via the HTML guide. This may require sometime if not experienced with Python, but there is good documentation. Once installed, become accustomed to the code with some of the example scripts given.

Step 2. Data Capture

It is explicit in the documentation that synchronised c3d motion capture data and DICOM sequences are needed for optimal post-processing of the data. Synchronisation can be achieved through hardware or digital means. For example, a hardware synchronisation would be possible with trigger out synchronisation ports on the ultrasound device. If these are not present, a digital synchronisation may be easier with the use of a National Instruments card and LabVEIW. **Note: this has only been tested with a Vicon motion capture system.**

To gain the ultrasound images in global space, the ultrasound probe is tracked by the motion capture system to obtain its roto-translational pose. This can be achieved through calibration with a generic cluster attached to the probe as extensively explained in the package, or through known measurements of the ultrasound image origin with respect to an accurately attached cluster. This can be attained if you have access to a high-quality 3D printer. An example of this technique is shown by a group based at Vanderbilt University (https://my.vanderbilt.edu/batlab/resources/motion-analysis). Once confident in obtaining ultrasound sweeps in known space, the post-processing can begin.

Step 3. Data Processing (Python)

1. Several example scripts are given within the Python package which form the basis of the processing needed to gain the data for the segmentation. It is advised to run the scripts within Spyder to gain relevant outputs which can be used to check the data and potentially debug any code.
2. Two files are needed to run the code; 1. The motion capture data in c3d format containing the position and names of the markers within the cluster attached to the probe. 2. The ultrasound data in DICOM format and completely void of RGB colour formatting within the ultrasound software during the export process. **This has only been tested in EchoWave which requires editing of several formats within the source code of the software***.
3. Additional information required to run the scripts; pixel to mm ratio dependent on the width and depth of the ultrasound image respectively, calibration/known measurements of the ultrasound image with respect to the probes' marker cluster (3 translations and 3 rotations), and sample frequency of motion capture system, choice on frames to be included in the voxel array, choice on calculation of pose of voxel array, choice on scale and size of voxel array (**IMPORTANT: scaling up voxel array will require scale down in the export**), choice on ultrasound image alignment, choice on gap filling parameters of voxel array, choice on export properties of voxel array. **All voxel array parameters and functions are described in detail within the documentation and a working example script will be added to this documentation.**
4. Two .vti files are saved which can be viewed, checked and processed in MeVisLab for the next step of the processing.

Step 4. Data Processing (MeVisLab)

Two MeVisLab (.mlab) files are used within this documentation for initial vti processing and then segmentation which were supplied by the same author of the Python package and will be explained in detail here.

1. View_vti.mlab: Views and re-orientates voxel-array for eventual export into DICOM format for segmentation. Each file contains a series of modules linked together, each serving individual purposes of which can be explained by right clicking the modules and finding the help sections. In the Figure A1 below, the .vti files are loaded in the bottom most module and will alert you if there are errors with the files. View3D will show the voxel array reconstruction and is a clear indication of the quality of the reconstruction. View2D is the voxel array broken back down into 2D slices and will also indicate the quality of processing so far. OrthoSwapFlip allows for manual orientation of the slices if there is a rotation offset. OrthoView2D visualises the slices in the three orthogonal planes. ImageSave allows the export of the slices into DICOM format in one file and is needed for the next step in this

format. DicomTool allows for the slices to be exported individually if needed for processing in other software.
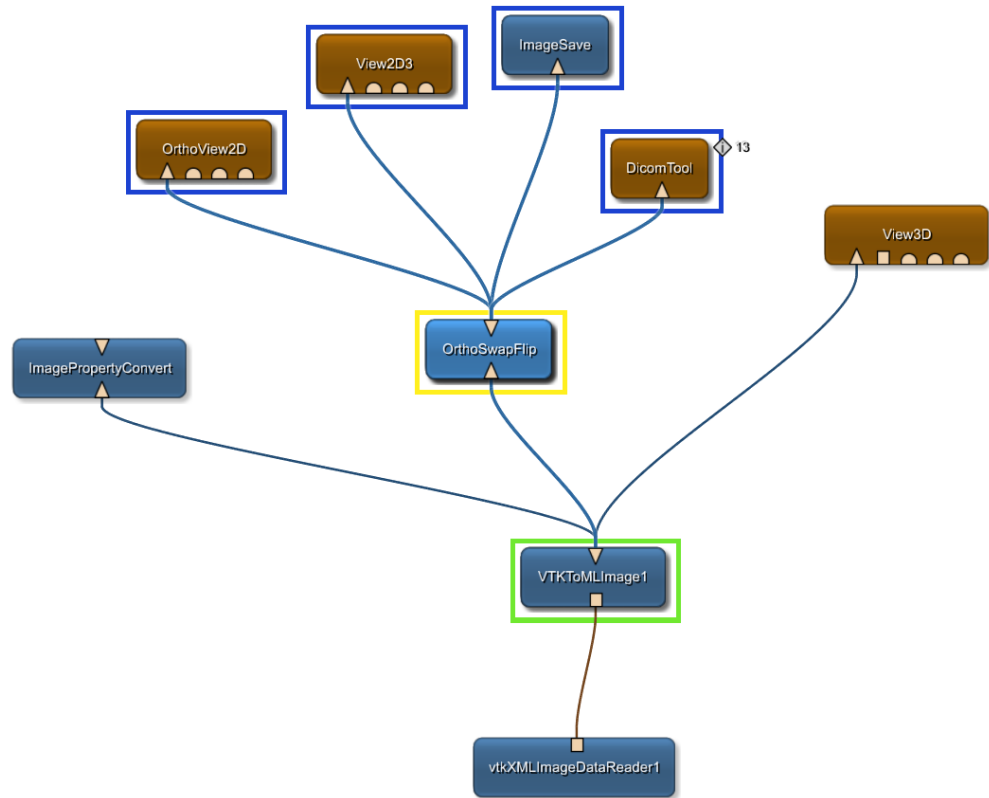

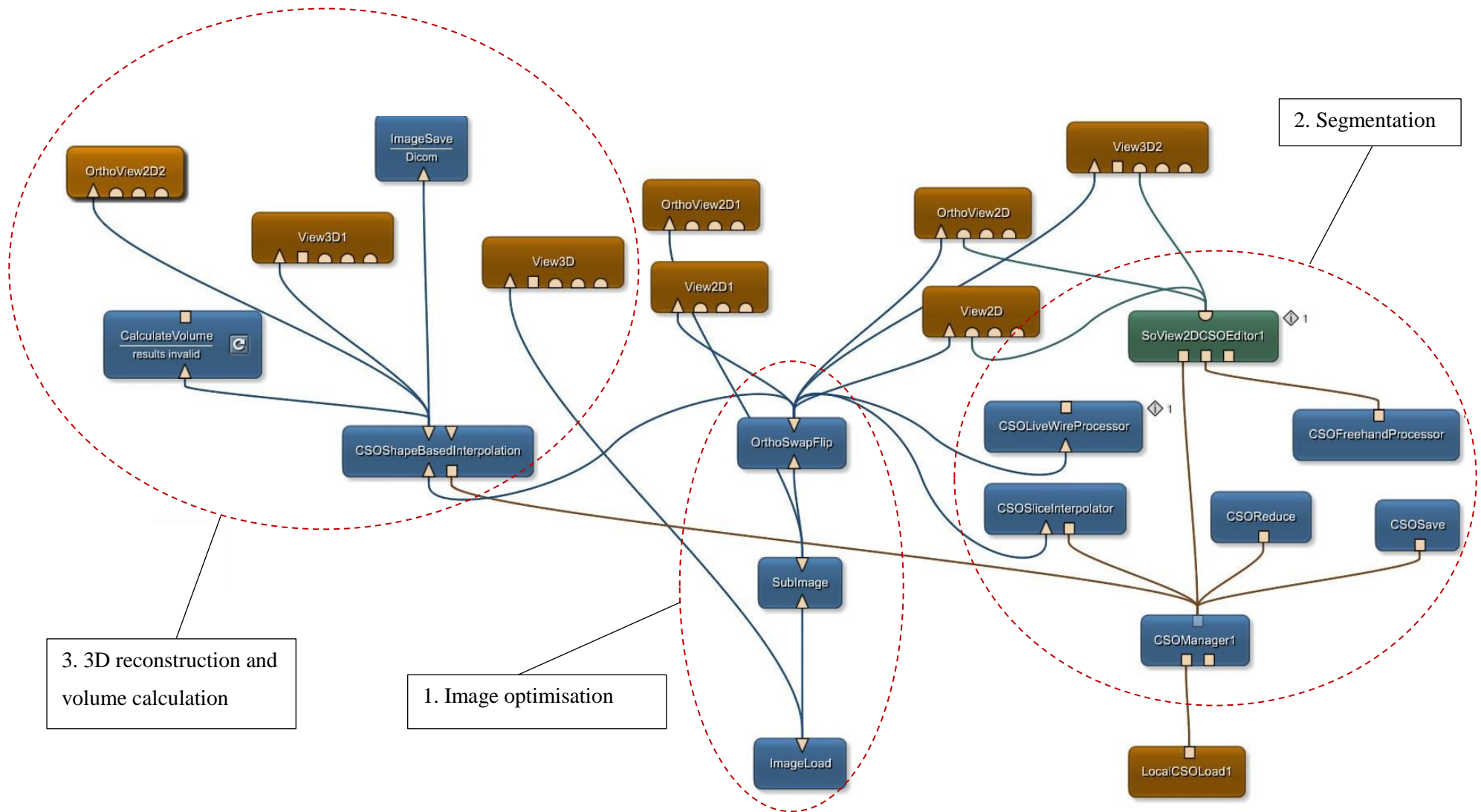Figure A.1. View_vti.mlab file for voxel array check and export in DICOM format for further processing.

Figure A.2. CSO Segmentation linear inter final.mlab*: workflow for image loading, resizing and reorientation (middle), segmentation (right), and 3D reconstruction, volume calculation, and export (left).

2. CSO Segmentation linear inter final.mlab: Figure A2 on the previous page represents the workflow needed to manually segment the structures you have previously captured if they are in the correct format as guided by the previous .mlab file. It consists of three main sections which will be discussed in detail here.

1. **Image optimisation:** Load the DICOM file saved from the previous step within ImageLoad. SubImage is important as it fits the size of the DICOM images to an ideal fit in View2D. Double-click SubImage and click 'Full Size', the X, Y and Z parameters should adjust accordingly, and make sure the 'Mode' is on 'Voxel Start and End'. This process should be repeated every time you load a new image sequence. Finally, if necessary, use OrthoSwapFlip to orientate the images in user friendly manner, this should have been achieved in the previous .vti file.

2. **Segmentation:** Firstly, double click CSOSave and save a new .cso file for each sequence of images you segment to avoid over-writing previous .cso files. This keeps an associated CSO (contour segment object) with each segmentation you perform. View2D opens the main image plane of the loaded DICOM sequence, this is where you perform the segmentations. OrthoView2D allows for segmentation in the other two orthogonal planes if necessary. CSOManager saves each contour drawn during segmentation and is useful to keep open so that each contour can be investigated and deleted if a mistake is made. CSOFreehandProcessor gives options on the way the contours are mapped onto the images (spline, polyline, freehand etc.) which can be adjusted according to personal preference. All other CSO modules for the segmentation should not need adjusting.

3. **3D reconstruction:** Once you have finished the segmentation, you should save the .cso file and then close the CSOManager. Then double click the CSOShapeBasedInterpolation module and make sure Update is selected next to 'On Input Change Behaviour' and then click Update. This produces and a 3D output viewed in View3D1 based on the linear interpolation performed between the drawn contours. Whilst a 3D model can be viewed, saving the model surface as a .stl file is not currently an option from MeVisLab. Therefore, the next step is to save it as a final DICOM file in ImageSave which can then be automatically segmented in other image processing software (ITK-snap for example) and then saved as a .stl.

4. **Further processing:** Dependent on your required final output, this walkthrough will go through the necessary steps needed to obtain articular surfaces (representing the rotation of the hip, knee and ankle joints) from the final MeVisLab output. This is achieved by following step 1.3 in the 'guide to building an MSK model' attached in this document.

Step 5. Alternative to part 2 of Step 4

It is clear from the segmentation in part 2 of step 4 and the further processing needed that this has a lot of potential operator variability which can introduce unwanted errors in the final outputs. In this section, an alternative is suggested which allows the direct, automatic processing of the required surfaces with minor 'cleaning up' to remove unwanted artefacts.

1. Step 4, part 1 explains the final DICOM export of the voxel array reconstruction. This same sequence can be exported; however, this must be processed through DicomTool which exports the sequence in their individual slices to a new folder.
2. This sequence can then be loaded into nmsBuilder for automatic construction of a .stl file containing the all the surfaces captured in the ultrasound sweep. (EXPLAIN PROCESS).
3. Load the final version into MeshLab for final processing which just involves 'cleaning up' the file. Use the 'Select Connected Components in a Region' tool to select and remove all artefacts which aren't connected to the articular surfaces desired. Then use the 'Select Faces in a Rectangular Region' tool to remove the remaining surfaces.
4. Surface fitting algorithms can then be applied to the joint surfaces for estimations of the position and size of the measurements conducted.

*For optimising the ultrasound image (especially if you need to calibrate the system) for raw DICOM exports after measurements, the following parameters need to be adjusted:

1. Deselect 'save video with surrounding information' which should be under menu/option/tools.
2. The Telemed logo cannot be removed. However, scale lines can be permanently removed by changing their color to black in skin file "...\Config\Skins\PhantomDark\data.dat" (if is used default PhantomDark skin):

<b_scale_lines_color_red value="0"/>

<b_scale_lines_color_green value="0"/>

<b_scale_lines_color_blue value="0"/>

Set all these values to.

B.   Wand design

To facilitate precise palpation of bony landmarks, a palpating wand was designed. Such devices have been used in the past and have shown to be more efficient and more accurate than skin markers in using the CAST (calibrated anatomical systems technique) method (Cappozzo *et al.*, 1995; Donati *et al.*, 2007).

Design evaluation

Several iterations were produced before arriving at a design which was best suited for fast and accurate palpation, and for simple post-processing steps. A decision matrix, shown in Table 4.1 was constructed to help quantify the best design.

Table B.1. Wand decision matrix including five weighted factors to help quantify the best initial design. The red and blue shaded rows show the worst and best designs respectively.

Weightings						Total
/10	8	6	10	4	1	29
% Total	28%	21%	34%	14%	3%	100%
	Handling	**Weight**	**Palpation Factor**	**Marker Occlusion**	**Aesthetics**	**/100**
Cardboard	50	90	60	30	10	58
Antenna	30	90	85	30	50	62
Steel Rod	10	5	20	60	20	20
Pencil	70	90	50	30	30	60
Paintbrush	85	85	90	80	80	86

It was decided that an object which could be readily found and amended was suitable for the task. Design preferences included handling, weight, palpation factor (appropriateness of the end point for palpation), marker occlusion (how effective the motion capture system was at locating the attached markers) and aesthetics. Five ideas were conceived including a piece of cardboard (lightweight), an antenna (clear tip and light), a large rod (like in Cappozzo, 1994), pencil and paintbrush. The cardboard cut-out proved, before testing, and by feel, to be highly unusable for motion capture experiments. The antenna was too difficult to adapt for motion capture experiments, for example, there was difficulty in attaching the reflective markers. The large rod was too heavy (2.3kg) to easily palpate the landmarks. The pencil was difficult to amend due to its size and inability to successfully attach markers onto.

A paint brush was found to be the best candidate as it covers several of the design considerations, including a convenient taper towards the tip, which meant it

was ideal for palpation. In terms of amending the paint brush to hold the skin markers, three screws were implemented perpendicularly to one another to form an out of plane, robust cluster for the calculation of the tip, like that shown in the literature (Donati *et al.*, 2007).

Figure B1. Paint brush wand design with three retro-reflective markers implemented and masking tape applied to minimise unwanted reflection.

A batch of pilot experiments went ahead with this design to see whether it could accurately locate palpable landmarks.

Final design

It was decided that accuracy in calculating the tip was key and the previous devices could not provide this. Therefore, a wand was designed using SolidWorks (Dassault Systèmes, Waltham, MA) based on the shape and size of the paint brush. This was 3D printed using an Ultimater 3 (Ultimaker B.V., Geldermalsen, The Netherlands), as one, solid part. One key problem with using this device is the resolution of the printing nozzle. This is only problematic when printing fine geometries, such as the location of the tip in this design which tapers from the main shaft. It was therefore difficult to avoid slight warping, which could offset the tips real location in global space. The design and main dimensions are shown in Figure B2.
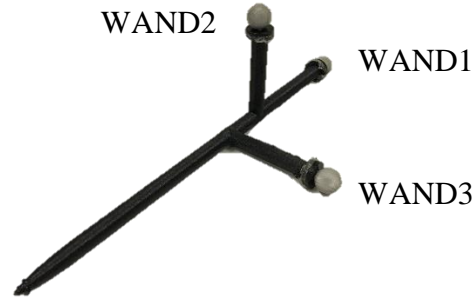
Figure B2. Final wand design. Max length: 279.5mm. One 14mm diameter reflective marker is attached to each offset arm to form a cluster.

Wand tip calculation

To calculate the tip of the wand from the three markers, a three-sphere trilateration method was used. The three retroreflective markers (14mm ø), WAND1, WAND2 and WAND3 each had centre co-ordinates (x_n, y_n, z_n) which subsequently represented the centre of a sphere which had known radii with respect to the tip of the wand. The intersection of three spheres produces two points, therefore the tip of the wand could be located accurately. This was calculated by the following method:

Firstly, two vectors were defined:

$$\overrightarrow{v_{21}} = \overrightarrow{WAND2} - \overrightarrow{WAND1} \qquad \text{(B.1)}$$

$$\overrightarrow{v_{31}} = \overrightarrow{WAND3} - \overrightarrow{WAND1} \qquad \text{(B.2)}$$

Where $\overrightarrow{v_{21}}$ and $\overrightarrow{v_{31}}$ define the centre of WAND2 and WAND3 with respect to WAND1. The cross product of these two vectors is then computed to define the third direction with respect to the plane formed by the three sphere centres:

$$\vec{c} = \overrightarrow{v_{21}} \times \overrightarrow{v_{31}} \qquad \text{(B.3)}$$

Each sphere has its respective equation, which are necessary for determining the intersection points and are as follows:

$$(x - x_n)^2 + (y - y_n)^2 + (z - z_n)^2 = r_n{}^2 \qquad \text{(B.4)}$$

r_n is the radius of each sphere. Two linear equations are obtained by subtracting the 2nd and 3rd sphere equation from the first. This generates two unique planes. A third plane is also needed which is defined by the three sphere centres ($\vec{c}$). With this information, the three-plane intersection, L, a unique point relative to WAND1 can be found by:

$$L =$$

$$\frac{\left(\frac{(sum(\overrightarrow{v_{21}})^2) + r_1{}^2 - r_2{}^2).* \overrightarrow{v_{31}} - (sum(\overrightarrow{v_{31}})^2) + r_1{}^2 - r_3{}^2).* \overrightarrow{v_{21}}}{2} \times \vec{c}\right)}{sum(\vec{c}.^2)} \qquad (B.5)$$

From here, two solutions are found which are defined from this point L in the positive and negative direction of $\vec{c}$ after being tested for real roots by the following equation:

$$\vec{u} = \pm \sqrt{(r_1{}^2 - sum(L^2)) * \left(\frac{\vec{c}}{\sqrt{sum(\vec{c}.^2)}}\right)} \qquad (B.6)$$

The tip of the wand is then found by:

$$WAND_{tip} = WAND1 + L - u \qquad (B.7)$$

C.   Phantom bottle

For the 3D freehand ultrasound reconstructions, an initial validation experiment was performed on a bottle of known dimensions. To gauge whether the setup could accurately estimate the radii of the main body of the bottle, one plastic bottle was filled with water and placed into a water bath and scanned by the ultrasound transducer at 15Hz. The 2D ultrasound images were manually segmented and the radii was calculated from fitting a cylinder to the main body of the bottle. The mean value from the five repeats was carried forward and compared to the real value (27mm). The difference between the calculated radii and reconstructed radii was defined as the accuracy.

Water bottle reconstructions showed an overestimation 0.5mm. Table C.1 shows the mean and standard deviations of the measurements.

Table C.1. Accuracy of water bottle volume calculations from the reconstruction of 2D ultrasound scans conducted in two sessions and as a function of the main body radius.

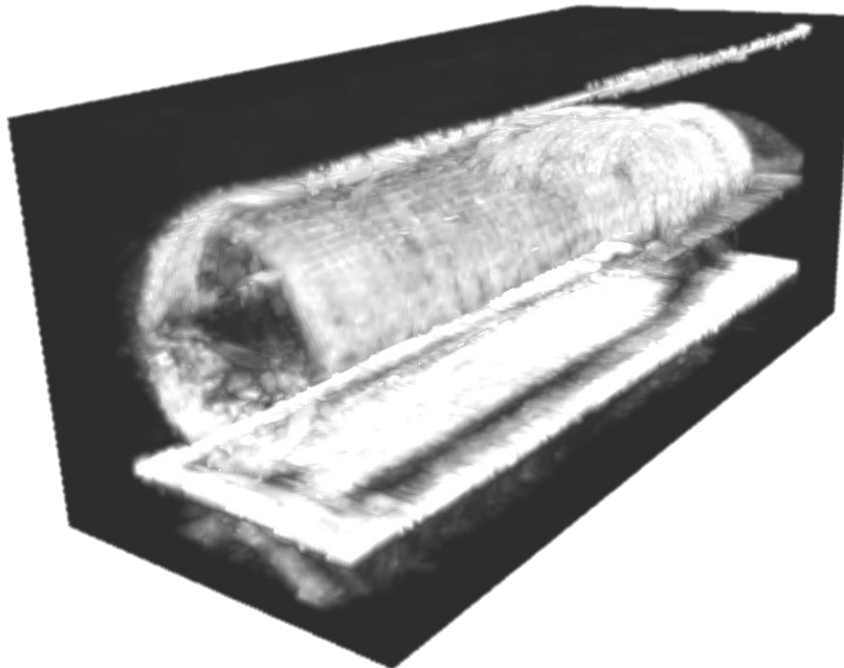| Radius (r=27mm)		Accuracy (mm)	% Error
Mean (mm)	*SD (mm)*		
27.5	0.1	0.5	2

Figure C.1 Voxel array construction of the aligned ultrasound images from a water-bottle scan
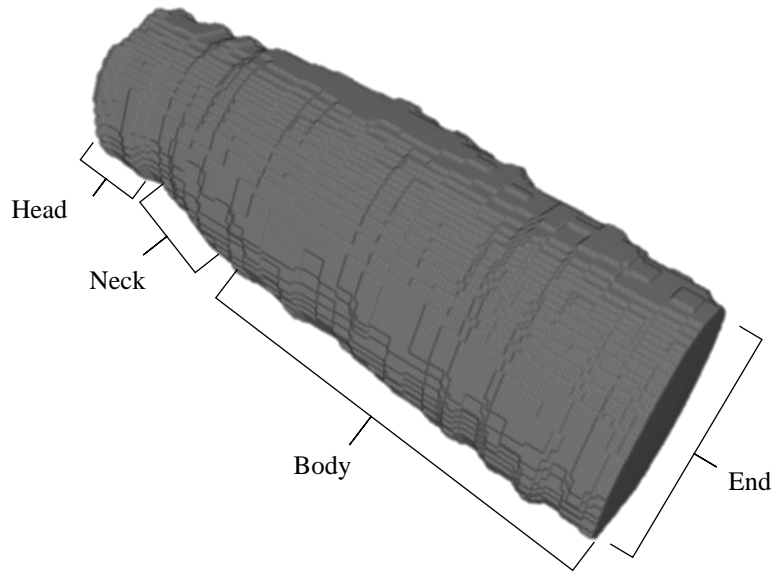
133

Figure C.2. Reconstructed water bottle from the ultrasound segmentation with bottle sections indicated.
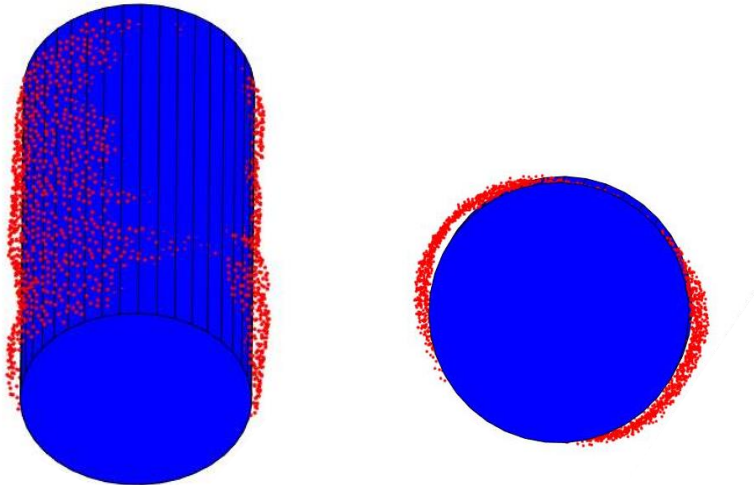

Figure C.3. Cylinder fitting to the circumference of the main body ultrasound reconstruction.

An object which could be easily analysed with ultrasound and fit within the field of view of the probe was chosen for preliminary accuracy measurements. A bottle filled with water allowed its entire circumference to be visible during a scan. This meant potentially accurate reconstruction and segmentation.

It was shown that the reconstructions overestimated the real radius by 2% (0.5mm) by approximately. Whilst artefacts not associated with the features of the water bottle are present in both, this was considered not to have an impact in the segmentation process. This analysis showed that fitting a cylinder to known geometries from ultrasound reconstruction was a robust procedure.